Summer 8-15-2017

Effects of Nucleosome Structure on DNA Photoproduct Formation and Deamination

Kesai Wang
Washington University in St. Louis

WASHINGTON UNIVERSITY IN ST. LOUIS

Department of Chemistry

Dissertation Examination Committee:
John-Stephen Taylor, Chair
Douglas Chalker
Michael L. Gross
Jay Ponder
Timothy Wencewicz

Effects of Nucleosome Structure on DNA Photoproduct Formation and Deamination

by

Kesai Wang

A dissertation presented to
The Graduate School of
Washington University in
partial fulfillment of the
requirements for the degree
of Doctor of Philosophy

August 2017
St. Louis, Missouri

Table of Contents

List of Figures

List of Tables

Acknowledgments

I would like to express the deepest appreciation to my advisor Dr. John-Stephen Taylor, who has the wisdom of a genius and the passion for science. He continually and convincingly conveyed an attitude of integrity in regard to scholarship, a practice of rigorousness in regard to research, and an excitement in regard to teaching. Without his guidance and persistent help this dissertation would not have been possible.

I would like to thank my Doctoral Advisory Committee members, Dr. Michael Gross and Dr. Jay Ponder, for their service in annual committee meetings, and their insightful ideas that directed the course of my PhD. I would like to thank my Doctoral Examination Committee members, Dr. Douglas Chalker and Dr. Timothy Wencewicz, for their willingness to bring their perspectives to my work and their service on my defense committee.

I am grateful to all my wonderful group members, previous and current, for making the Taylor lab a pleasant place to work in. I am especially thankful to Dr. Vincent Cannistraro, a teacher and a friend, who unreservedly guided me into the field of biochemistry, patiently helped with my experimental designs, as well as the less scientific side of my life.

In addition, I would like to thank Graduate School of Arts and Sciences, American Society of Biochemistry and Molecular Biology, and National Institutes of Health, for their financial support granted through Dean's Dissertation Fellowship, Travel Award for Graduate Students, and research fund R0140463, respectively.

I thank my parents and my little sister for their unconditional love and support, my first and last boyfriend Chong for his caring and encouragement, and most importantly, my deceased grandfather for his unwavering belief and pride in me. As a man who valued knowledge, I know he would have been very proud, as always, to see me complete my doctoral studies.

Kesai Wang

Washington University in St. Louis

August 2017

Dedicated to my Grandfather Wang Yongfeng (1929-2015).

ABSTRACT OF THE DISSERTATION

Effects of Nucleosome Structure on DNA Photoproduct Formation and Deamination

by

Kesai Wang

Doctor of Philosophy in Chemistry

Washington University in St. Louis, 2017

Professor John-Stephen Taylor

Cyclobutane pyrimidine dimers (CPDs) are DNA photoproducts linked to skin cancer, whose mutagenicity depends in part on their frequency of formation and deamination. Nucleosomes modulate CPD formation, favoring outside facing sites, and disfavoring inward facing sites. A similar pattern of CPD formation in protein-free DNA loops suggest that DNA bending causes the modulation of photoproduct formation in nucleosomes. To systematically study the cause and effect of nucleosome structure on CPD formation and deamination, we had developed a circular permutation synthesis strategy for positioning a target sequence at different superhelix locations (SHLs) across a nucleosome in which the DNA has been rotationally phased with respect to the histone octamer by TG motifs. We had used this system to show that the nucleosome dramatically modulates CPD formation in a T_{11}-tract that covers one full turn of the nucleosome helix at seven different SHLs, and that the position of maximum CPD formation at all locations is shifted to the 5'-side of that found in mixed-sequence nucleosomes. We have also shown that an 80-mer minicircle DNA using the same TG motifs faithfully reproduces the CPD pattern in the nucleosome, indicating that it is a good model for protein-free rotationally phased bent DNA of the same curvature as in a nucleosome, and that bending is modulating CPD formation. Furthermore, we have used the mono-nucleosome system to show that nucleosome moderately

modulates TC CPD deamination in poly $(TC)_n$ (n = 6 and 35) tracts that covers almost all seven SHLs in one full nucleosome helix. Unlike a previous study of deamination at TCG sites, the position of maximum CPD deamination rate is shifted 3 nucleotides to the 5'-side of the base pairs whose major groove face the nucleosome.

Chapter 1 Introduction

1.1 Motivation

Skin cancer is the most common cancer in the United States (1). It is estimated that one in five Americans will develop skin cancer in their lifetime and that nearly 9,500 people in the U.S. are diagnosed with skin cancer every day (2,3). There are mainly two types of skin cancers, melanoma and keratinocyte carcinoma (including 20% of squamous and 75% of basal cell carcinoma). Keratinocyte carcinoma accounts for most skin cancers diagnosed, and are highly curable if detected early and treated properly. In contrast, melanoma accounts for majority of skin cancer deaths, whose five-year survival rates for regional and distant stage are 62% and 18%, respectively (4).

High exposure to either natural or artificial ultraviolet (UV) radiation is a risk factor for skin cancers, especially for keratinocyte carcinoma. This risk can be reduced simply by minimizing skin exposure to UV radiation, such as by applying sunscreen; however, commercially available sunscreens only provides reliable protection against UVB and little protection against UVA. There are other less controllable risk factors, including personal/family history of skin cancers (especially melanoma), skin sun-sensitivity, and previous sunburns (4). Increased exposure to UV light almost certainly leads to the increased incidence of all types of skin cancers (5). One of the main molecular mechanisms involved in photocarcinogenesis is the signature C to T or CC to TT mutations that are frequently observed in tumor-suppressor genes and thought to arise from CPDs (6). Furthermore, UV contributes to photoaging, characterized by wrinkles, loss of skin tone and resilience.

Most living organisms on the surface of the earth are exposed to UV radiation at some point in their life cycle. Therefore, it is extremely meaningful to systematically investigate the formation frequency of UV-induced DNA photoproducts, as well as their subsequent deamination rates as they relate to C to T or CC to TT signature UV mutations associated with skin cancers. In the following sections, I will consider the background in more details and describe other studies so that readers can understand my dissertation studies.

1.2 Background

1.2.1 Photophysics of skin and ultraviolet (UV) light

Skin is the largest and highly protective organ in human body and highly protective (Figure ***1.1***). The thin epidermis (or the outermost layer of skin) contains melanocytes that can generate melanin, the pigment that determines our skin color and protects us from UV by light absorption. The dermis beneath the epidermis is, in contrast, a thick layer containing connective tissue, hair follicles, and sweat glands that provides UV-protection by light-scattering (6). The penetration of UV into skin is wavelength-dependent.

Conventionally, the UV spectrum (Figure ***1.2***) of sunlight is divided into short wavelengths UVC ($200 < \lambda < 280$ nm), middle wavelengths UVB ($\lambda = 280–320$ nm), and long wavelengths UVA ($320 < \lambda < 400$ nm) (7,8). UVC is extremely efficient at forming DNA photoproducts, but can be completely absorbed by the ozone layer. UVB is mostly absorbed by the ozone layer, whereas UVA passes the ozone layer without absorption. Consequently, only UVA (95% of terrestrial sunlight) and UVB (5% of terrestrial sunlight) can finally reach the surface of earth and are thus the primary photocarcinogenic agents (9). UVA, due to its long wavelength, penetrates

the most deeply into the skin with little scattering in the dermis layer compared with middle wavelength UVB.

The type (or chemical nature), formation frequency and mechanism of UV-induced DNA damage are wavelength-dependent. UVB and high energy UVC mainly induce *cis-syn* cyclobutane pyrimidine dimers (CPDs) and pyrimidine (6-4) pyrimidone photoproducts [(6-4) photoproducts; (6-4)PPs], with (6-4)PPs in significantly lower abundance (10,11). UVA radiation can also induce CPDs albeit mainly TT CPDs and at much lower levels, compared with UVB (12-15). Both UVA and UVB can also promote oxidative DNA damages (16). All in all, as determined in studies using laser irradiation, CPDs are the principal DNA lesions produced by terrestrial sunlight (9).

1.2.2 Cyclobutane pyrimidine dimers (CPDs) and photocarcinogenesis

CPDs form between two adjacent pyrimidines via [2 + 2] cycloaddition (Figure ***1.3***), in which the 4 π electrons of 2 C5-C6 double bonds form a 4-membered ring. A previous study in our group found that the formation of a CPD causes approximately 7-9° deformation relative to the B-form DNA structure at the lesion site (17). Compared with (6-4)PPs that cause 44° deformation (18), the structural disruptions by CPDs are relatively small and difficult to be recognized and repaired, making them potential mutagenic.

There are four types of CPDs between adjacent pyrimidines, depending on the spatial alignment of the two bases and their conformations around the N-glycosidic bond (Figure ***1.4***). Among them, the *cis-syn* CPD (with *anti-anti* glycosyl conformations) is the predominant type in double-stranded DNA, owing to geometric constraints (19-21). Depending on the sequence content, there are four types of *cis-syn* CPDs, namely TT, TC, CT, and CC. Under UVB irradiation, the overall relative proportion of CPDs forming at TT, TC, CT and CC sites is ~28, ~26, ~16 and

~30%, respectively (13). Although *cis-syn* TT CPD is the most abundant type, C-containing CPDs are the most photocarcinogenic ones that generate the C-to-T or CC-to-TT signature mutations found in skin cancer patients (22).

There are two principal mechanisms that have been proposed to explain the origin of these UV signature mutations. One is called the "tautomer-bypass mechanism" in which the C in a CPD adopts a tautomeric form that resembles T, which would direct the erroneous insertion of A during regular DNA replication thereby causing a C to T mutation (23,24). The other mechanism is the "deamination-bypass mechanism", which is proposed by our group and summarized in Figure ***1.5***. Unlike T=T CPDs which are chemically stable, the cytosine in C-containing CPDs can rapidly deaminate to a uracil within hours to days (25), which then directs the insertion of an adenine in the opposite strand by polymerase η in an error-free way (26). To summarize, the two mechanisms leading to mutations are: 1) direct error-prone replication of the CPD; 2) deamination of C within the CPD followed by error-free replication of the deaminated DNA photoproduct.

Chemically, C or ^{m}C deamination occurs in three steps under acidic conditions: protonation of C at N3 position, followed by a water attack at C4, and the loss of ammonia resulting in the formation of U (Figure ***1.6***). Mechanistically, the presence of a saturated 5,6 bond in the dimer as well as the presumably reduced hydrogen bonding and base stacking in a CPD most likely lead to increased nucleophilic attack by a hydroxide ion or water molecule at the C4 of the exposed cytosine base (27). Various studies by our group and others have shown that the deamination rates highly depend on the sequence context, pH, temperature and salt concentration (25,27,28). For example, a 3'-C deaminates faster than a 5'-C, and a G flanking the C accelerates deamination in duplex DNA owing to the catalysis of the O6-carbonyl group on the G (25). Furthermore, high salt

concentrations slow down the deamination presumably by stabilizing the duplex structure and thereby inhibiting protonation of C and addition of water. The overall frequency of C to T or CC to TT mutations depends on the competition between the rate of C-containing CPD formation, the rate of deamination, repair and translesion synthesis by polymerase η. When the UV-induced mutations affect the function of sufficient oncogenes and tumor suppressor genes, transformation of the keratinocytes and the melanocytes occurs (6,29). Besides direct mutation of genes, reduced level of DNA repair, or reduced time left for DNA repair in cell cycles caused by UV-altered cell signaling may also affect mutation frequency and lead to skin cancers (30).

Every living cell is potentially cancerous, but a functioning tumor suppressor gene (TSG, or antioncogene) protects a cell from one step on the path to cancer. When mutation causes loss or reduction of TSG function, a normal cell can progress to a cancer cell. Several TSGs are involved in photocarcinogenesis, including *p53* and *PTGH* genes that are responsible for keratinocyte carcinoma, and *p16* gene that is responsible for melanoma (6). It is worth mentioning that the status of the entire pathways regulated by these genes plays a more dominant role in photocarcinogenesis as opposed to the status of the genes themselves (31). For example, p53 protein binds DNA and stimulates production of a protein called p21, which can interact with a cell division-stimulating protein (cdk2) that causes the arrest of cell division, to enable time for repair. Mutant p53 protein cannot bind DNA effectively, resulting in less or no production of the p21 protein. Therefore, cells will divide uncontrollably, and acquire additional mutations that lead to tumors (32).

1.2.3 DNA damage and repair in human cells and *in vitro*

Luckily, the mutagenic consequences are minimized by various repair pathways in humans, among which, nucleotide excision repair (NER) is the sole repair system for bulky DNA adducts such as TT CPDs and (6-4)PPs (33). NER repairs DNA by making dual incisions on both sides of the

lesion with an excision nuclease. The damaged nucleotide is released in an oligomer (27-29 nt in eukaryotes), and the resulting gap is then filled in and sealed (33). Uracil in DNA originates from deamination of cytosine can be repaired via base excision repair (BER) by uracil-DNA glycosylase (UDG) present in human cells. In this repair pathway, the single uracil is removed by UDG that hydrolyzes the glycosylic bond, resulting in an abasic site (AP site) which can then be removed by AP lyase, and thus the nucleotide is replaced.

In our experiments, we made use of the *cis-syn* CPD-specific DNA repair enzymes not found in humans, DNA photolyase (34) and T4 endonuclease V (or T4 pyrimidine dimer glycosylase; T4-pdg) (35). Photolyase is a photoreactivating enzyme that breaks the 4-membered cyclobutane ring and converts a CDP back to 2 pyrimidines under black light (mainly long wavelength UVA and not much visible light). Mechanistically, photolyase acts by bending the DNA and flipping out the pyrimidine dimer from the double helix into the active site of the enzyme after which the cyclobutane ring is cleaved through a photocatalytic electron transfer process (36,37).

In the dissertation, photolyase is used for photoreversing CPDs in order to detect the presence of uracil resulting from the deamination of cytosine in a CPD, using UDG cleavage (Figure ***1.7***). Briefly, after UVB irradiation, the C-containing CPDs were allowed to deaminate for specific times at certain a temperature and pH condition. Then the CPDs were photo-reverted to non-dimerized ones containing C or U depending on the extent of deamination, by use of *E. coli* photolyase. Following that, the DNA was treated with *E. coli* UDG to release the U and generate an AP-site, which was then further treated with hot piperidine to lead to strand cleavages at AP-sites. Lastly, the ^{32}P-labeled cleavage products of different lengths were separated and visualized by gel electrophoresis.

T4-pdg locates and binds to pyrimidine dimers in dsDNA (ds, double strand DNA) due to locally perturbed structures. The enzyme then cleaves the N-glycosylic bond of the 5´ pyrimidine of the dimer with its glycosylase activity and then breaks the phosphodiester bond 3´ to the resulting AP-sites with its AP lyase activity (Figure ***1.8***) (38). T4-pdg is used in this dissertation for detection of *cis-syn* CPDs in dsDNA generated by UVB irradiation. Again, despite its AP lyase activity, hot piperidine treatment was applied after enzymatic degradation to ensure complete strand cleavage.

1.2.4 DNA packaging in chromatin

To compact the long DNA strands inside eukaryotic cells, genomic DNA is incorporated into chromatin in the nuclei. In a diploid human cell, 6 billion base pairs of DNA are packaged into 23 pairs of chromosomes (39). Given that each base stack is about 0.34 nm, the length of human DNA when extended would be 2 meters! Thanks to the histone proteins, chromosomal DNA can be condensed into the microscopic space of the nucleus (10 microns in diameter), resulting in a DNA-protein complex called chromatin. The condensation process is believed to involve several key steps as summarized in Figure ***1.9*** (39). First, the genomic DNA forms a "bead-on-a-string" structure by assembling with histones mainly via electrostatic interactions, resulting in a five- to ten-fold compaction of the DNA. In this process, the DNA wraps around histone octamers to form a string of nucleosome core particles (NCP), each of which has a cross-section diameter of about 11 nm. The H1 linker histone is attached to the entry and exit points of the nucleosomal DNA, acting like a "lock" to maintain the structure. The DNA between two adjacent nucleosome core particles is called the linker DNA, and varies in size between 20 to 60 bp. As demonstrated by high-resolution X-ray structural analysis, each nucleosome, which contains both the nucleosome core particle and the linker DNA, compacts around 200 bp of DNA into almost two left-handed

superhelical turns (40). In a second step, the poly-nucleosome string is folded into a "30-nm chromatin fiber" resulting in a net compaction of about 50-fold. This 30-nm fiber serves as a protofiber to produce coiled fibers of larger sizes in higher-order structures, which are eventually condensed into chromosomes.

Given the compact state of DNA in chromatin, one may wonder how replication and transcription machineries overcome barriers and access the individual strands of DNA. While the initiation of these processes in the context of chromatin is not fully understood, it is likely that chromatin remodeling plays a role in the spatial and temporal control of initiation of replication (41). During S phase of the cell division cycle when the entire genomic DNA is replicated, it is widely assumed that the chromatin is locally and transiently disassembled to free the DNA to allow for the passage of a replication fork (42).

Compaction of DNA into chromatin not only packages the genetic information, but also provides an additional level for the control of gene expression (43). Histone posttranslational modifications (PTMs), or commonly viewed as "histone epigenetic code", play a key role in transcription activation and silencing by regulating chromatin structure and accessibility (44-46). Histone modifications, including methylation, acetylation, phosphorylation and ubiquitination of basic amino acids (lysine and arginine), have the effect of altering the charge of the core histones and may thus influence chromatin structure through an electrostatic mechanism. Histone modifications also function by influencing the ability of regulatory complexes to come into contact with chromatin (45). For example, acetylation of Lys 14 in histone H3 can direct the binding of the ATP-dependent nucleosome-remodeling complex, thereby stimulating the gene activation (47).

In eukaryotic cells, there are two types of chromatin: heterochromatin and euchromatin. Heterochromatin is a tightly packed chromatin localized to nuclear envelope, characterized by hypoacetylation and hypomethylation of lysines 4 and 79 of histone H3 in *Saccharomyces cerevisiae* (48), and is silent in transcription. Euchromatin is a lightly packed chromatin with numerous PTMs and is often under active transcription. From the structural perspective, euchromatin is made of highly heterogeneous histones, whereas heterochromatin, in contrast, is made of highly homogeneous histones. This is also why chicken erythrocytes containing exclusively heterochromatin were chosen as the source of nucleosomal core particles in our study. Unlike mature human red blood cells that do not possess nuclei, evolution allows birds to keep their nuclei in mature red blood cells. The sole function of these cells is to transport oxygen with a protein called haemoglobin that was expressed in "precursor" red blood cells, and thus the mature red blood cells are not involved in active transcription. Therefore, in chicken erythrocytes, the chromatin is almost completely repressed heterochromatin that lacks modifications. Upon enzymatic digestion or physical fragmentation, heterochromatin produces very homogeneous nucleosome core particles, with which we carried out all experiments.

To prepare nucleosome core particles from chicken erythrocytes, we adopted a simplified protocol previously developed in Smerdon lab at Washington State University. In their original protocol, the whole procedure involves isolation of nuclei from chicken erythrocytes, chromatin digestion by Micrococcal Nuclease (MNase) to generate nucleosome, depletion of linker histone H1, purification of nucleosome core particles through ion-exchange and gel-filtration chromatography. The biggest disadvantage is that the overall procedure is extremely time consuming due to the tedious enzymatic digestion steps and resulting purification to remove MNase. In our simplified protocol, we replace the MNase digestion with physical fragmentation

by sonication so that no contaminant MNase is introduced in the purification step. As a result, the laborious gel-filtration step is omitted, and a great amount of time is saved by leaving out two rounds of enzymatic digestion. The nucleosome core particles prepared by the simplified method are obtained with quality and in high yields, and are stable for at least a year when stored at 4 ºC.

1.2.5 Nucleosome structure and DNA positioning

As the basic repeating unit of chromatin, a nucleosome core particle (NCP) is made of two parts: a histone octamer that is made of two copies of each of histones H2A, H2B, H3 and H4, as is shown in different colors in Figure ***1.10***, and a 147 bp DNA wrapping approximately 1.65 times around the octamer (49). The nucleosome core particle, or NCP, has a C2 symmetry axis called the dyad axis. Relative to the dyad axis, there are different superhelical locations (SHLs). Conventionally, the super helix on dyad axis is assigned as SHL 0. The superhelices to the 5'-side of DNA include SHL -1, -2, -3, so on and so forth, and to the 3'-side, negative numbers. On average, there are ten base pairs within each superhelix, each posing a unique rotation angle relative to the histone surface, and therefore, there are ten rotational positions (Figure ***1.11***) in each SHL. Again, the base pair on the dyad axis is numbered 0. The bases to the 5'-side are assigned negative numbers, and to the 3'-side, positive numbers. This numbering system for SHL and rotational positions will be repeatedly used throughout this dissertation.

All four core histones share a similar structural motif constructed from three α helices connected by two loops, denoted by α1-L1-α2-L2-α3. The histone octamer has a molecular weight of approximately 108 kDa, and is divided into four "histone-fold" dimers defined by H3-H4 and H2A-H2B histone pairs. In the assembly, two H3-H4 pairs interact through a 4-helix bundle and form a H3-H4 tetramer. Each H2A-H2B pair interacts with the tetramer through a second 4-helix bundle and form the histone octamer. The histone-fold regions of the H3–H4 tetramer bind to the

center of the DNA covering SHL - 3 to +3, whereas those of the H2A–H2B dimers bind from -6 to -3 and +3 to +6 (49).

Summarizing from the high-resolution crystal structure, five predominant histone-DNA interactions are observed (40): (1) electrostatic interactions between the positive charge generated by the histone helix dipole and the negative charge generated by the DNA phosphate backbone; (2) hydrogen-bonding between the DNA phosphates and the amide nitrogen atoms; (3) insertion or penetration of the arginine side chains from either the histone-folds or the histone tails into the DNA minor groove; (4) extensive non-polar contacts between the deoxyribose groups of the DNA and non-polar amino acid side chains; (5) frequent salt links between the DNA phosphate oxygen atoms and protein basic and hydroxyl side chain groups.

The binding affinity of DNA around histones and the nucleosome organization are highly sequence-dependent both *in vivo* and *in vitro (50,51)*. Several nucleosome positioning sequences in genomic DNA have been identified in the most stable nucleosomes, including TATA tetranucleotides and CA repeats (52). Artificial positioning sequences showing high binding affinities have also been utilized to incorporate DNA into rotationally phase nucleosomes, including TG motifs and "601 Widom DNA sequences" (53,54). The TG motif, $(A/T)_3NN(G/C)_3NN$, is widely used for its superior ability to rotationally phase nucleosomes *in vitro*. The ten nucleotides make up one full nucleosomal helical turn, with the major groove of the G·C base pairs preferentially facing the histone octamer surface, which is consistent with its tendency to bend into the major groove. In contrast, the minor groove of the A·T base pairs has a strong preference for facing the histone octamer surface, which is consistent with its tendency to bend into the minor groove. In the dissertation, all nucleosomal binding sequences were designed based on TG bending motifs.

To determine the rotational positioning of nucleosomes, both chemical and enzymatic approaches have been developed, among which, DNase I mapping and hydroxyl radical footprinting are the two most widely used techniques (55-57). Both methods show a cleavage preference for outward-facing sugar phosphate backbones, though hydroxyl radicals exhibit much less sequence specificity and thus can probe the DNA backbone at a single nucleotide level (58,59).

In this dissertation, we adopted hydroxyl radical footprinting technique to probe the rotational phasing of reconstituted nucleosomes. The hydroxyl radicals can be easily generated by the Fenton chemistry: $[Fe(EDTA)]^{2-} + H_2O_2 \rightarrow [Fe(EDTA)]^{-} + \bullet OH + OH^{-}$, and are believed to mainly attack the hydrogen at the C5'-position (H-5') of the sugar ring of DNA, and 2- to 5-fold less at other sugar sites in the order of C4' > C3' > C2'> C1' (60). In the proposed H-5' abstraction pathway, the principle cleavage products include a nucleotide 3'-phosphate and a nucleotide 5'-aldehyde, as shown in Figure ***1.12*** (61,62). When nucleosomal DNA is exposed to hydroxyl radical, the outward-facing backbones are more accessible to attack compared with inward-facing ones, resulting in darker bands on a DNA sequencing gel. Since the rotational position of the nucleotides is repeated every 10-11 bp, the hydroxyl radical cleavage pattern of nucleosomal DNA is characterized by a pronounced 10-11 bp periodicity (Figure ***1.13***).

1.3 Dissertation overview

Previous studies in our group found that UV preferably induces the formation of CPDs in nucleosome at sites where the phosphodiester bond is positioned away from the histone surface and DNA bending is towards the major groove (Figure ***1.14***) (63,64). The broadly accepted explanation for this preference is that the outward-facing region has a higher decompression and rotational flexibility that allow the adjacent pyrimidines additional freedom to adopt a more

favorable photoreactive conformation for forming CPDs. The formation of CPDs causes a 7-9º structural distortion onto the DNA, the outward-facing positions can accommodate this distortion better than the inward-facing region, where the DNA conformation is more compressed and rigid. In these studies, however, only ten rotational positions on the dyad superhelix were examined, little is known about the CPD formation as a function of other SHLs and rotational positions. The goal of this dissertation is to systematically study the structural effect of nucleosome structure on CPD formation at every superhelical and rotational positions. In Chapter 2, we developed a system for studying CPD photoproduct formation and properties in any given sequence context at any superhelical location in a rotationally phased nucleosome. This enabled us to investigate: CPD frequency as a function of translational and rotational positions; nucleosome binding affinities; temperature effects on nucleosome stabilities.

Using a protein-free DNA loop, Pehrson and coworkers observed a 10-11 bp periodicity in CPD formation similar to that in heterogeneous DNA, implying that bending, not protein-DNA interactions are the primary cause of the modulation of photoproduct formation (65). However, the exact shape, curvature, and rotational phasing of the DNA loop is unknown, therefore cannot be directly correlated with nucleosomal DNA. In Chapter 3, we developed a DNA minicircle system for determining the extent to which DNA bending might play a role in CPD formation in nucleosomes. Using this system, we were able to conclude that dominant factor in determining CPD formation frequency in a nucleosome was DNA curvature, rather than DNA-histone interactions.

Previously, Dr. Cannistraro in our group found that there were several factors that can affect C or ^{m}C deamination rates, including salt concentration, temperature and sequence context (Figure ***1.15***) (25). For example, the deamination rate of T=^{m}C CPDs is appoximately 25-fold

faster when flanked directly by G's than by A's, T's or C's on the 3'-side, probably owing to catalysis by the O6 group of guanine. Dr. Song in our group investigated the deamination rates of CPDs at T^{m}CG sites in the context of nucleosomes and found that deamination was greatly enhanced for outermost CPDs (63,64). Again, these studies are limited to the ten rotational positions on the dyad superhelix. What's more, sequences of other contexts were not studied. In Chapter 4, we expanded the investigation to two other sequence contexts (CT=CT and TC=TC) by incorporating a poly $(TC)_n$ tracts into nucleosomes. By varying the length of TC-tracts, we were able to study more SHLs and rotational positions, and found that nucleosome structure modulates CPD deamination at all nucleosomal positions.

Finally, Chapter 5 summarizes the conclusions of this study, and proposes future research.

1.4 References

1. Guy Jr, G.P., Thomas, C.C., Thompson, T., Watson, M., Massetti, G.M., Richardson, L.C., Control, C.f.D. and Prevention. (2015) Vital signs: melanoma incidence and mortality trends and projections—United States, 1982–2030. *MMWR Morb Mortal Wkly Rep*, **64**, 591-596.

2. Stern, R.S. (2010) Prevalence of a history of skin cancer in 2007: results of an incidence-based model. *Archives of Dermatology*, **146**, 279-282.

3. Rogers, H.W., Weinstock, M.A., Feldman, S.R. and Coldiron, B.M. (2015) Incidence estimate of nonmelanoma skin cancer (keratinocyte carcinomas) in the US population, 2012. *JAMA Dermatology*, **151**, 1081-1086.

4. Siegel, R.L., Miller, K.D. and Jemal, A. (2017) Cancer statistics, 2017. *CA: A Cancer Journal for Clinicians*, **67**, 7-30.

5. Woodhead, A.D., Setlow, R.B. and Tanaka, M. (1999) Environmental factors in nonmelanoma and melanoma skin cancer. *Journal of Epidemiology*, **9**, 102-114.

6. Hussein, M.R. (2005) Ultraviolet radiation and skin cancer: molecular mechanisms. *Journal of Cutaneous Pathology*, **32**, 191-205.

7. Diffey, B.L. (2002) Sources and measurement of ultraviolet radiation. *Methods*, **28**, 4-13.

8. Setlow, R.B. (1974) The wavelengths in sunlight effective in producing skin cancer: a theoretical analysis. *Proceedings of the National Academy of Sciences*, **71**, 3363-3366.

9. Besaratinia, A., Yoon, J.-i., Schroeder, C., Bradforth, S.E., Cockburn, M. and Pfeifer, G.P. (2011) Wavelength dependence of ultraviolet radiation-induced DNA damage as determined by laser irradiation suggests that cyclobutane pyrimidine dimers are the principal DNA lesions produced by terrestrial sunlight. *The FASEB Journal*, **25**, 3079-3091.

10. Yoon, J.-H., Lee, C.-S., O'Connor, T.R., Yasui, A. and Pfeifer, G.P. (2000) The DNA damage spectrum produced by simulated sunlight. *Journal of Molecular Biology*, **299**, 681-693.

11. MITCHELL, D.L. and NAIRN, R.S. (1989) The biology of the (6–4) photoproduct. *Photochemistry and Photobiology*, **49**, 805-819.

12. Douki, T., Reynaud-Angelin, A., Cadet, J. and Sage, E. (2003) Bipyrimidine photoproducts rather than oxidative lesions are the main type of DNA damage involved in the genotoxic effect of solar UVA radiation. *Biochemistry*, **42**, 9221-9226.

13. Rochette, P.J., Therrien, J.P., Drouin, R., Perdiz, D., Bastien, N., Drobetsky, E.A. and Sage, E. (2003) UVA - induced cyclobutane pyrimidine dimers form predominantly at thymine – thymine dipyrimidines and correlate with the mutation spectrum in rodent cells. *Nucleic Acids Research*, **31**, 2786-2794.

14. Besaratinia, A., Synold, T.W., Chen, H.-H., Chang, C., Xi, B., Riggs, A.D. and Pfeifer, G.P. (2005) DNA lesions induced by UV A1 and B radiation in human cells: comparative analyses in the overall genome and in the p53 tumor suppressor gene. *Proceedings of the National Academy of Sciences of the United States of America*, **102**, 10058-10063.

15. Mouret, S., Baudouin, C., Charveron, M., Favier, A., Cadet, J. and Douki, T. (2006) Cyclobutane pyrimidine dimers are predominant DNA lesions in whole human skin exposed to UVA radiation. *Proceedings of the National Academy of Sciences*, **103**, 13765-13770.

16. Kielbassa, C., Roza, L. and Epe, B. (1997) Wavelength dependence of oxidative DNA damage induced by UV and visible light. *Carcinogenesis*, **18**, 811-816.

17. Wang, C.-I. and Taylor, J.-S. (1991) Site-specific effect of thymine dimer formation on dAn. dTn tract bending and its biological implications. *Proceedings of the National Academy of Sciences*, **88**, 9072-9076.

18. Kim, J.K., Patel, D. and Choi, B.S. (1995) Contrasting structural impacts induced by cis - syn cyclobutane dimer and (6–4) adduct in DNA duplex decamers: implication in mutagenesis and repair activity. *Photochemistry and Photobiology*, **62**, 44-50.

19. Iwai, S. (2008) Pyrimidine dimers: UV‐induced DNA damage. *Modified Nucleosides: in Biochemistry, Biotechnology and Medicine*, 97-131.

20. Cadet, J., Sage, E. and Douki, T. (2005) Ultraviolet radiation-mediated damage to cellular DNA. *Mutation Research/Fundamental and Molecular Mechanisms of Mutagenesis*, **571**, 3-17.

21. Yamamoto, J., Nishiguchi, K., Manabe, K., Masutani, C., Hanaoka, F. and Iwai, S. (2010) Photosensitized [2+ 2] cycloaddition of N-acetylated cytosine affords stereoselective formation of cyclobutane pyrimidine dimer. *Nucleic Acids Research*, **39**, 1165-1175.

22. Ziegler, A., Leffell, D.J., Kunala, S., Sharma, H.W., Gailani, M., Simon, J.A., Halperin, A.J., Baden, H.P., Shapiro, P.E. and Bale, A.E. (1993) Mutation hotspots due to sunlight in the p53 gene of nonmelanoma skin cancers. *Proceedings of the National Academy of Sciences*, **90**, 4216-4220.

23. Jiang, N. and Taylor, J.S. (1993) In vivo evidence that UV-induced C. fwdarw. T mutations at dipyrimidine sites could result from the replicative bypass of cis-syn cyclobutane dimers or their deamination products. *Biochemistry*, **32**, 472-481.

24. Danilov, V., Les, A. and Alderfer, J. (2001) A theoretical study of the cis-syn pyrimidine dimers in the gas phase and water cluster and a tautomer-bypass mechanism for the origin of UV-induced mutations. *Journal of Biomolecular Structure and Dynamics*, **19**, 179-191.

25. Cannistraro, V.J. and Taylor, J.-S. (2009) Acceleration of 5-methylcytosine deamination in cyclobutane dimers by G and its implications for UV-induced C-to-T mutation hotspots. *Journal of Molecular Biology*, **392**, 1145-1157.

26. Song, Q., Sherrer, S.M., Suo, Z. and Taylor, J.-S. (2012) Preparation of site-specific T= mCG cis-syn cyclobutane dimer-containing template and its error-free bypass by yeast and human polymerase η. *Journal of Biological Chemistry*, **287**, 8021-8028.

27. Tu, Y., Dammann, R. and Pfeifer, G.P. (1998) Sequence and time-dependent deamination of cytosine bases in UVB-induced cyclobutane pyrimidine dimers in vivo. *Journal of Molecular Biology*, **284**, 297-311.

28. Barak, Y., Cohen-Fix, O. and Livneh, Z. (1995) Deamination of Cytosine-containing Pyrimidine Photodimers in UV-irradiated DNA SIGNIFICANCE FOR UV LIGHT MUTAGENESIS. *Journal of Biological Chemistry*, **270**, 24174-24179.

29. Krämer, M., Stein, S., Mai, S., Kunz, E., König, H., Loferer, H., Grunicke, H., Ponta, H., Herrlich, P. and Rahmsdorf, H. (1990) Radiation-induced activation of transcription factors in mammalian cells. *Radiation and Environmental Biophysics*, **29**, 303-313.

30. Daya-Grosjean, L., Dumaz, N. and Sarasin, A. (1995) The specificity of p53 mutation spectra in sunlight induced human cancers. *Journal of Photochemistry and Photobiology B: Biology*, **28**, 115-124.

31. Hussein, M.R.A.-E. and Wood, G.S. (2002) Molecular aspects of melanocytic dysplastic nevi. *The Journal of Molecular Diagnostics*, **4**, 71-80.

32. Levine, A.J., Momand, J. and Finlay, C.A. (1991) The p53 tumour supressor gene. *Nature*, **351**, 453.

33. Sancar, A. (1995) DNA repair in humans. *Annual Review of Genetics*, **29**, 69-105.

34. Kim, S.T., Malhotra, K., Smith, C.A., Taylor, J.S. and Sancar, A. (1993) DNA photolyase repairs the trans-syn cyclobutane thymine dimer. *Biochemistry*, **32**, 7065-7068.

35. Smith, C.A. and Taylor, J.-S. (1993) Preparation and characterization of a set of deoxyoligonucleotide 49-mers containing site-specific cis-syn, trans-syn-I,(6-4), and Dewar photoproducts of thymidylyl (3'--> 5')-thymidine. *Journal of Biological Chemistry*, **268**, 11143-11151.

36. Mees, A., Klar, T., Gnau, P., Hennecke, U., Eker, A.P., Carell, T. and Essen, L.-O. (2004) Crystal structure of a photolyase bound to a CPD-like DNA lesion after in situ repair. *Science*, **306**, 1789-1793.

37. Carell, T., Burgdorf, L.T., Kundu, L.M. and Cichon, M. (2001) The mechanism of action of DNA photolyases. *Current Opinion in Chemical Biology*, **5**, 491-498.

38. Hoffman, L. (1996), *Epicentre Forum*, **3**, 4.

39. Annunziato, A. (2008) DNA packaging: nucleosomes and chromatin. *Nature Education*, **1**, 26.

40. Luger, K., Mader, A.W., Richmond, R.K., Sargent, D.F. and Richmond, T.J. (1997) Crystal structure of the nucleosome core particle at 2.8 angstrom resolution. *Nature*, **389**, 251.

41. Demeret, C., Vassetzky, Y. and Mechali, M. (2001) Chromatin remodelling and DNA replication: from nucleosomes to loop domains. *Oncogene*, **20**, 3086.

42. Krude, T. (1995) Chromatin: Nucleosome assembly during DNA replication. *Current Biology*, **5**, 1232-1234.

43. Wade, P.A., Jones, P.L., Vermaak, D. and Wolffe, A.P. (1998) A multiple subunit Mi-2 histone deacetylase from Xenopus laevis cofractionates with an associated Snf2 superfamily ATPase. *Current Biology*, **8**, 843-848.

44. Jenuwein, T. and Allis, C.D. (2001) Translating the histone code. *Science*, **293**, 1074-1080.

45. Zhang, L., Eugeni, E.E., Parthun, M.R. and Freitas, M.A. (2003) Identification of novel histone post-translational modifications by peptide mass fingerprinting. *Chromosoma*, **112**, 77-86.

46. Strahl, B.D. and Allis, C.D. (2000) The language of covalent histone modifications. *Nature*, **403**, 41.

47. Kasten, M., Szerlong, H., Erdjument‐Bromage, H., Tempst, P., Werner, M. and Cairns, B.R. (2004) Tandem bromodomains in the chromatin remodeler RSC recognize acetylated histone H3 Lys14. *The EMBO Journal*, **23**, 1348-1359.

48. Katan‐Khaykovich, Y. and Struhl, K. (2005) Heterochromatin formation involves changes in histone modifications over multiple cell generations. *The EMBO Journal*, **24**, 2138-2149.

49. Luger, K., Mäder, A.W., Richmond, R.K., Sargent, D.F. and Richmond, T.J. (1997) Crystal structure of the nucleosome core particle at 2.8 Å resolution. *Nature*, **389**, 251-260.

50. Stein, A., Takasuka, T.E. and Collings, C.K. (2009) Are nucleosome positions in vivo primarily determined by histone–DNA sequence preferences? *Nucleic Acids Research*, **38**, 709-719.

51. Zhang, Y., Moqtaderi, Z., Rattner, B.P., Euskirchen, G., Snyder, M., Kadonaga, J.T., Liu, X.S. and Struhl, K. (2009) Intrinsic histone-DNA interactions are not the major determinant of nucleosome positions in vivo. *Nature Structural & Molecular Biology*, **16**, 847-852.

52. Widlund, H.R., Cao, H., Simonsson, S., Magnusson, E., Simonsson, T., Nielsen, P.E., Kahn, J.D., Crothers, D.M. and Kubista, M. (1997) Identification and characterization of genomic nucleosome-positioning sequences. *Journal of Molecular Biology*, **267**, 807-817.

53. Shrader, T.E. and Crothers, D.M. (1989) Artificial nucleosome positioning sequences. *Proceedings of the National Academy of Sciences*, **86**, 7418-7422.

54. Lowary, P. and Widom, J. (1998) New DNA sequence rules for high affinity binding to histone octamer and sequence-directed nucleosome positioning. *Journal of Molecular Biology*, **276**, 19-42.

55. Vitolo, J.M., Thiriet, C. and Hayes, J.J. (2001) DNase I and hydroxyl radical characterization of chromatin complexes. *Current Protocols in Molecular Biology*, 21.24. 21-21.24. 29.

56. Ober, M. and Lippard, S.J. (2007) Cisplatin damage overrides the predefined rotational setting of positioned nucleosomes. *Journal of the American Chemical Society*, **129**, 6278-6286.

57. Hampshire, A.J., Rusling, D.A., Broughton-Head, V.J. and Fox, K.R. (2007) Footprinting: a method for determining the sequence selectivity, affinity and kinetics of DNA-binding ligands. *Methods*, **42**, 128-140.

58. Tullius, T.D. and Dombroski, B.A. (1986) Hydroxyl radical" footprinting": high-resolution information about DNA-protein contacts and application to lambda repressor and Cro protein. *Proceedings of the National Academy of Sciences*, **83**, 5469-5473.

59. Tullius, T. (1988) DNA footprinting with hydroxyl radical. *Nature*, **332**, 663-664.

60. Balasubramanian, B., Pogozelski, W.K. and Tullius, T.D. (1998) DNA strand breaking by the hydroxyl radical is governed by the accessible surface areas of the hydrogen atoms of the DNA backbone. *Proceedings of the National Academy of Sciences*, **95**, 9738-9743.

61. Pogozelski, W.K. and Tullius, T.D. (1998) Oxidative strand scission of nucleic acids: routes initiated by hydrogen abstraction from the sugar moiety. *Chemical reviews*, **98**, 1089-1108.

62. Jain, S.S. and Tullius, T.D. (2008) Footprinting protein-DNA complexes using the hydroxyl radical. *Nature Protocols*, **3**, 1092.

63. Song, Q., Cannistraro, V.J. and Taylor, J.-S. (2014) Synergistic modulation of cyclobutane pyrimidine dimer photoproduct formation and deamination at a TmCG site over a full helical DNA turn in a nucleosome core particle. *Nucleic Acids Research*, **42**, 13122-13133.

64. Song, Q., Cannistraro, V.J. and Taylor, J.-S. (2011) Rotational position of a 5-methylcytosine-containing cyclobutane pyrimidine dimer in a nucleosome greatly affects its deamination rate. *Journal of Biological Chemistry*, **286**, 6329-6335.

65. Pehrson, J.R. and Cohen, L.H. (1992) Effects of DNA looping on pyrimidine dimer formation. *Nucleic Acids Research*, **20**, 1321-1324.

66. Biswas, M., Voltz, K., Smith, J.C. and Langowski, J. (2011) Role of histone tails in structural stability of the nucleosome. *PLoS Computational Biology*, **7**, e1002279.

1.5 Figures

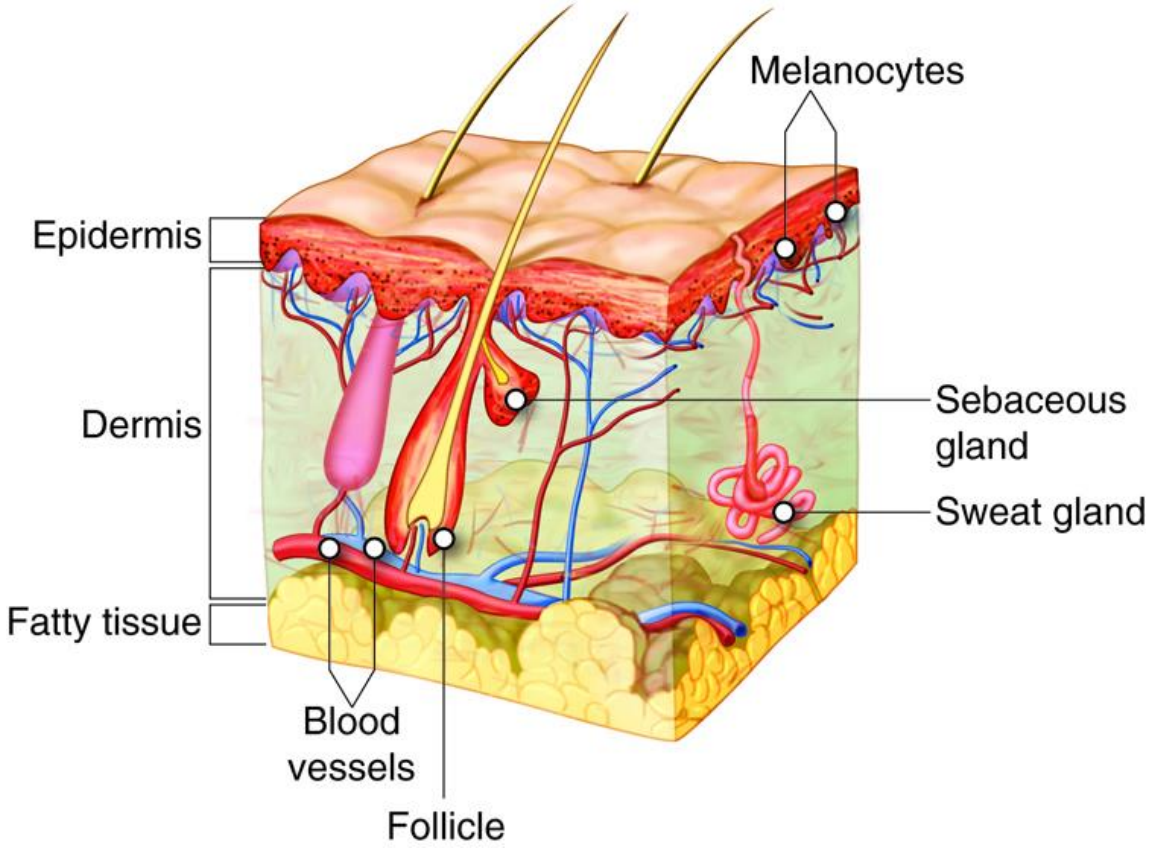

Figure 1.1: Structure of the skin.

*This figure is from an online course: Open Learning Initiative Introduction to Anatomy and Physiology (http://www.savingstudentsmoney.org/OLI/AnPpost.html)

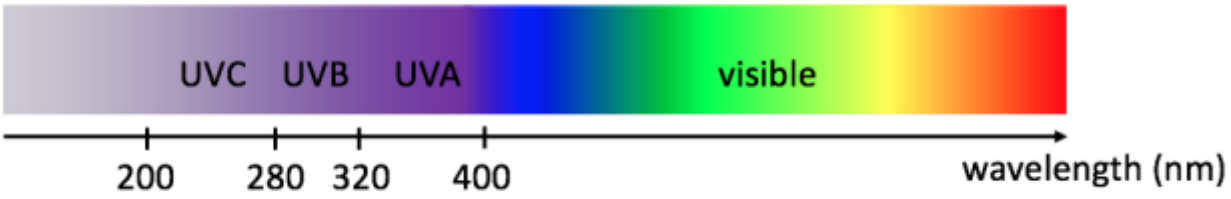

Figure 1.2: UV/Vis spectrum.

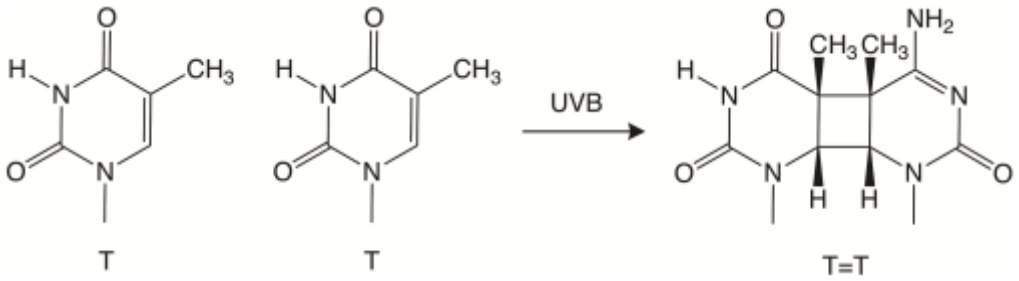

Figure 1.3: Formation of T=T CPD at a dipyrimidine site via [2+2] cycloaddition.

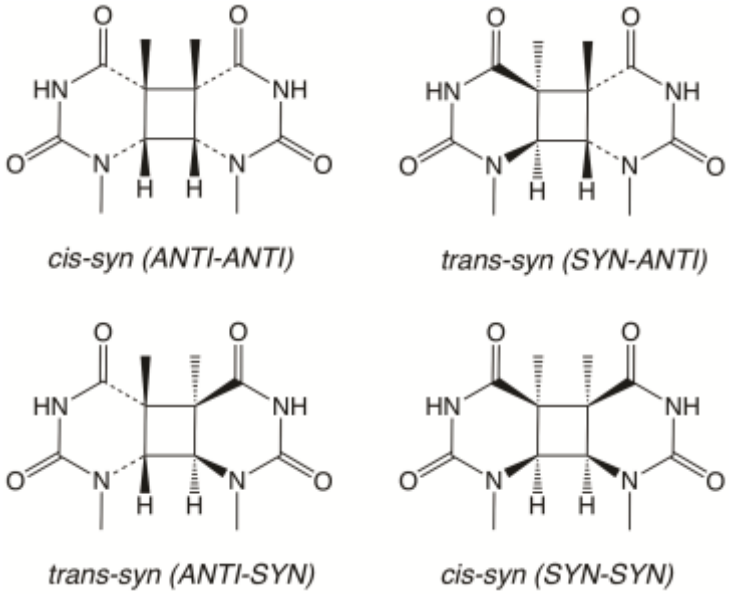

Figure 1.4: Four possible structures of *syn*-CPDs formed between adjacent thymine bases viewed according to their glycosyl conformation. The conformations around the *N*-glycosidic bond of the 5′- and 3′-components are shown in parentheses next to the CPD structures.

*This figure is adapted from Ref. (21).

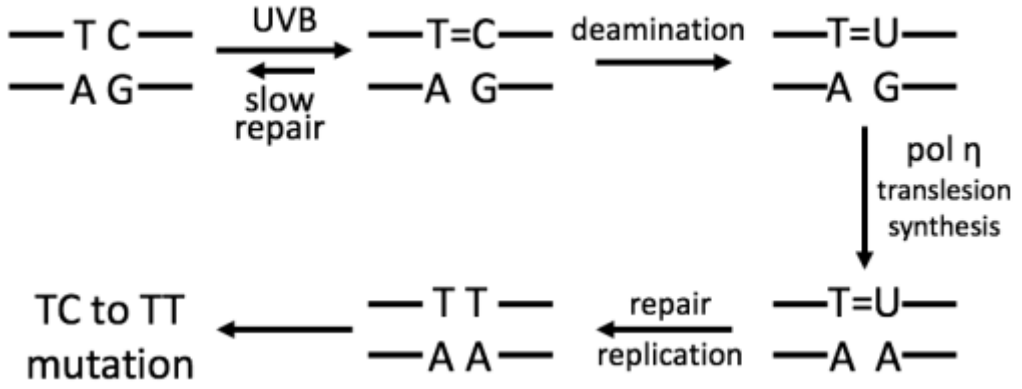

Figure 1.5: Origin of C-to-T or CC-to-TT mutations from CPD deamination and/or translesion synthesis.

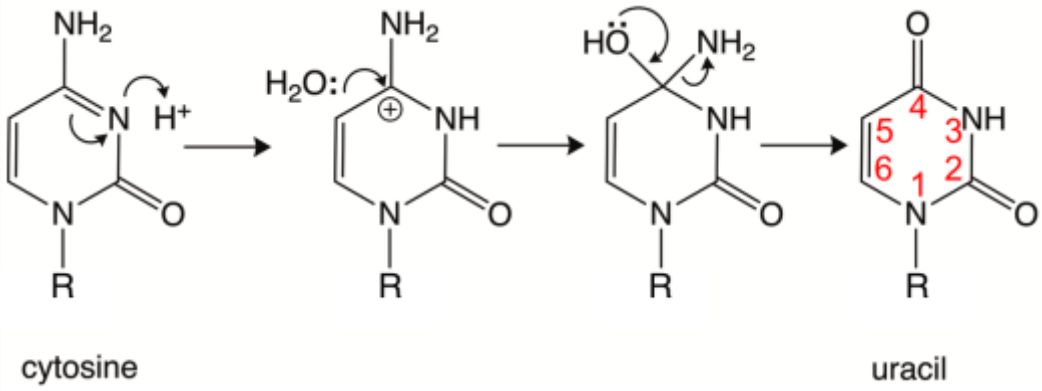

Figure 1.6: Deamination of cytosine into uracil in a T=C CPD.

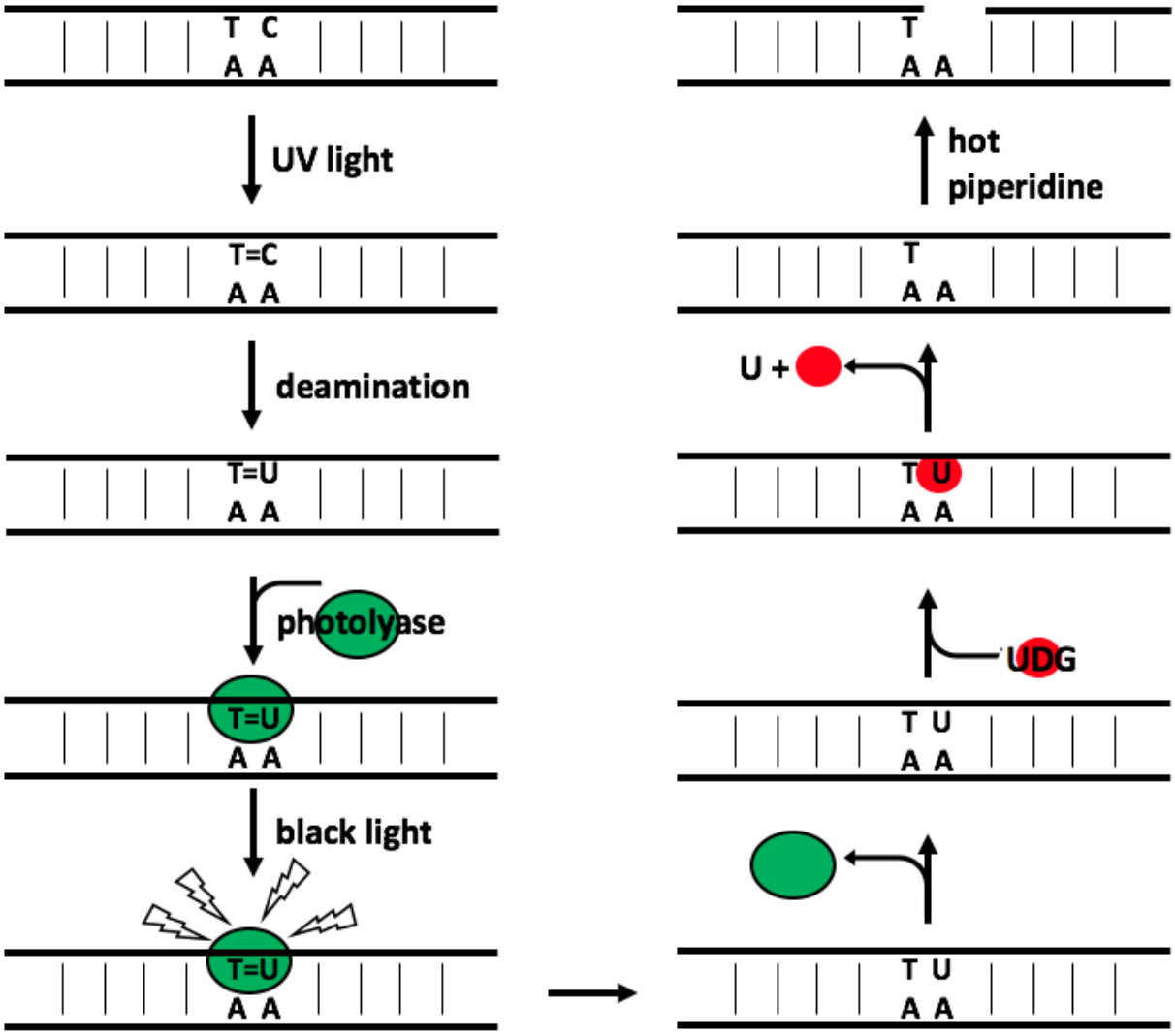

Figure 1.7: Detection of T=C CPD deamination sites by photolyase and DNA-uracil glycosylase. The deaminated (and undeaminated) CPDs are reverted by photolyase (green) under black light. DNA-uracil glycosylase (UDG) (red) catalyzes the release of free uracil from uracil-containing DNA, resulting in an abasic site (AP-site). Heating in basic buffer condition leads to the strand cleavage at AP-sites, which can then be determined by gel electrophoresis.

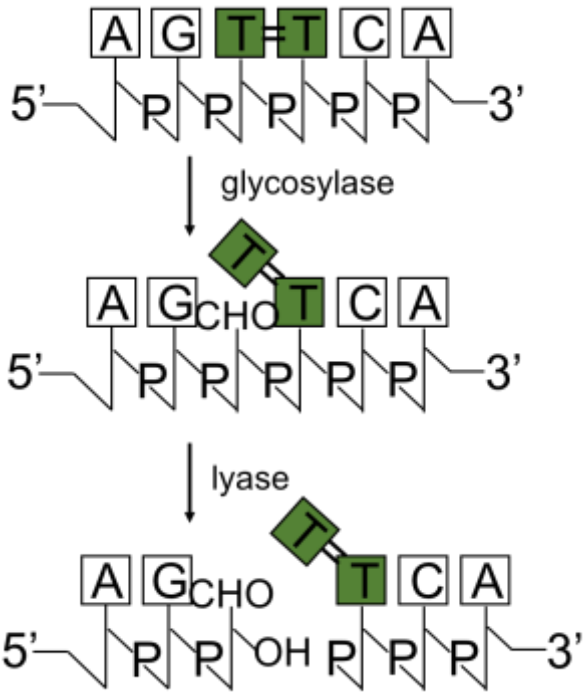

Figure 1.8: Mechanism of pyrimidine dimer cleavage by T4-pdg.

*The figure is adapted from Ref. (38).

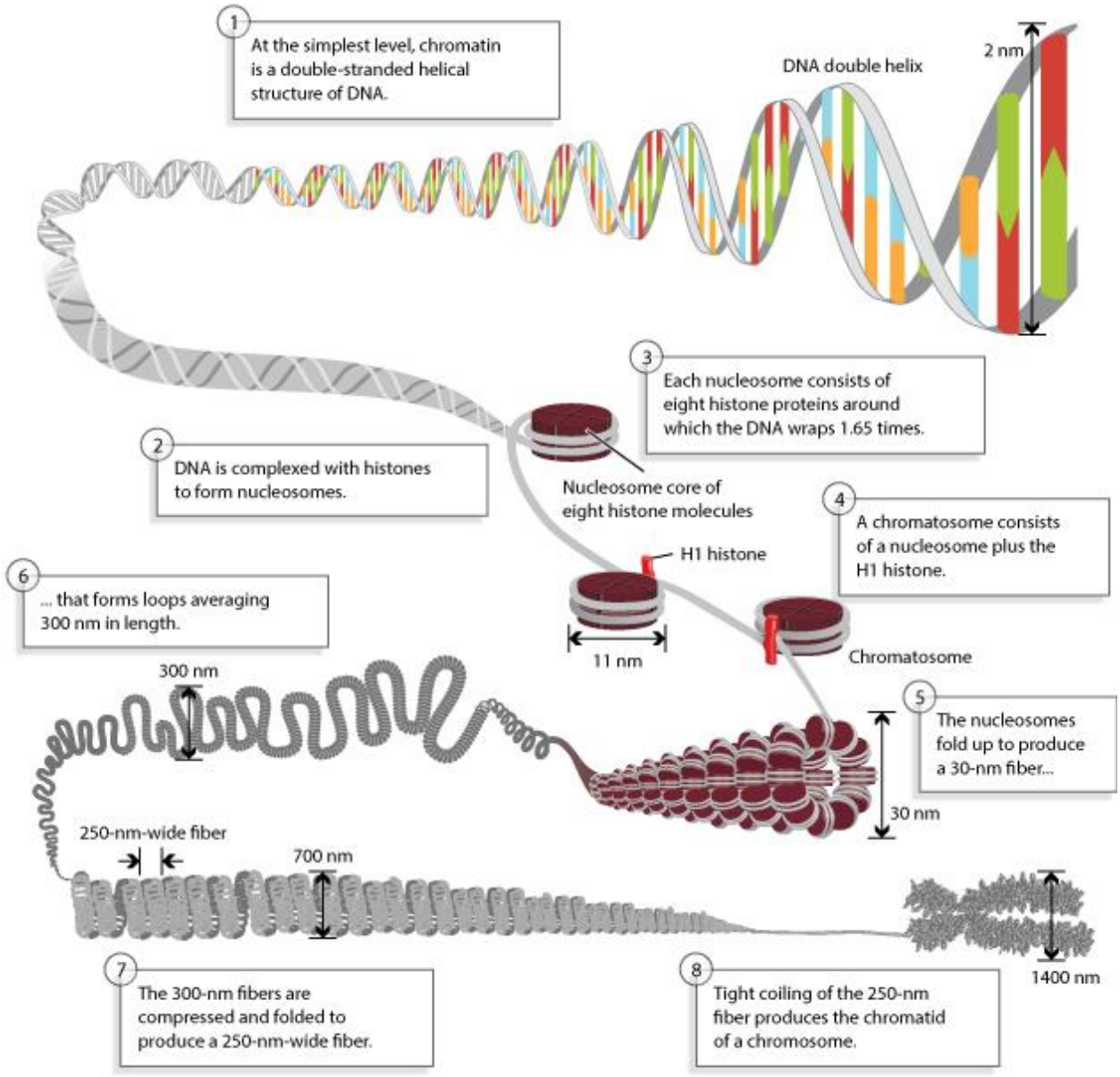

Figure 1.9: Chromosomes are composed of DNA tightly-wound around histones. Eukaryotic DNA is packaged inside microscopic nuclei with the help of histones. Nucleosomes fold up to form a 30-nanometer chromatin fiber, which serves as a protofiber to produce coiled fibers of larger sizes to form higher-order structures.

*This figure is taken from Ref. (39).

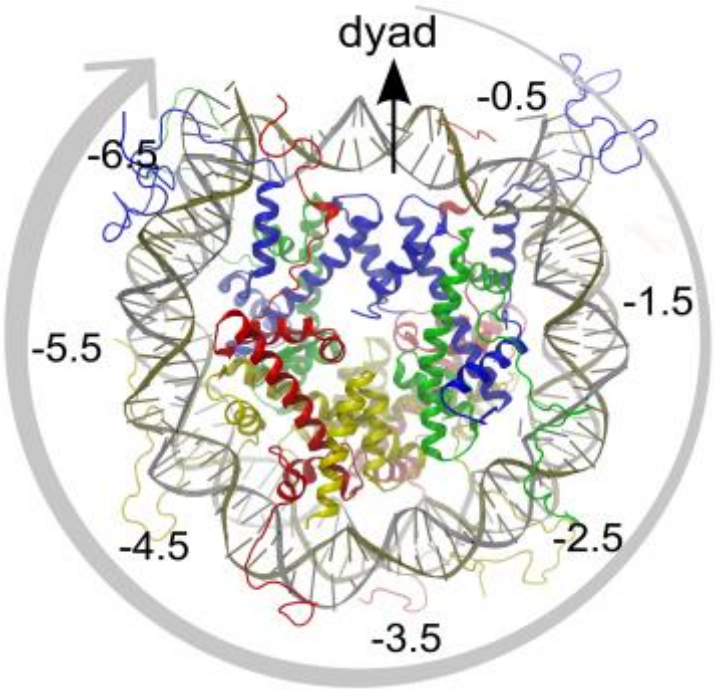

Figure 1.10: Structure of a nucleosome core particle and positions of superhelical locations. A nucleosome core particle is made of a 147bp DNA and a histone octamer core which contains two copies of each of H2A (yellow), H2B (red), H3 (blue) and H4 (green). The structure has a C2 symmetry axis called dyad axis. Superhelical locations (SHL) are the different locations of superhelices relative the dyad axis. The superhelix on the dyad is assigned as SHL0. The SHLs 5'-to the dyad axis are assigned negative numbers.

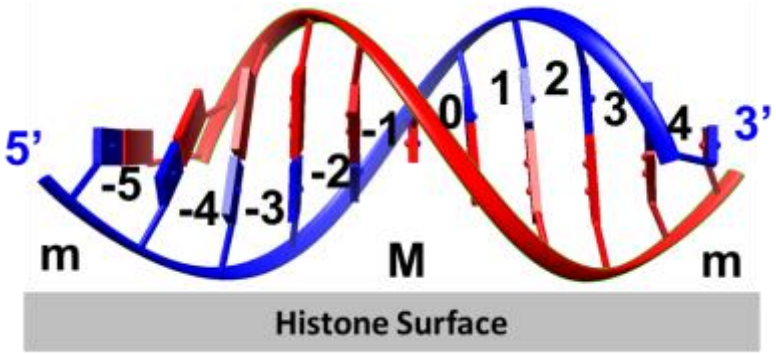

Figure 1.11: Rotational positions within each superhelix on nucleosomes. On average, there are ten bases in a superhelix, each having a unique rotating angle relative to the histone surface. The base on the dyad is assigned as 0. The bases 5'-to the dyad axis are assigned negative numbers.

*The top figure is taken from Ref. (66).

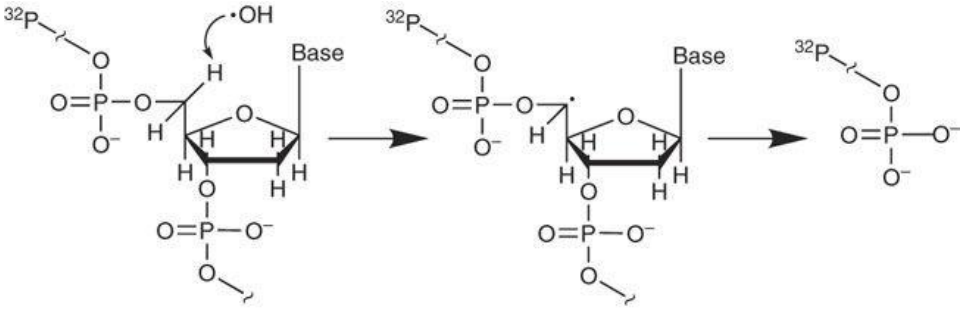

Figure 1.12: Proposed hydrogen abstraction at C5'-position pathway for DNA strand cleavage. The major reaction of the hydroxyl radical with the DNA backbone is to abstract a deoxyribose 5'-hydrogen atom, leading to the formation of a free radical intermediate, which reacts with oxygen and eventually undergoes backbone cleavage to form products. Only the radio-labeled product (oligonucleotide 3'-phosphate) is shown. The other cleavage product is oligonucleotide 5'-aldehyde.

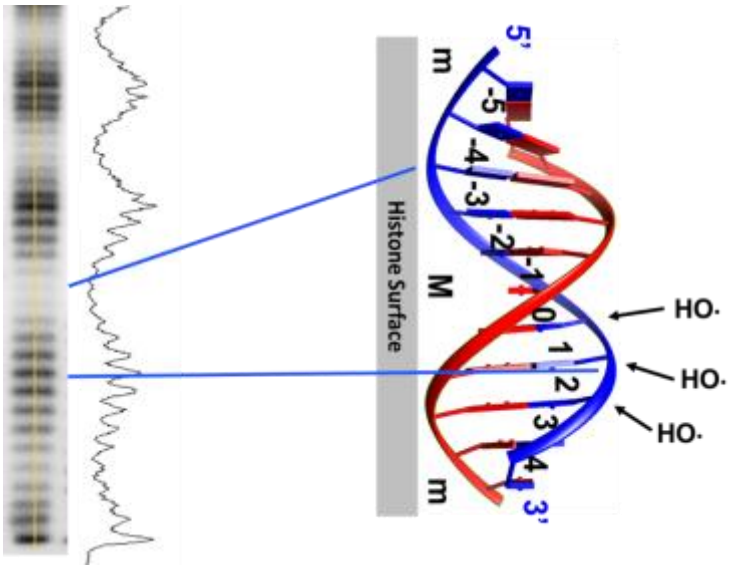

Figure 1.13: Hydroxyl radical footprinting pattern of nucleosomal DNA. The outside facing positions are more accessible to attack compared with inside facing positions, resulting in a darker band on a DNA sequencing gel. A pronounced 10-11 bp periodicity is observed.

*The top figure is taken from Ref. (62)

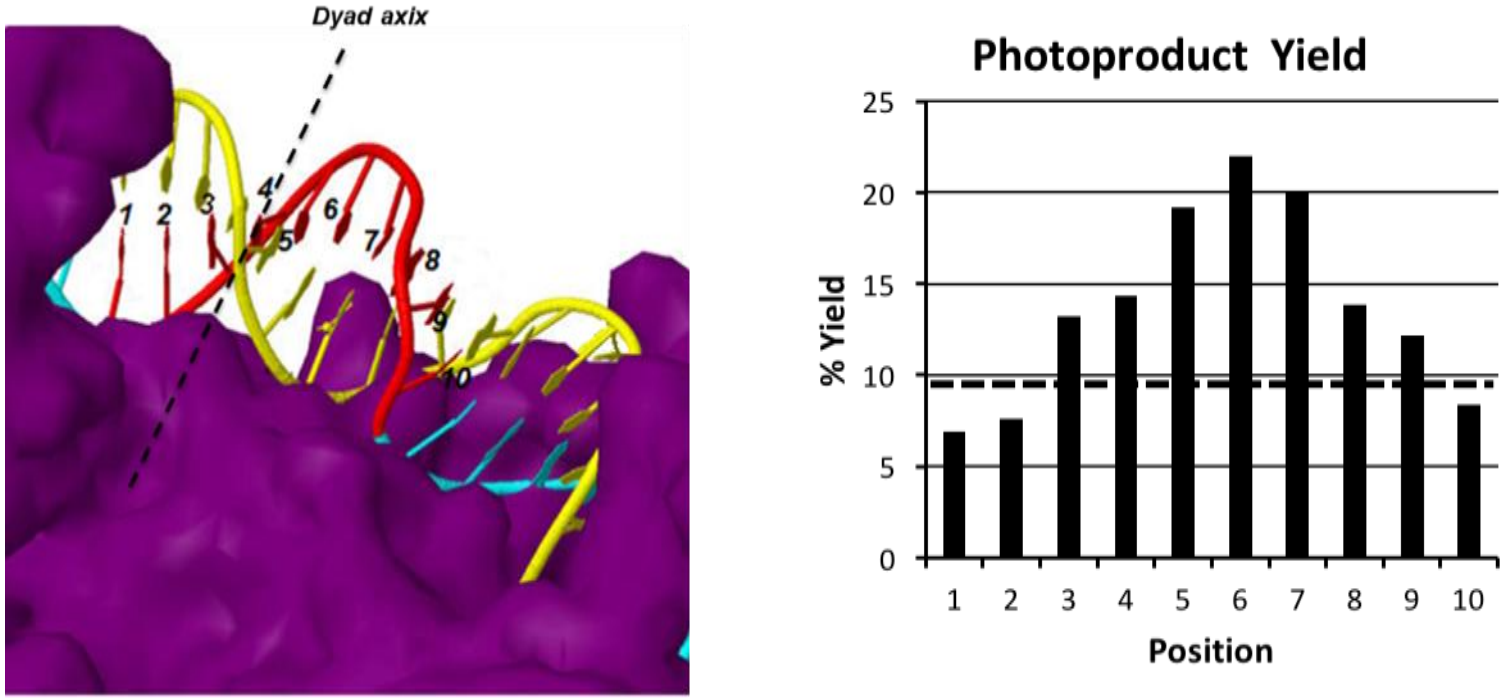

Figure 1.14: The rotational position of a T^{m}CG site in a full turn of nucleosome at the dyad axis greatly affects the rate of CPD formation. Left: Rotational positions of the ^{m}C of the T^{m}CG sites in the nucleosome. Right: Bar graph of TmC CPD yield at each rotational position compared to that in free DNA (dashed line).

*This figure is taken from Ref. (63)

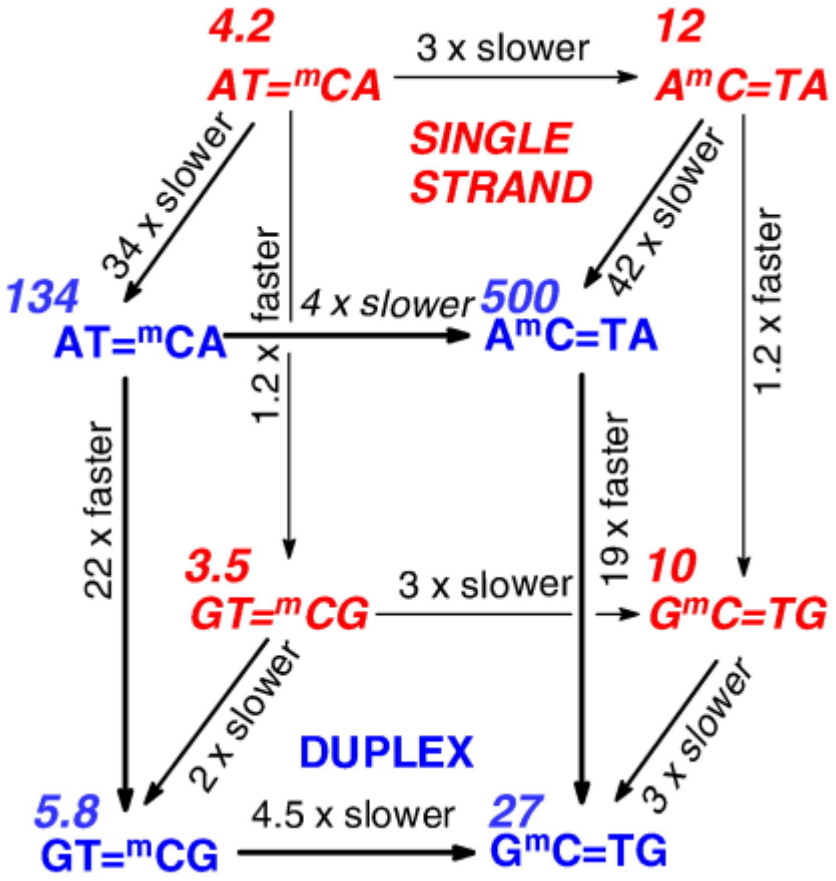

Figure 1.15: Effects of sequence context and duplex formation on deamination rates. Sequences in italic and red on the back face of the cube refer to the single stranded form. Sequences in bold and blue on the front face of the cube refer to the double stranded form. Numbers in italics are the deamination half-lives in hours.

*This figure is taken from Ref. (25)

Chapter 2 Effects of Rotational and Translational Position on T=T CPD Formation in a T_{11}-Tract in a Nucleosome [1]

2.1 Introduction

It is well established that DNA photoproducts produced by sunlight are responsible for the majority of the mutations associated with skin cancers (1-4). What is not so well established is the physical or mechanistic origin of the variation in mutation type and frequency within a gene, which must result from a complex interplay between the frequency of photoproduct formation, chemical transformation, repair, and translesion synthesis. To begin to dissect the various contributions of these factors, we have been examining the role of chromatin structure on DNA photoproduct formation.

The original studies of CPD modulation by nucleosomes were carried out with nucleosomes containing mixed-sequence DNA obtained from the degradation of chromatin. Such sequences may be biased to bend around the nucleosome and obscure the relationship between sequence, rotational position and CPD formation. In a study of 254 nm induced CPD formation in nucleosome-bound 5S rRNA gene with a defined sequence, a less than 2-fold modulation of CPD formation could be detected only after carefully subtracting the CPD pattern produced in free DNA (5). In contrast, HISAT DNA containing various length T-tracts showed strong modulation of CPD formation, but with maxima that were shifted to the 5'-side of what was observed with mixed sequence nucleosomal DNA (6). A more recent study measuring rates of CPD formation and

[1] All contents in this chapter have been published in Wang K and Taylor JS. Modulation of Cyclobutane Thymine Photodimer Formation in T_{11}-Tracts in Rotationally Phased Nucleosome Core Particles and DNA Minicircles. Nucleic Acids Res (2017) 45 (12): 7031-7041.

photostationary state levels induced by 254 nm light concluded that there was no modulation of photoproduct formation in 5S and Widom 601 defined sequence DNAs (7). In contrast, UVB-induced CPD formation of TCG CPDs at every rotational position in a full turn of DNA at the dyad axis of a rotationally phased artificial DNA sequence was modulated in a similar way to what was observed with mixed-sequence DNA.

To investigate the modulation of CPD formation by nucleosomes, we have first chosen to develop methodology to study CPD formation at different translational positions in a nucleosome (Figure ***2.1***). A T_{11}-tract was chosen as a model system for study because it contains all 10 possible CPD sites in a full turn of DNA. To hold the T_{11}-tract in a single rotational orientation in a nucleosome, we have made use of TG bending motifs $(T/A)_3NN(G/C)_3NN$ discovered by Crothers and coworkers to rotationally fix nucleosomal DNA when spaced every 10 bp (8). To position the T_{11}-tract at different superhelical locations, we made use of a circular permutation synthesis strategy of the type initially developed by Crothers for localizing bends (9). We will show that CPD formation in the T_{11}-tracts is strongly modulated by a nucleosome, with maxima that are shifted to the 5'-side of the T_{11}-containing strand compared to heterogeneous DNA as previously observed for a mixed T-tracts (6). The precise position of the maxima, however, varied with the translational position, and did not always correlate with the maxima in hydroxyl radical cleavage sites used to assign rotational orientation of the DNA.

2.2 Materials and Methods

2.2.1 Materials

ODNs were from IDT. T4-pdg (previously T4 endonuclease V) was prepared from a clone provided from Stephen Llyod as previously described (10).

2.2.2 Nucleosomal DNA dimers

The 168 bp parental nucleosomal DNA duplex was synthesized by hybridization of 95-mer and 96-mer ODNs (IDT) to form a 23 bp duplex at their 3'-ends by slowly cooling from 95 °C to room temperature in 50 mM NaCl, and extended by 3' to 5'-exo$^-$ Klenow Fragment (New England BioLabs) in 50 mM NaCl, 10 mM Tris-HCl (pH 7.5), 10 mM $MgCl_2$, 100 µM dNTPs and 1 mM DTT, for 30 min at 37 °C. The 168 bp duplex DNA was then digested by EcoRI (Promega) in 90 mM Tris-HCl (pH 7.5), 50 mM NaCl and 10 mM $MgCl_2$, for 30 min at 37 °C, and multimerized with T4 DNA ligase (Promega) in 30 mM Tris-HCl (pH 7.8), 10 mM $MgCl_2$, 10 mM DTT and 1 mM ATP, for 3 h at room temperature. The dimer product was separated by electrophoresis on a 3% agarose gel run at 200 V and isolated using a Promega Wizard SV gel and PCR clean-up system. The dimeric DNA was then cloned into pBlueScript II SK- vector DNA (Agilent) that had been restricted with EcoRI and then dephosphorylated with calf intestinal phosphatase (CIP) (New England BioLabs) in 100 mM NaCl 50 mM Tris-HCl (pH 7.5), 10 mM $MgCl_2$ and 1 mM DTT, for 30 min, at 37 °C, to prevent re-circularization. The cloning was performed using 1:1, 1:3 and 3:1 molar ratios of vector:insert with T4 DNA ligase and 1 mM ATP at 10 °C overnight. The pBS vector with the dimer insert was then transfected into TOP10 chemically competent *E.coli* cells (Invitrogen) and plated on solid LB media (15 g/L agar, 25g/L LB broth, 100 µg/mL ampicillin). A clone containing the desired dimer plasmid was identified by restriction analysis and the sequence verified by DNA sequencing.

2.2.3 Circular permutation synthesis of nucleosomal DNA

The pBS dimer-containing clone was cultured in liquid LB media (25 g/L LB broth and 100 µg/ml ampicillin) and the plasmid was harvested with Promega PureYield plasmid miniprep system. Translationally permuted 150 bp nucleosomal DNAs were prepared from this plasmid by PCR

amplification with LongAmp Taq DNA polymerase (New England BioLabs) for 35 cycles followed by phenol extraction and ethanol precipitation. A typical 100 µL PCR reaction contained 0.5 µM of forward and reverse primers, 300 µM of dNTPs, 300 ng template DNA, 4 µL DNA polymerase (2.5 U/ µL) in 1× reaction buffer 60 mM Tris-SO_4 (pH 9.0), 20 mM $(NH_4)_2SO_4$, 2 mM $MgSO_4$, 3% glycerol, 0.06% IGEPAL CA-630, and 0.05% Tween 20.

2.2.4 Nucleosome reconstitution

Nucleosome core particles were isolated and purified from chicken erythrocytes following a simplified procedure provided by Dr. Michael Smerdon. DNA duplex 150-mers corresponding to seven different translational positions were incorporated into the nucleosomes by a salt mediated exchange process. Briefly, 150 bp duplex was incubated with nucleosomes at various ratios in 300 µL of 2 M NaCl, 10 mM Tris-HCl, 5 mM EDTA at pH 7.5 and room temperature for 2 h, and then dialyzed against 50 mM NaCl and 10 mM Tris-HCl (pH 7.5) at 4 °C, overnight. The reconstituted nucleosomal core particles were recovered from the dialysis tubing and equilibrated at 54 °C for 2 h to fix the nucleosomal phasing. The reconstituted particles were assayed by native PAGE (6% acrylamide, 0.2% bisacrylamide) in 100 mM Tris-borate, 2 mM EDTA (TBE), and the ratio of nucleosome-bound DNA to free DNA was quantified by Quantity One software.

2.2.5 Relative binding affinity of circular permutated sequences

The relative binding affinities for the nucleosomal DNAs for the histone core particle were determined by a competitive nucleosome reconstitution experiment with chicken DNA that was purified from isolated nucleosomes by phenol extraction and ethanol precipitation by a general procedure (8, 11). In a first step, a fixed amount of radiolabeled nucleosomal SHL 0 DNA was incubated with chicken blood nucleosome core particles (1:550) and increasing amounts of

competitor chicken nucleosomal DNA at 2 M NaCl, after which the salt concentration was lowered to 50 mM, and the reaction mixtures electrophoresed on a native polyacrylamide gel (6% acrylamide, 0.2% bisacrylamide in TBE). In this way, it was determined that 385 parts of chicken DNA was needed to give approximately 50% binding of the radiolabeled nucleosomal SHL 0 DNA. Then radiolabeled SHL 0 to -6 DNAs were incubated in triplicate with the competitor DNA and nucleosome core particles at a 1:385:550 ratio, and the average ratios of bound to free DNA were calculated relative to that for the SHL 0 DNA.

2.2.6 Hydroxyl radical footprinting

Sodium ascorbate, $Fe(NH_4)_2(SO_4)_2 \cdot 6H_2O$ and H_2O_2 (15 mM, 1.5 mM, and 0.18% final concentrations respectively) were quickly added to 100 µL of the nucleosome-bound DNA sample in 50 mM NaCl, 10 mM Tris-HCl, pH 7.5 reaction buffer with gentle vortexing after the addition of each reagent. The reaction was incubated for 120 s at room temperature and quenched by addition of glycerol and EDTA solution to final concentrations of 5% and 12 mM, respectively. The samples were electrophoresed on a native PAGE (6% acrylamide, 0.2% bisacrylamide in TBE), and gel sections containing the nucleosome bands were excised, crushed, and soaked in 1% SDS and 0.2 M NaCl. The proteins were then extracted with phenol:chloroform:isopropanol 25:24:1, and the DNA was ethanol precipitated. To align the bands, a Maxam-Gilbert G sequencing reaction was carried out on the nucleosome-free DNA sample in 50 mM cacodylate, 50 mM NaCl, 5 mM EDTA at pH 8.2. For a 100 µL reaction, 1µL of dimethyl sulfate was added to initiate the reaction. After 120 s of incubation at room temperature, 60 µL of mercaptoethanol was added to quench the reaction. The DNA was ethanol-precipitated and the resulting pellet was solubilized in 100 µL of 1 M piperidine, followed by 5 min heating at 90 °C and evaporating to dryness at 60 °C.

2.2.7 T4-pdg assay for CPDs

DNA substrates were irradiated with broadband UVB (280-400 NM, centered at 312 nm) (Spectroline model XX-15B) at 0 and 40 °C at a measured intensity of 1.5 mW/cm^2 for 40 min for a dose of 36 kJ/m^2. Nucleosome-bound DNA was first extracted with phenol:chloroform:isopropanol 25:24:1 twice, and ethanol-precipitated twice. The DNA samples were incubated with 8 μg of T4-pdg in 10 mM Tris-HCl, 50 mM NaCl, 5 mM EDTA, pH 7.5 for 30 min at 37 °C to and then heated in 1M piperidine for 5 min to insure complete elimination of the sugar ring. Residual piperidine was evaporated by heating at 60 °C in vacuo. The resulting pellets were brought up in 20 μL formamide-dye and sequentially loaded on a 10% denaturing PAGE (7 M urea, 10% acrylamide, 0.33% bisacrylamide in TBE) so that the T-tracts would be aligned.

2.2.8 Peak analysis

The volume tool in Quantity One was used to quantitatively determine the relative amounts of HO• cleavage and TT CPD formation as a function of nucleotide position x, and the relative peak volumes I were fit to a Gaussian function, $I = C + a*\exp(-(x-b)^2/(2*c^2))$ where C is a constant, a is the amplitude, b is the position of the maximum, and c is the standard deviation.

2.2.9 Relative photoreactivity of T_{11}-tracts at different SHLs

To determine the relative efficiency of CPD formation in different SHLs, the 5'-radiolabeled duplex 41-mer sequence was separately mixed with 5'-radiolabeled duplex SHL -1 and -2 nucleosomal DNA. The mixtures were electrophoresed to determine the exact ratio of the 41-mer to the nucleosomal DNA by volume integration of the bands in a radioimage of the gel. The mixtures were then exchanged with the chicken nucleosome core particles, irradiated, and then

subjected to the T4-pdg assay described above to determine the relative photoreactivity of the T-tracts at the SHL -1 and -2 positions in the nucleosome core particle DNA relative to that of the unbound 41-mer DNA. Two separate mixtures of 5'-radiolabeled duplex DNA, one consisting of SHL 0, -2, -4 and -6 DNA, and the other of SHL -1, -3 and -5 DNA were then prepared, a fraction of each which was assembled into a nucleosome core particle. The free and nucleosome core particles were then irradiated and subjected to the T4 endonuclease assay from which the relative reactivities of the T-tracts at the different SHLs were calculated.

2.3 Results and Discussion

2.3.1 Design and synthesis of DNA substrates

To facilitate the synthesis of nucleosomal DNA containing a T_{11}-tract at each of the seven superhelical positions in the 5'-half of a nucleosome core particle, we adopted a circular permutation synthesis strategy of the type originally developed by Crothers and coworkers to study DNA bending (9). The idea was to synthesize a single nucleosomal DNA sequence containing a T_{11}-tract and then to dimerize it, after which nucleosomal DNA containing the T_{11}-tract in any desired superhelical location could be obtained by PCR using the appropriate primers (Figure ***2.2***). The parental nucleosomal DNA was designed to have the T_{11}-tract centered at the dyad axis by incorporating TG bending motifs, $(T/A)_3NN(G/C)_3NN$, every 10 bp in the flanking DNA (8, 12). With this bending motif, bending is toward the major groove at the central GC base pair of the $(G/C)_3$ sequence and toward the minor groove at the central TA base pair of the $(T/A)_3$ sequence. In this way, the central T of the T_{11}-tract in the parent 150-mer maps to 0, the dyad axis, and the T's to the 5'-side are assigned negative numbers, and to the 3'-side, positive numbers. To make dimers of the nucleosomal DNA, EcoRI digestion sites were engineered into the ends of the sequence without interrupting the TG motifs, and were flanked by an extra 6 bp to ensure efficient

digestion. The resulting 168-mer sequence was also designed not to contain repetitive sequences as previously used (8, 12) to ensure that unique primers could be used to amplify any desired nucleosomal DNA sequence (Figure ***2.3***).

The designed 168-mer DNA was prepared by primer extension of two overlapping 95-mer and 96-mer synthetic ODNs. The dimer of the 150-mer nucleosomal DNA was prepared by digesting the 168-mer with EcoRI and ligating the digestion products with T4 DNA ligase. The dimer was purified from an agarose gel (Figure ***2.4***) and was cloned into the EcoRI site of a pBlueScript SK- vector. Individual clones were screened by enzyme digestion and PCR to identify those that had the tandem repeat in phase, and then verified by sequencing (Figure ***2.5***). For the circular permutation synthesis, seven sets of forward and reverse primers were used to produce a series of 150 bp nucleosomal DNAs that position the T_{11}-tract at 7 different superhelical locations (SHL) along a nucleosome core particle, at 0 (dyad), -1, -2, -3, -4, -5, and -6 (Table ***2.1***).

2.3.2 Nucleosome core particle reconstitution and assay by hydroxyl radical footprinting

To determine the optimal conditions for nucleosome core particle (NCP) reconstitution, the 150bp DNA duplexes were 5'-end labeled and titrated with NCPs isolated from chicken erythrocytes under high salt conditions that promote nucleosomal DNA exchange, followed by lowering of the salt concentration and thermal annealing (13). Electrophoresis on a native gel showed that about 95% of the 150-mer DNAs could be incorporated into a single NCP band at an NCP:DNA ratio of 600:1 (Figure ***2.6***). To determine the rotational and translational setting of the DNA on the nucleosome, the reconstituted NCPs were subjected to hydroxyl radical (HO•) footprinting. The HO• cleavage pattern exhibited a very pronounced 10-11 bp periodicity, indicating that the 150-

mer DNAs were rotationally phased. The cleavage pattern was mapped onto the DNA sequence by alignment with the Maxam-Gilbert G reaction bands (Figure ***2.7***).

The HO• footprinting pattern was used to verify the translational position of the T_{11}-tract based on the expectation that the periodic modulation of the HO• cleavage pattern would only be apparent where the DNA was in direct contact with the histone core. HO• preferentially cleaves DNA at sites where the sugar phosphate backbone is most exposed and faces away from the histone surface, and is inhibited where it faces the histone surface. For the dyad position, one can clearly see the expected six repeats of HO• cleavage bands above (to the 3'-side of) the band at the T_{11}-tract, with the last band appearing at the edge of the large uncleaved band corresponding to full length DNA. The number of repeats increased by one as the T_{11}-tract was moved an additional 10 bp towards the 5'-end. When the T_{11}-tract was positioned at SHL -6, 12 repeats are observed. These results, coupled with the observation of a single nucleosomal band in the electrophoresis gel following nucleosomal DNA exchange (Figure ***2.6***) indicate that the 150-mer DNA's are all largely adopting a single, centered translational position that maximizes histone-DNA contacts. Had the DNA shifted by 10 bp to either side, contact between one turn of the helix and the nucleosome would have been lost, and this would lead to thermodynamic instability.

There were differences, however, in the alignment of the HO• cleavage bands with the T-tract sequence at different SHLs (Figure ***2.8*** and Figure ***2.9***A). The HO• cleavage band pattern for each SHL could be fit to a Gaussian function with the average position of the band maximum at $+1 \pm 1$ relative to the base pair assigned as 0 in the T_{11}-tract. The spread of cleavage bands had an average standard deviation σ of 2.0 ± 0.3, corresponding to a band width at half peak height of $2.355\ \sigma$ or 4.8 ± 0.7 nucleotide. Previous HO• footprinting of a repetitive TG motif-containing

nucleosome (8) and one containing the Widom 601 sequence (14) also showed a variation of 2 or more in the position of maximum cleavage from that expected for a 10-11 base pair repeat. The variability in the position of the HO• cleavage band maxima could be due to differences in the precise translational position and hence rotational position of the nucleosomal DNA at difference SHLs caused by the T_{11}-tract. The variability could also be due to differences in DNA conformation or interactions with histone tails at different SHLs. Removing the histone tails, however, was not previously found to alter the HO• footprinting pattern, but the point to which the tails were truncated was not indicated (15).

2.3.3 T=T CPD distribution with in T_{11}-tracts as a function of SHL

Free or nucleosome-bound 150-mer DNA duplexes were irradiated with broadband UVB light centered at 312 nm light at 0 °C to produce the *cis-syn* T=T CPDs within the T_{11}-tracts. The irradiation time was chosen to maximize signal to noise of gel bands while still maintaining the pattern observed at lower doses (Figure ***2.10*** and Figure ***2.11***). The nucleosome-bound samples were then phenol extracted to remove histone core proteins, ethanol precipitated, and incubated with T4 pyrimidine dimer glycosylase or T4-pdg to reveal the locations of the CPDs. T4-pdg is a glycosylase that hydrolyzes the N-glycosidic linkage of the 5'-T of the CPD, and then causes strand cleavage by an associated lyase activity to first yield a 5'-phosphate terminated end by a β-elimination reaction, followed by formation of a 3'-phosphate terminated end by a slower δ-elimination reaction (16). These are the same ends that are produced by the Maxam-Gilbert reactions, and the 3'-phosphate is the major end produced by HO•-mediated hydrogen abstraction at C5 and C4 of the sugar ring (17). To ensure complete δ-elimination of the sugar, the samples were further incubated with 1 M piperidine at 90 °C for 5 minutes. The samples were sequentially loaded in time so that the cleavage bands at the T_{11}-tracts ran at approximately the same position

on the gel (Figure ***2.7***). Because hot piperidine is also known to cause cleavage at (6-4) and Dewar photoproducts (18), we treated an irradiated T_{11}-tract containing 41-mer under the same conditions without T4-pdg, and found no additional bands (Figure ***2.10***), confirming that the observed patterns in free DNA were due solely to CPDs. This is consistent with the fact that TT (6-4) and Dewar photoproducts form with 7% and 0.3%, respectively, of the frequency of CPDs with UVB light (19). These photoproducts are expected to form even less in nucleosomes, which are known to suppress (6-4) products about 6-fold compared to internucleosomal or linker DNA (20).

The CPD cleavage band patterns in free and nucleosome-bound DNA were completely different and showed essentially the opposite intensity pattern (Figure ***2.8***). In free DNA, all seven T_{11}-tract positions show the same T=T CPD band pattern, with the highest CPD frequency at the 3'-end, decreasing to a minimum in the center, and increasing slightly at the 5' end, as previously observed by others in T-tracts of various lengths (21, 22). In nucleosome-bound DNA, the band pattern was reversed, with the CPD frequency highest in the middle of the T-tract and tapering off towards the 5'- and 3'-ends. The pattern of CPD cleavage bands of the T_{11}-tracts at all seven SHLs could be fit to a Gaussian function with an average maximum band position at -0.9 ± 0.7 relative to the base pair translationally related to the dyad, and with a σ of 1.4 ± 0.3 (Figure ***2.9***A & B). While almost all of the CPD cleavage bands fit a Gaussian, outlier CPD cleavage bands were observed at -4 in the T_{11}-tract of the dyad NCP and at +4 in the -6 NCP, which map to positions in a nucleosome crystal structure (1AOI.pdb) that are in close contact with paired loops in histone folds.

The position of the CPD band pattern maximum within the T_{11}-tracts in the nucleosome core particle also varied with translational position much like that of the HO• cleavage band

patterns. A variation in the position of maximum CPD formation with translational position has also been observed for irradiated chromatin, but with a different average position (23). The average maximum position of CPD formation in the T_{11}-tracts was 1.8 ± 0.7 nucleotides to the 5'-side of the site of the average maximum position of HO• cleavage. For most translational positions, CPD formation tracked with HO• cleavage (Figure ***2.9***A), with the exception of the dyad and SHL -2 positions which showed differences of 2.4 and 3 nucleotides between sites of maximum CPD formation and HO• cleavage. Interestingly, the standard deviations for the Gaussian fits of the CPD band patterns tracked very closely with those for HO• cleavage and did not show any large deviation at the dyad and the SHL -2 positions (Figure ***2.9***B).

The progressive change of the position of maximal cleavage towards the 5'-end in the nucleosomal DNA's with an increase in the translational position away from the dyad can be explained in part by the fact that the helical repeat is not exactly 10 bp/turn in the nucleosome. Inspection of the crystal structure of a 147-mer DNA nucleosome (1KX5.pdb) shows that the base pair orientation equivalent to that at the dyad occurs at -10, -31, -52 and -73, which could explain the overall shift of the position of maximum CPD formation from 0.1 at the dyad to -2 for the SHL -6 T-tract (24). The variation in the position of maximum CPD formation or HO• cleavage is not linear with translational position, however, suggesting that the T-tract itself may lead to adjustments in the actual rotational and translational positioning of the T-tracts on the histone core particle as a function of position.

The 5'-shift in the position of the maximum CPD formation relative to the HO• cleavage is in accord with what was previously observed in a naturally occurring DNA sequence containing T-tracts of various lengths (6). This is different from what was observed for heterogeneous and non-T-tract sequences, where the maximum of CPD formation and HO• cleavage closely

coincided (25, 26). The frequency of CPD formation in the heterogeneous sequences was found to correlate with the amplitude of nucleotide motion as inferred from temperature factors of the nucleotides in the crystal structures of nucleosomes. The temperature factors in turn correlate with the degree to which the backbone faces away from the protein surface, and hence the sites most accessible to HO• (25). The average 1.8 bp shift in position of the maximum CPD cleavage in T-tracts relative to HO• cleavage would thus appear to be due to a difference in the DNA conformation, flexibility, or histone interactions between T-tracts and heterogeneous DNA.

In the crystal structure of a nucleosome containing a T_{16}-tract (2FJ7.pdb) (27) the temperature factors for the individual T's in the T_{16}-tract parallel those seen in non-T-tract DNA in a nucleosome (Figure ***2.12***A), suggesting that something other than nucleotide dynamics is controlling CPD formation frequency. We noted that the minor groove of the T_{16}-tract was significantly narrowed in the crystal structure, suggesting that this conformation might be an important determinant. Previous molecular dynamics studies of CPD formation suggested that CPD formation is most favorable when the distance between the centroids of the C5-C6 bonds of adjacent thymidines and the improper torsion angle (T_nC5-C6-$T_{n+1}C6$-C5) fall within the range of 0 to 3.6 Å and 0 to 48° (28). Analysis of these parameters within the T_{16}-tract show that among all the TT sites, only the T_{251}-T_{252} site comes close to these values, with a values of 3.7 Å and 38° (Figure ***2.12***B). This site corresponds to the -1 and 0 positions relative to the translated dyad axis, and occurs two nucleotides to the 5'-of the position of the maximum nucleotide temperature factor at positions +1 & +2. The next closest site is 252 and 253 which had values of 4.1 Å and 24°. Thus it is possible that the T-tract adopts a slightly different structure from heterogeneous DNA that shifts CPD formation frequency to the 5'-side.

2.3.4 Binding affinity as a function of T-tract translational position

If the observed differences in CPD formation and HO• cleavage patterns at the T-tracts at different SHLs are due to different alignments of the T_{11}-tract, then one might expect that they could have an effect on the binding affinity of the DNA. To test this possibility, we determined the binding affinity of the various DNAs relative to the DNA at SHL 0 by previously described competition experiments (8, 11). Briefly, the concentration of chicken nucleosomal DNA required to reduce the binding of radiolabeled SHL 0 DNA to 50% was first determined by titration. The other radiolabeled DNAs were incubated with this same amount of chicken nucleosomal DNA and the fraction bound was determined. The results are graphed in Figure ***2.9***C, and show that the relative binding affinity dropped slightly from 1 for SHL 0 to 0.7 for SHL -1 & -2, and then increased from 0.8 for SHL -3 to 1 for SHL -4 and then to 1.5 for SHL -5 & -6. The relative binding affinities are what one might expect for the presence of a destabilizing sequence which would cause least disruption of binding when it is placed at the end of the nucleosomal DNA. The observed binding trend, however, does not appear to correlate with the observed CPD and HO• cleavage patterns.

2.3.5 CPD yield as a function of T-tract translational position

While the study of individual T_{11}-tract DNAs revealed differences in the pattern of CPD formation as a function of SHL, it did not reveal whether or not the overall formation of CPDs at a particular SHL was enhanced or inhibited. To determine this, we first irradiated radiolabeled SHL 0 & -1 DNAs with radiolabeled 41-mer DNA before and after assembly with nucleosomal core particles, where it was expected that the 41-mer DNA would remain free in solution under both conditions. Then a mixture of SHL 0, -2, -4 and -6 DNA was irradiated before and after assembly into a nucleosome, and the same was done for a mixture of SHL -1, -3 and -5 DNA. After quantifying and normalizing the band volumes, the CPD yields could be calculated as a function of

translational position relative to free DNA (Figure ***2.9***C). As can be seen the CPD yield at SHL 0 was greater than for free DNA and then dramatically rose 4.5-fold for SHL -5, after which it dropped back down to 1.5-fold for SHL -6. The results are generally in accord with what has been observed for CPD formation in mixed-sequence nucleosome core particles in which CPD yield increased on going from the dyad to the 5'-end (23) though this may also reflect some sort of sequence bias. There does not, however, appear to be any correlation between CPD yield and the position of maximum for CPD formation in the T_{11}-tracts as a function of translational position.

2.3.6 Temperature study of T=T CPD formation in nucleosome at the dyad and SHL -6

Because it is known that the frequency of CPD formation within a T-tract in free DNA is temperature dependent (21), we examined the effect of temperature on CPD formation in both free and nucleosome-bound DNA. First, a 41 bp free DNA duplex containing a T_{11}-tract in the center was irradiated with UVB light at 0, 10, 20, 30, and 40 °C. The CPD band pattern shifted from one with a major peak at the 3'-end to a more even distribution of peaks as the temperature increased (Figure ***2.13***) in accord with a previous study on T-tracts of various different lengths (21). This change was attributed to a shift from the T-tract structure to a normal B DNA structure at higher temperatures.

Because the greatest difference in CPD band patterns for the nucleosome free 41-mer was observed at 0 and 40 °C, the free and nucleosome-bound DNA were irradiated with UVB light at these two temperatures. Only the DNAs with the T_{11}-tract at the dyad and -6 SHL positions were subjected to this temperature study because they represent two extreme positions of conformational flexibility in a nucleosome (29). As expected, the CPD band pattern in the two nucleosome-free DNAs changed in the same way as in the 41-mer duplex when heated from 0 to

40 °C, in which the major bands were at the 3'-end of the T-tract at 0 °C and more evenly distributed at 40 °C, though favoring the 5'-side (Figure ***2.14***). The bias for the 5'-side may be due to the fact that CPD formation was more efficient at 40 °C than at 0 °C, as evidenced by the decrease in the % uncleaved substrate, which would favor shorter fragments resulting from a greater number of multiple hits per strand. In contrast, CPD formation at both the dyad and SHL -6 positions in the nucleosome showed similar Gaussian band patterns at 0 °C that did not change significantly upon heating to 40 °C, except perhaps for a small shift in the position of the maximum peak to the 5'-side, possibly due to the increased cleavage efficiency. For the dyad NCP, the Gaussian band pattern was centered at +0.2 at 0 °C and shifted slightly 5' to -0.3 upon heating to 40 °C, whereas σ also increased slightly from 1.3 to 2.1. Likewise, the center of the Gaussian band pattern for SHL -6 NCP moved slightly 5' from -1.5 to -1.9 with a similar small increase in σ from 1.3 to 1.8. The small changes in the pattern of CPD formation in the NCP with an increase in temperature suggest that the flexibility of the DNA does not increase significantly with temperature. The small changes also suggest that the 5'-end of the nucleosomal DNA is not much more flexible than that at the dyad, and remains largely bound to the histone core even at 40 °C.

2.4 Conclusion

We have shown by way of CPD formation that the nucleosome is capable of modifying the conformation of T_{11}-tracts at all SHLs, including -6. Considering that the -6 SHL is only one turn away from where the DNA exits the nucleosome, and is therefore the least constrained, the T_{11}-tract must be quite bendable. The ability of the T_{11}-tract to smoothly bend across all SHLs along a nucleosome core particle is in accord with previous studies that found that T-tracts enhanced the bendability of DNA (30), and further begs an answer to the question of why T-tracts are excluded from nucleosomes in yeast (31, 32). In Chapter 4, we expand the study to poly $(TC)_n$ tracts and we

will show that nucleosomes strongly modulate CPD deamination, with rate maxima shifted 3 nucleotides (nt) to the 3' side of the dyad axis.

2.5 Acknowledgements

We thank Vincent Cannistraro and Santhi Pondugula for advice and help with various experimental procedures. We also thank Stephen Lloyd for T4-pdg. Research reported in this chapter was supported by the National Cancer Institute of the National Institutes of Health under award number R01CA40463.

2.6 References

1. Brash, D.E. (2015) UV signature mutations. *Photochemistry and Photobiology*, **91**, 15-26.

2. Pfeifer, G.P. and Besaratinia, A. (2012) UV wavelength-dependent DNA damage and human non-melanoma and melanoma skin cancer. *Photochemistry and Photobiology Sciences*, **11**, 90-97.

3. Ikehata, H. and Ono, T. (2011) The mechanisms of UV mutagenesis. *Journal of Radiation Research*, **52**, 115-125.

4. Pfeifer, G.P., You, Y.H. and Besaratinia, A. (2005) Mutations induced by ultraviolet light. *Mutatation Research*, **571**, 19-31.

5. Liu, X., Mann, D.B., Suquet, C., Springer, D.L. and Smerdon, M.J. (2000) Ultraviolet damage and nucleosome folding of the 5S ribosomal RNA gene. *Biochemistry*, **39**, 557-566.

6. Schieferstein, U. and Thoma, F. (1996) Modulation of cyclobutane pyrimidine dimer formation in a positioned nucleosome containing poly(dA.dT) tracts. *Biochemistry*, **35**, 7705-7714.

7. Finch, A.S., Davis, W.B. and Rokita, S.E. (2013) Accumulation of the cyclobutane thymine dimer in defined sequences of free and nucleosomal DNA. *Photochemistry and Photobiology Sciences*, **12**, 1474 1482.

8. Shrader, T.E. and Crothers, D.M. (1989) Artificial nucleosome positioning sequences. *Proceedings of the National Academy of Sciences*, **86**, 7418-7422.

9. Levene, S.D., Wu, H.M. and Crothers, D.M. (1986) Bending and flexibility of kinetoplast DNA. *Biochemistry*, **25**, 3988-3995.

10. Ryabinina, O.P., Minko, I.G., Lasarev, M.R., McCullough, A.K. and Lloyd, R.S. (2011) Modulation of the processive abasic site lyase activity of a pyrimidine dimer glycosylase. *DNA Repair*, **10**, 1014-1022.

11. Jayasena, S.D. and Behe, M.J. (1989) Competitive nucleosome reconstitution of polydeoxynucleotides containing oligoguanosine tracts. *Journal of Molecular Biology*, **208**, 297-306.

12. Svedruzic, Z.M., Wang, C., Kosmoski, J.V. and Smerdon, M.J. (2005) Accommodation and repair of a UV photoproduct in DNA at different rotational settings on the nucleosome surface. *Journal of Molecular Chemistry*, **280**, 40051-40057.

13. Kosmoski, J.V. and Smerdon, M.J. (1999) Synthesis and nucleosome dtructure of DNA containing a UV photoproduct at a specific site. *Biochemistry*, **38**, 9485-9494.

14. Syed, S.H., Goutte-Gattat, D., Becker, N., Meyer, S., Shukla, M.S., Hayes, J.J., Everaers, R., Angelov, D., Bednar, J. and Dimitrov, S. (2010) Single-base resolution mapping of H1 nucleosome interactions and 3D organization of the nucleosome. *Proceedings of the National Academy of Sciences*, **107**, 9620-9625.

15. Hayes, J.J., Clark, D.J. and Wolffe, A.P. (1991) Histone contributions to the structure of DNA in the nucleosome. *Proceedings of the National Academy of Sciences*, **88**, 6829-6833.

16. Latham, K.A. and Lloyd, R.S. (1995) Delta-elimination by T4 endonuclease V at a thymine dimer site requires a secondary binding event and amino acid Glu-23. *Biochemistry*, **34**, 8796-8803.

17. Balasubramanian, B., Pogozelski, W.K. and Tullius, T.D. (1998) DNA strand breaking by the hydroxyl radical is governed by the accessible surface areas of the hydrogen atoms of the DNA backbone. *Proceedings of the National Academy of Sciences*, **95**, 9738-9743.

18. Kan, L.S., Voituriez, L. and Cadet, J. (1992) The Dewar valence isomer of the (6-4) photoadduct of thymidylyl-(3'-5')-thymidine monophosphate: formation, alkaline lability and conformational properties. *Journal of Photochemistry and Photobiology B: Biology*, **12**, 339-357.

19. Douki, T. and Cadet, J. (2001) Individual determination of the yield of the main UVinduced dimeric pyrimidine photoproducts in DNA suggests a high mutagenicity of CC photolesions. *Biochemistry*, **40**, 2495-2501.

20. Mitchell, D.L., Nguyen, T.D. and Cleaver, J.E. (1990) Nonrandom induction of pyrimidine-pyrimidone (6-4) photoproducts in ultraviolet-irradiated human chromatin. *Journal of Biological Chemistry*, **265**, 5353-5356.

21. Lyamichev, V. (1991) Unusual conformation of (dA)n.(dT)n-tracts as revealed by cyclobutane thymine-thymine dimer formation. *Nucleic Acids Research*, **19**, 4491-4496.

22. Suter, B., Schnappauf, G. and Thoma, F. (2000) Poly(dA.dT) sequences exist as rigid DNA

structures in nucleosome-free yeast promoters in vivo. *Nucleic Acids Research*, **28**, 4083-4089.

23. Gale, J.M. and Smerdon, M.J. (1988) Photofootprint of nucleosome core DNA in intact chromatin having different structural states. *Journal of Molecular Biology*, **204**, 949-958.

24. Davey, C.A., Sargent, D.F., Luger, K., Maeder, A.W. and Richmond, T.J. (2002) Solvent mediated interactions in the structure of the nucleosome core particle at 1.9 a resolution. *Journal of Molecular Biology*, **319**, 1097-1113.

25. Song, Q., Cannistraro, V.J. and Taylor, J.-S. (2014) Synergistic modulation of cyclobutane pyrimidine dimer photoproduct formation and deamination at a TmCG site over a full helical DNA turn in a nucleosome core particle. *Nucleic Acids Research*, **42**, 13122-13133.

26. Song, Q., Cannistraro, V.J. and Taylor, J.S. (2011) Rotational position of a 5-methylcytosine-containing cyclobutane pyrimidine dimer in a nucleosome greatly affects its deamination rate. *Journal of Biological Chemistry*, **286**, 6329-6335.

27. Bao, Y., White, C.L. and Luger, K. (2006) Nucleosome core particles containing a poly(dA.dT) sequence element exhibit a locally distorted DNA structure. *Journal of Molecular Biology*, **361**, 617-624.

28. Law, Y.K., Azadi, J., Crespo-Hernandez, C.E., Olmon, E. and Kohler, B. (2008) Predicting thymine dimerization yields from molecular dynamics simulations. *Biophysical Journal*, **94**, 3590-3600.

29. Dobrovolskaia, I.V. and Arya, G. (2012) Dynamics of forced nucleosome unraveling and role of nonuniform histone-DNA Interactions. *Biophysical Journal*, **103**, 989-998.

30. Vafabakhsh, R. and Ha, T. (2012) Extreme bendability of DNA less than 100 base pairs long revealed by single-molecule cyclization. *Science*, **337**, 1097-1101.

31. Yuan, G.C., Liu, Y.J., Dion, M.F., Slack, M.D., Wu, L.F., Altschuler, S.J. and Rando, O.J. (2005) Genome-scale identification of nucleosome positions in S. cerevisiae. *Science*, **309**, 626-630.

32. Segal, E. and Widom, J. (2009) Poly(dA:dT) tracts: major determinants of nucleosome organization. *Current Opinion in Structural Biology*, **19**, 65-71.

2.7 Tables and Figures

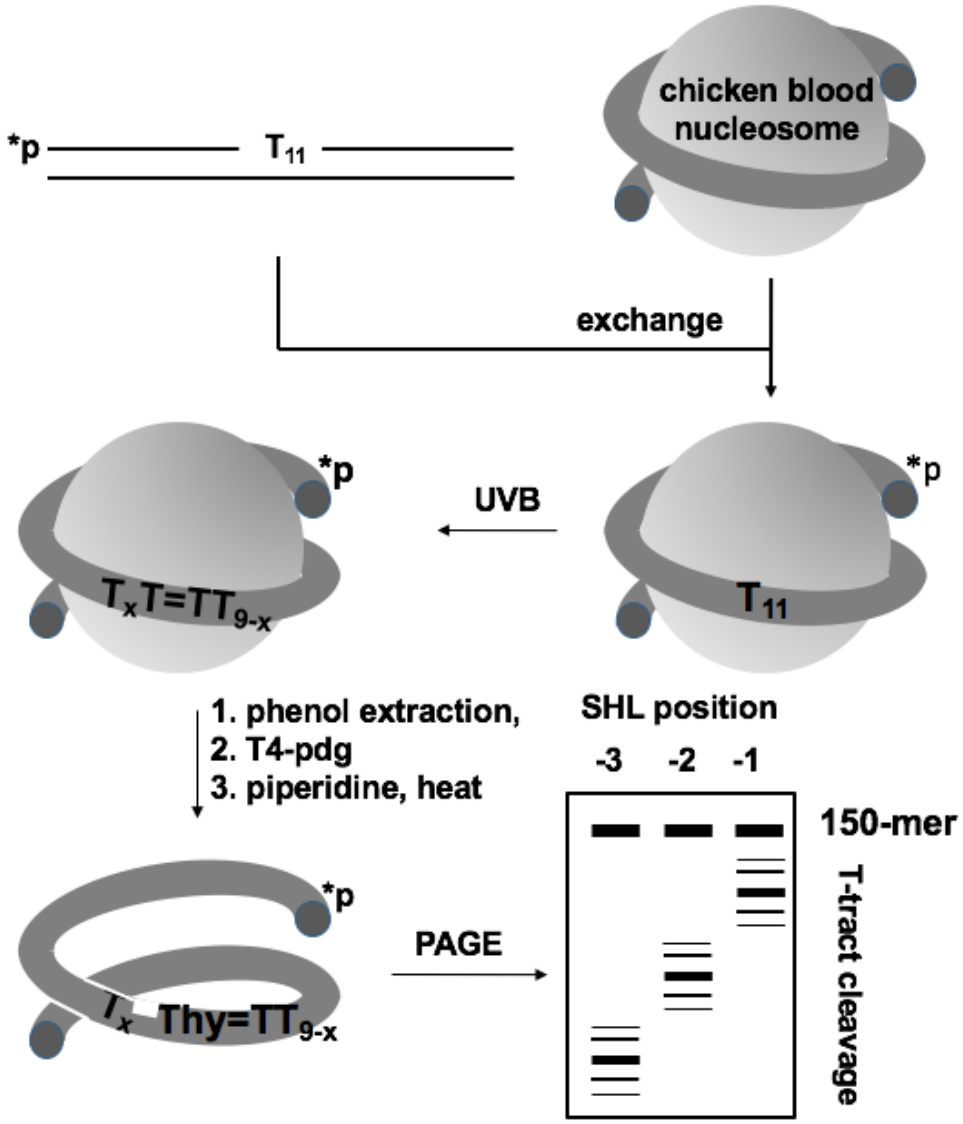

Figure 2.1: Strategy for studying CPD formation as a function of rotational and translational positions in a nucleosome. A 150-mer, 5'-32P-endlabeled duplex DNA containing a T11-tract at various translational positions is incorporated into a nucleosome by a salt-mediated exchange mechanism and then irradiated with UVB light. The DNA is then treated with T4-pdg which cleaves the DNA at sites of CPDs, and electrophoresed on a denaturing polyacrylamide gel to visualize the sites of cleavage.

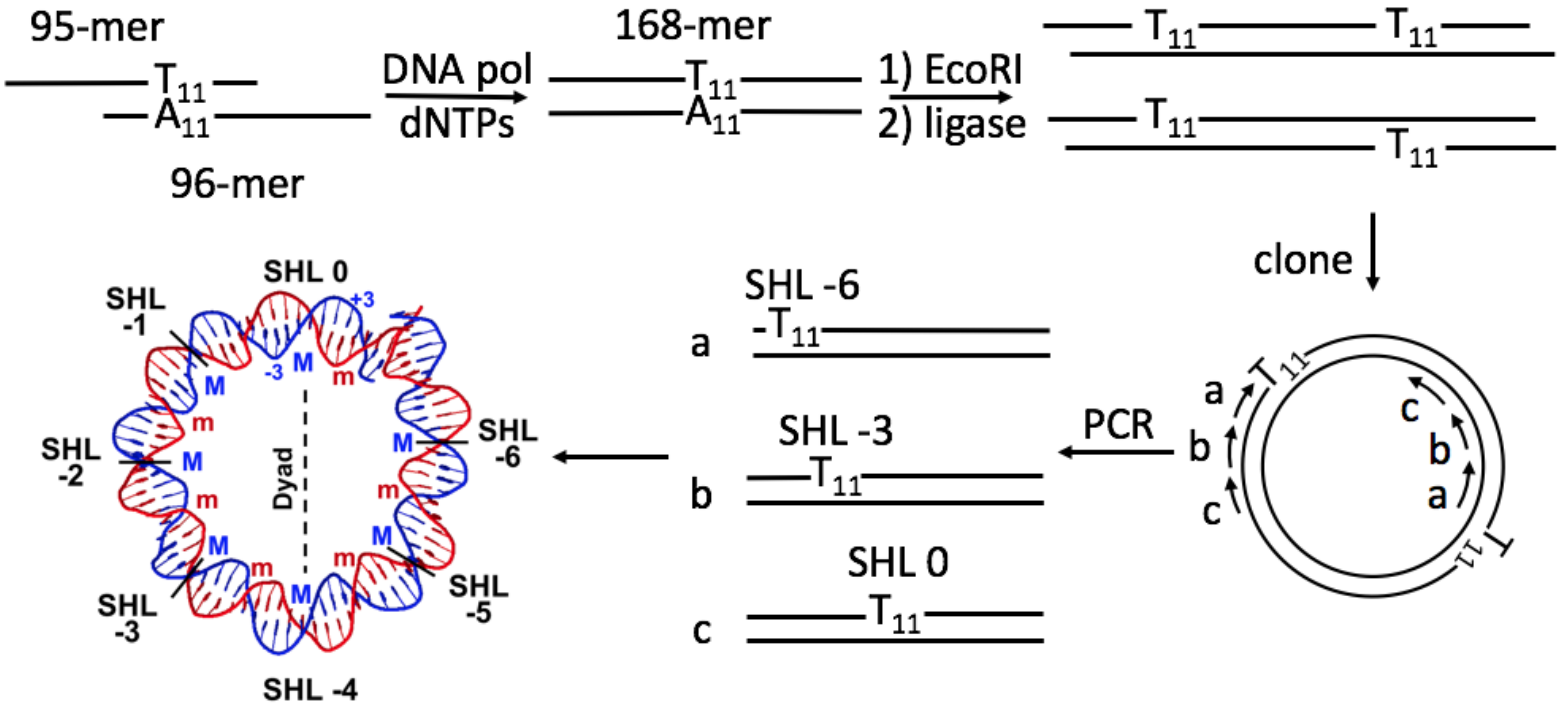

Figure 2.2: Circular permutation PCR strategy used for preparing nucleosomal DNA with T_{11}-tracts at specific SHLs. A DNA 168-mer with a centrally located T_{11}-tract was prepared by primer extension of two overlapping 95 and 96-mers. The resulting product was cleaved with EcoRI and multimerized with T4 DNA ligase and ATP, and the dimer excised from a gel and cloned. Nucleosomal DNAs with T_{11}-tracts at specific SHLs were prepared from the clone by PCR using specific pairs of forward and reverse primers (Table 2.1) whose positions are shown as solid and dashed arrows respectively on the sequence in Figure 2.3. The SHLs correspond to the number of helical turns from the dyad axis on the blue strand containing the T_{11}-tract. They are negative to correspond with the numbering system in which the nucleotides on the T_{11}-tract decrease from 0 at the dyad axis as they approach the 5'-end. The -3 (inside) and +3 nucleotide (outside) positions are shown in blue. The positions at which the major and minor grooves face the histone surface are indicated by M and m, respectively, and are colored coded to match the major groove and minor groove bending motifs in Figure 2.3.

SHL	Primer pairs
dyad	f 5′-AATTC GGCTC ATTCA GCGTC TATG
	r 5′- CA GCGTC ATTGT CGCAG TATCA C
-1	f 5′-ATTCA GCGTC TATGT CGGTC TTAG
	r 5′-GAGCC GAATT CAGCG TCATT G
-2	f 5′-TATGT CGGTC TTAGA GGCTG ATAC
	r 5′-GACGC TGAAT GAGCC GAATT
- 3	f 5′-TTAGA GGCTG ATACA CCGAG AATG
	r 5′-GACCG ACATA GACGC TGAAT G
-4	f 5′-ATACA CCGAG AATGT CGCTC TAAC
	r 5′-CAGCC TCTAA GACCG ACATA GAC
-5	f 5′-AATGT CGCTC TAACT CGCTC ATT
	r 5′-CTCGG TGTAT CAGCC TCTAA GAC
-6	f 5′-TAACT CGCTC A TTTTTTTTTTT A GTGGC
	r 5′-GAGCG ACATT CTCGG TGTAT C

Table 2.1: Primer sets used in circular permutation synthesis.(f = forward primer, r = reverse primer).

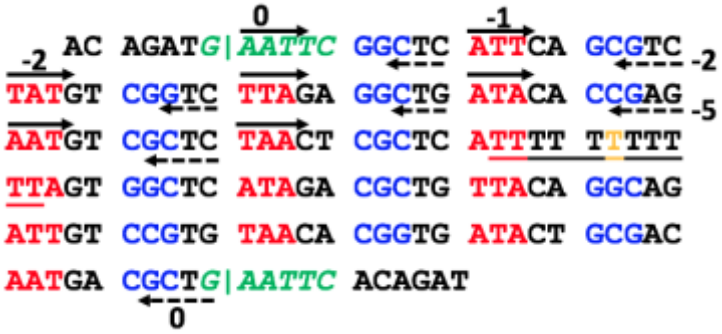

Figure 2.3: Sequence design of 168-mer nucleosomal DNA. A 168-mer DNA duplex was designed to have a centrally located T_{11}-tract (underlined), terminal EcoRI restriction sites (green italic), phased minor groove bending $(T/A)_3$ sequences in red, and major groove bending $(G/C)_3$ sequences in blue. The T in orange in the T_{11}-tract corresponds to the position at which the major groove is expected to bend towards the histone surface at the dyad axis.

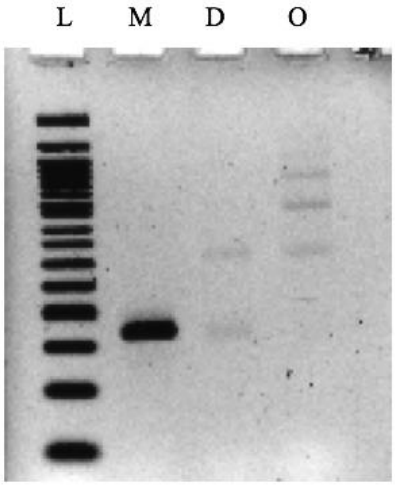

Figure 2.4: Ligation products of digested primary 168bp nucleosomal DNA. L: 100 bp ladder, M: monomer used in ligation, D: monomer and dimer fraction from ligation product mixture, O: oligomers from ligation reaction

Figure 2.5: Sequencing analysis of clone 8.

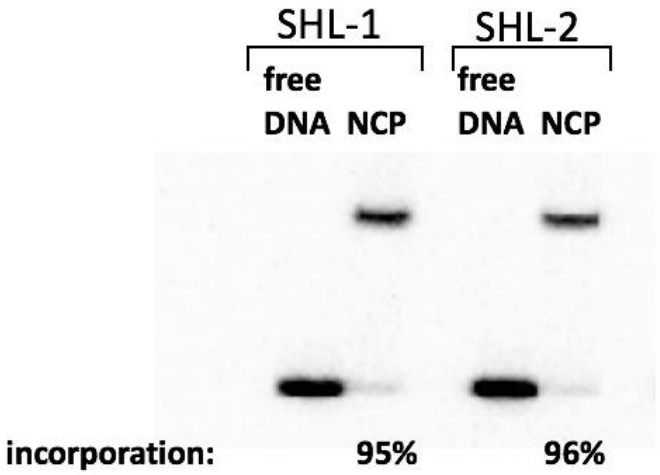

Figure 2.6: Native PAGE analysis of the salt mediated exchange of nucleosomal DNA into nucleosomes. Incorporations of >95% could be achieved at a ratio of 1:600 (DNA: NCP) by this method.

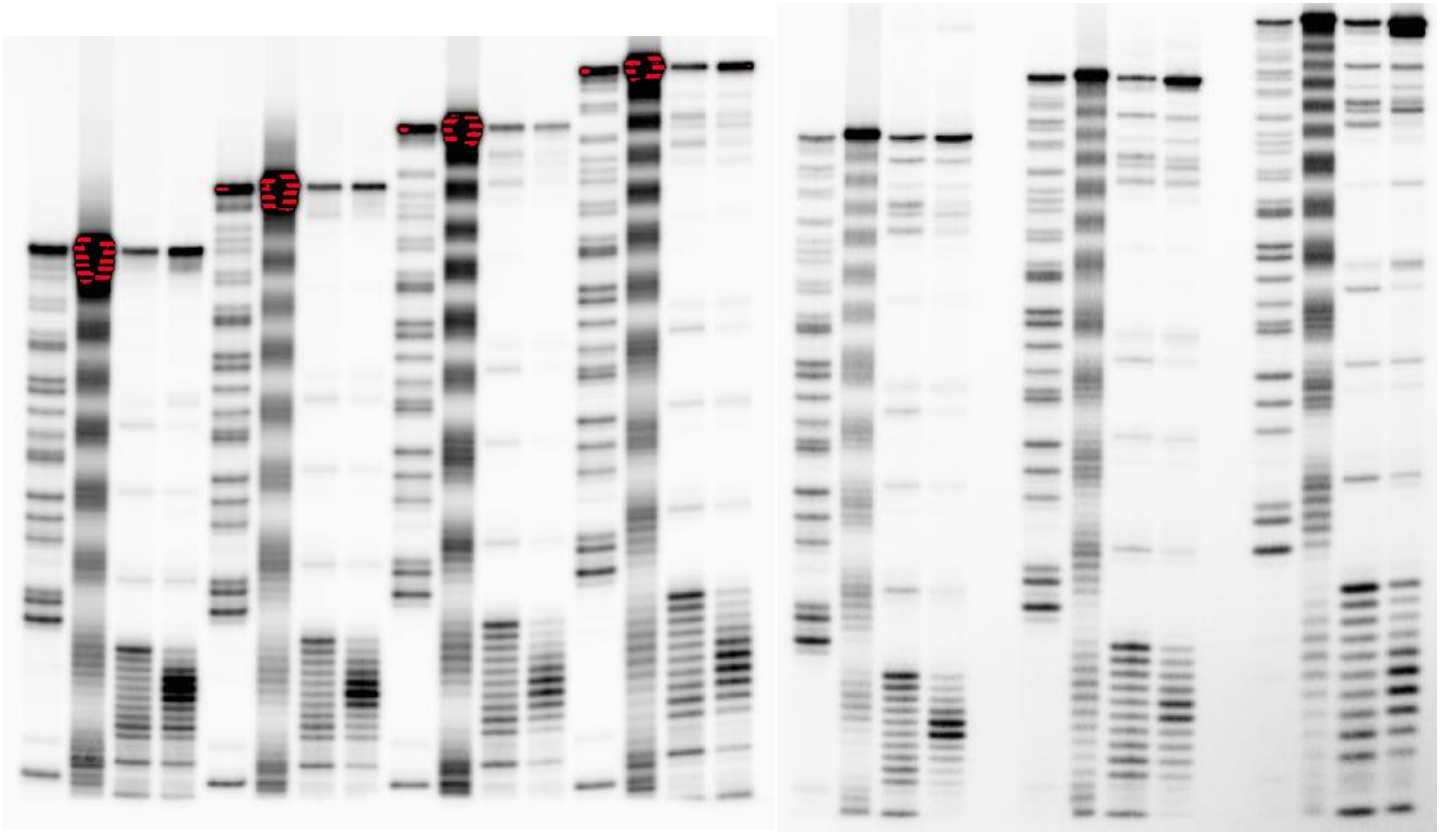

Figure 2.7: PAGE analysis of the hydroxyl radical footprinting of the nucleosome core particles and assay of CPD formation in free and nucleosome-bound DNA. The first lane of each set of four lanes is the Maxam Gilbert G ladder, the second lane is the HO• footprint of the DNA in the nucleosome core particle, the third lane is CPD specific T4-pdg treated UVB irradiated free DNA, and the fourth lane is the CPD specific T4-pdg treated irradiated nucleosome-bound DNA. From left to right, SHLs 0, -1, -2, -3, -4, -5 and -6.

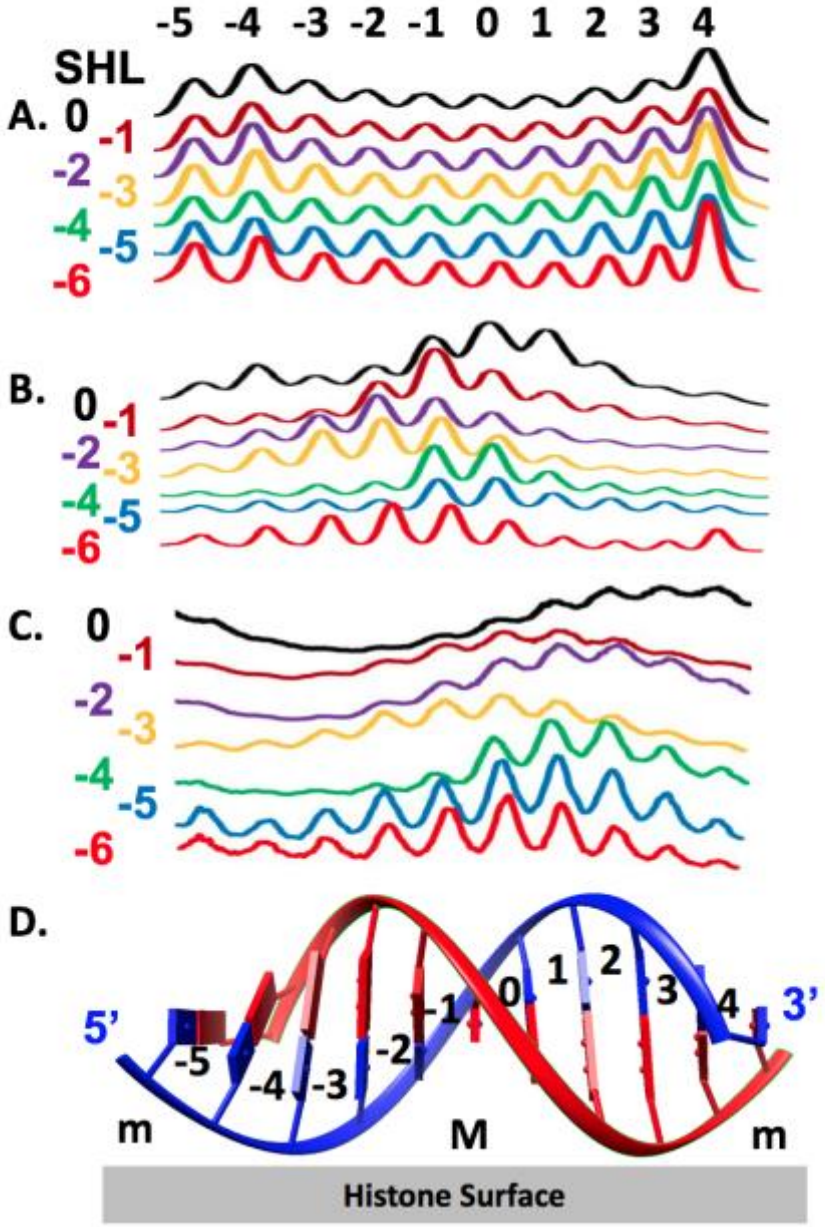

Figure 2.8: Footprinting and CPD patterns in nucleosome-bound DNA compared to the CPD pattern in free DNA. Traces of the T_{11}-tract section of the lanes in Figure 2.6 of A) CPD formation in free DNA, B) CPD formation in nucleosome-bound DNA, and C) HO• cleavage in nucleosome-bound DNA. The numbers to the left are the SHLs of the T_{11}-tract, while the numbers above correspond to the position of the cleaved T in the T_{11}-tract in which the 0 position is expected to align with the dyad in the SHL 0 construct. M and m refer to where the major and minor grooves face the nucleosome surface.

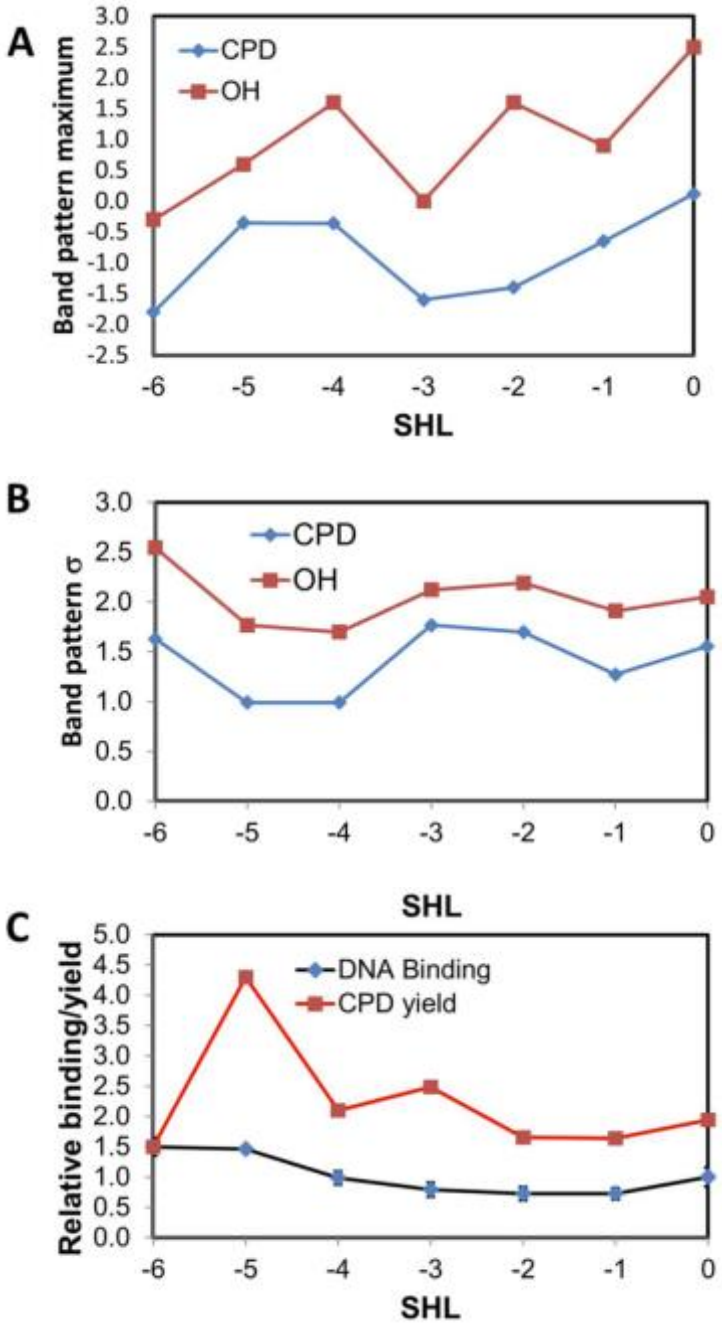

Figure 2.9: Quantification of the CPD and footprinting band patterns, relative CPD yields, and nucleosomal DNA binding affinities. A) Comparison of the position of maximum CPD formation and HO• cleavage in the T_{11}-tracts of the nucleosome-bound DNA as a function of SHL calculated from Gaussian analysis of the pattern of bands in Figure 2.8. B) Comparison of the standard deviation of the Gaussian function used to fit the CPD and HO• cleavage patterns. C) Yield of CPDs in the nucleosome core particle relative to free DNA for the T_{11}-tracts as a function of SHL, together with the binding affinity of the DNA for the nucleosome relative to SHL 0.

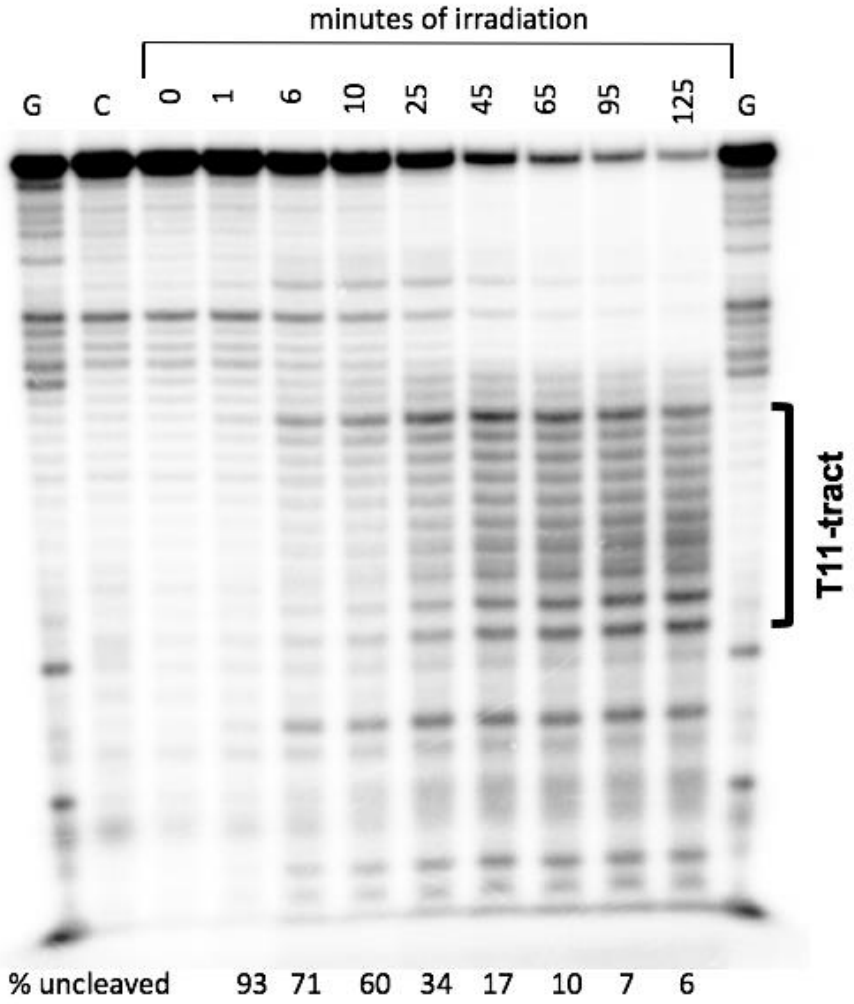

Figure 2.10: Test for (6-4) photoproduct formation and CPD formation as a function of UV dose in the 41-mer duplex. Lane G: Maxam Gilbert A+G ladder; Lane C: UVB-irradiation for 40 min at 0 °C, then treated with 1M piperidine at 90 °C for 5 min. Lanes 0-125: UVB irradiation for 0, 1, 6, 10, 25, 45, 65, 95, and 125 min of irradiation at 0 °C, then treated with T4-pdg followed by treatment with 1 M piperidine at 90 °C for 5 min. The percent uncleaved is calculated following subtraction of the 0 min lane.

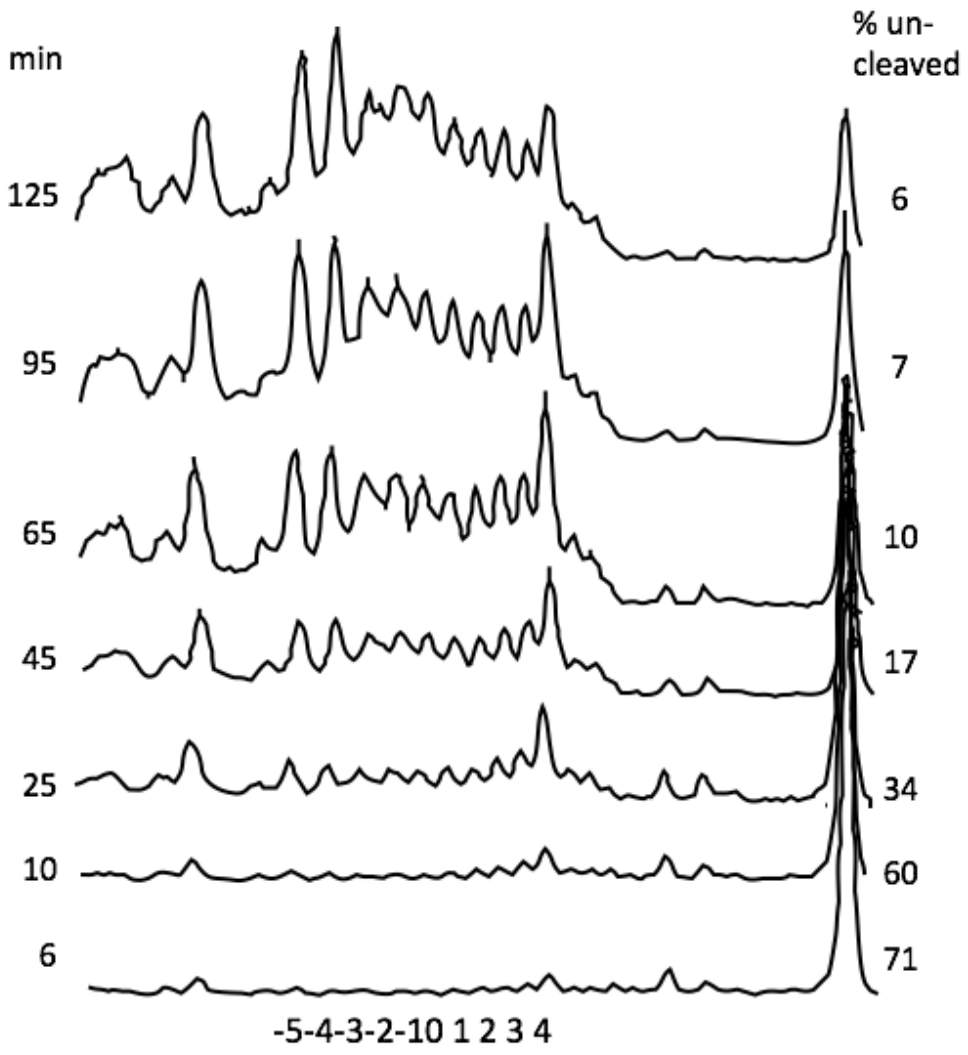

Figure 2.11: Traces of lanes in Figure 2.10. Traces of lanes for the irradiation times shown on the left.

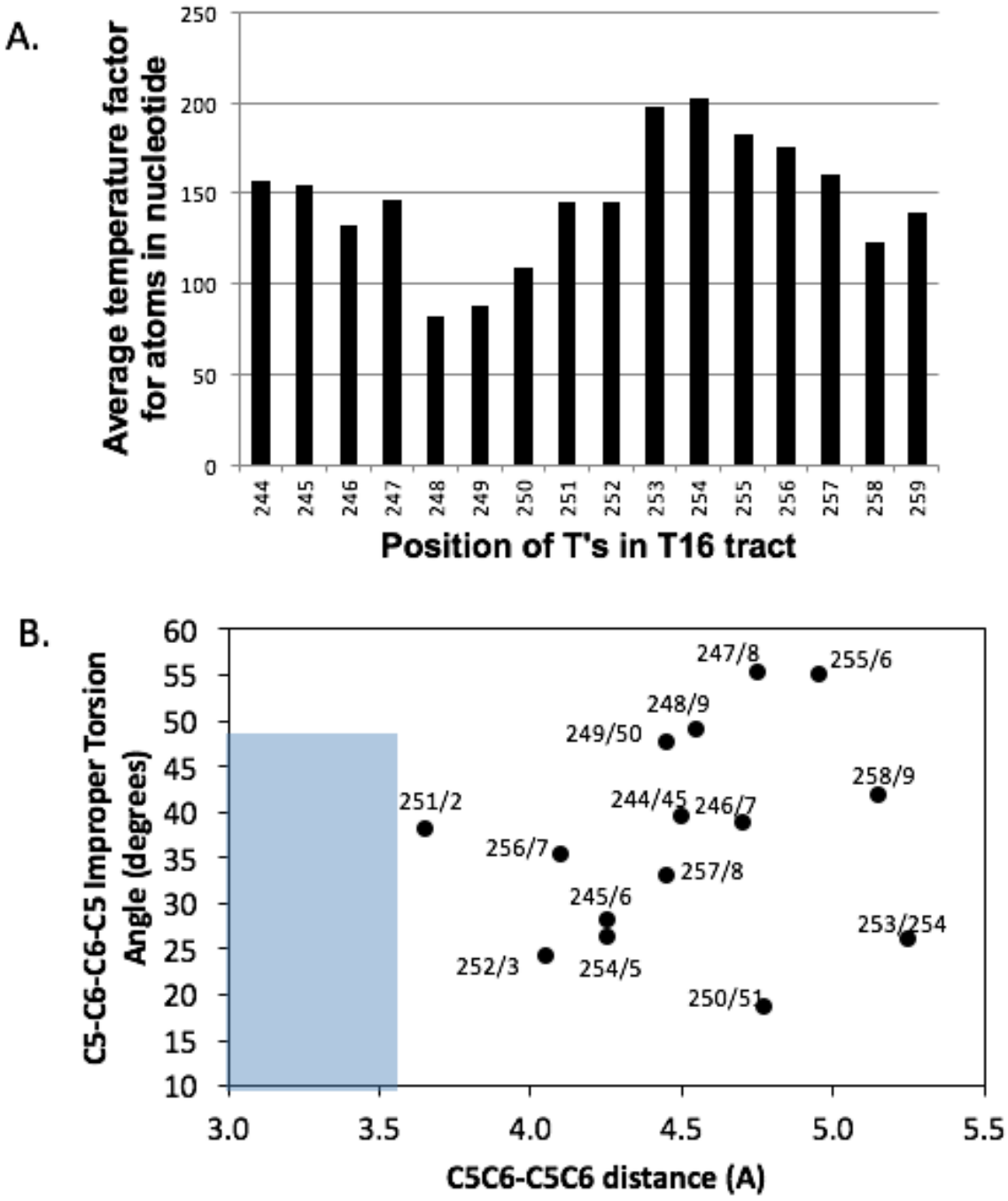

Figure 2.12: Temperature factors and geometry of nucleotides within T16-tract of nucleosome crystal structure 2FJ7.pdb.A) Temperature factors as a function of translational position. B) Geometric parameters relevant to CPD formation for the T16-tract. Shaded in blue is the region thought to be required for CPD formation.

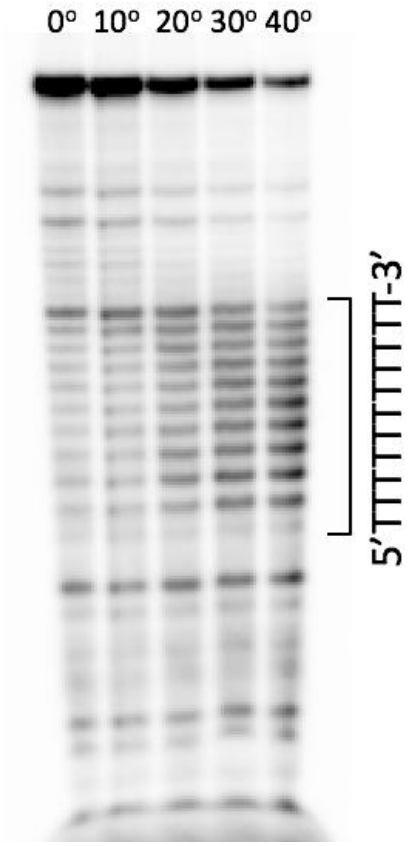

Figure 2.13: CPD photoproduct distribution in the 41mer duplex DNA irradiated with UVB over a temperature range from 0 to 40 ℃.

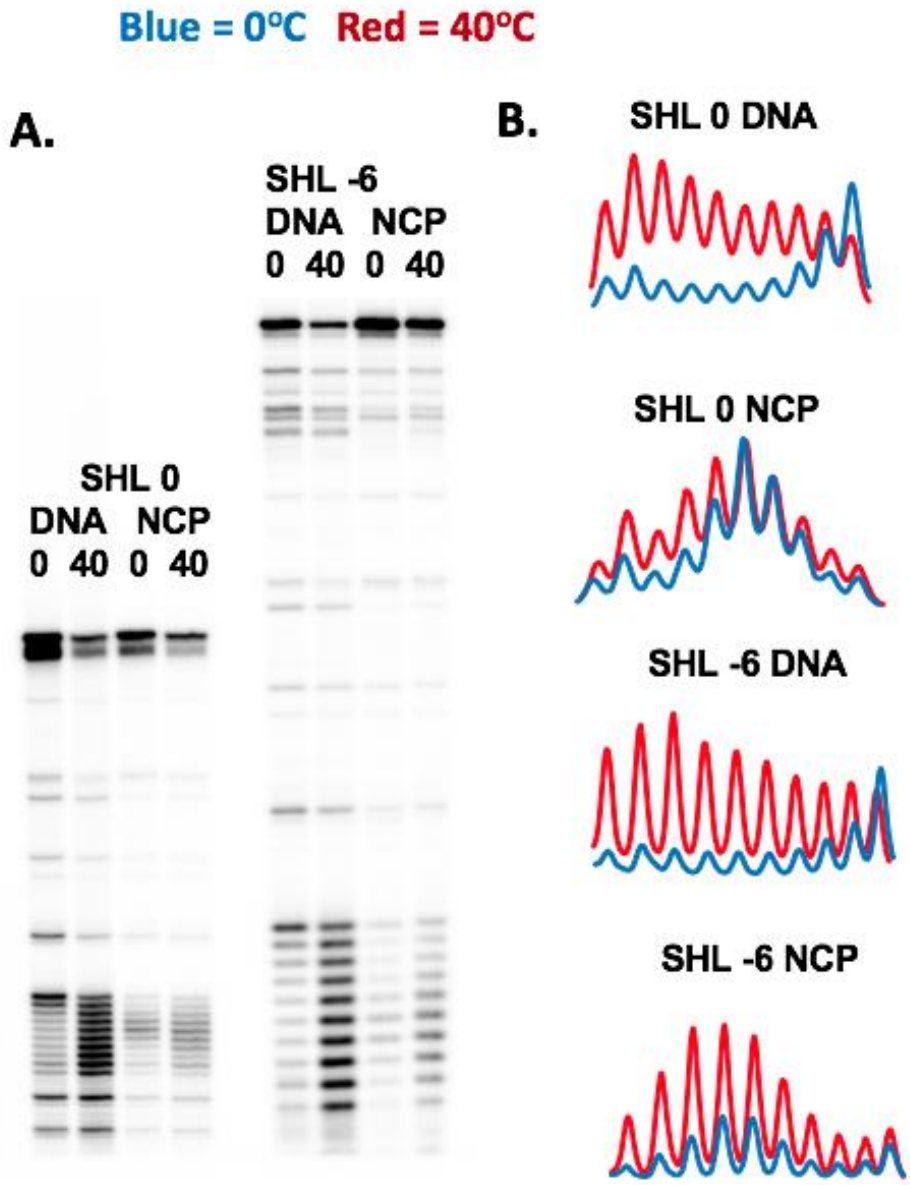

Figure 2.14: PAGE assay of the effect of temperature on the frequency of CPD formation in T_{11}-tracts in free DNA (DNA) and in nucleosome-bound DNA (NCP) at two different SHLs. A) Radioimage of the PAGE gel of the T4-pdg cleavage products at SHL 0 and -6, at 0 °C and 40 °C, and B) scans of the lanes at the sites of the T_{11}-tracts.

Chapter 3 Effects of DNA Bending on T=T CPD Formation in a Rotationally Phased T_{11}-tract in a DNA Microcircle[1]

3.1 Introduction

It was demonstrated many decades ago that nucleosomes can modulate cyclobutane pyrimidine dimer (CPD) formation in heterogeneous genomic DNA with a 10-11 bp periodicity that was attributed to the effect of bending on the conformation and dynamics of DNA (1, 2). A similar effect was observed to occur in a protein-free DNA loop which supported the idea that bending, and not protein DNA interactions were the primary cause of the modulation of photoproduct formation (3). We also discovered that the deamination of C and 5-methylcytosine (^{m}C) in the CPDs was modulated with the same rotational phasing as their formation (4). Because deamination of C and ^{m}C in CPDs has been correlated with the signature C to T mutations induced by UV light (5, 6), it would be of interest to know whether the deamination is also being modulated by bending or by some other effect.

To study CPD formation in protein-free DNA with the same curvature as in the nucleosome, we prepared a rotationally phased 80-mer microcircle DNA. The sequence of microcircle DNA was directly adapted from the nucleosomal DNA sequence (Figure ***2.3***), containing the same TG bending motif and a T_{11}-tract in the middle. CPD formation in the microcircle DNA was also found to be modulated in the same way as in the nucleosome (modulation by nucleosome structure can be found in Chapter 2), indicating that the TG motifs

[1] All contents in this chapter have been published in Wang K and Taylor JS. Modulation of Cyclobutane Thymine Photodimer Formation in T_{11}-Tracts in Rotationally Phased Nucleosome Core Particles and DNA Minicircles. Nucleic Acids Res (2017) 45 (12): 7031-7041.

were rotationally phasing the microcircles, and that bending was the major factor in controlling CPD formation frequency.

3.2 Materials and Methods

3.2.1 Materials

ODNs were from IDT. T4-pdg (previously T4 endonuclease V) was prepared from a clone provided from Stephen Llyod as previously described (7).

3.2.2 Circular 80-mer DNA substrates: microcircle DNA mimic of nucleosomal DNA

The single strand circular 80-mer DNA containing an A_{11}-tract was prepared by ligation of the linear DNA with T4 DNA ligase and 1 mM ATP in the presence of a scaffold DNA at 10 °C overnight and purified by denaturing PAGE on a 10% acrylamide 0.33% bisacrylamide gel in 7 M urea in 1× TBE. Purified ligation products were then treated with 5 μL of exonuclease I (New England BioLabs) in 67 mM glycine-KOH, 6.7 mM $MgCl_2$, 10 mM 2-mercaptoethanol, pH 9.5 for 1 h at 37 °C to eliminate any unligated, and ligated, single-stranded, linear DNAs. The circular DNA was then annealed with complementary single strand T_{11}-tract containing ODNs of different lengths in 50 mM NaCl by slowly cooling from 90 °C to room temperature. Annealed products were purified by native PAGE on 6% acrylamide, 0.2 % bisacrylamide gel in TBE before further treatment.

3.2.3 T4-pdg assay for CPDs

DNA substrates were irradiated with broadband UVB (280-400 NM, centered at 312 nm) (Spectroline model XX-15B) at 0 and 40 °C at a measured intensity of 1.5 mW/cm^2 for 40 min for a dose of 36 kJ/m^2. Nucleosome-bound DNA was first extracted with

phenol:chloroform:isopropanol 25:24:1 twice, and ethanol-precipitated twice. The DNA samples were incubated with 2 μg of T4-pdg in 10 mM Tris-HCl, 50 mM NaCl, 5 mM EDTA, pH 7.5 for 30 min at 37 ℃ to and then heated in 1M piperidine for 5 min to insure complete elimination of the sugar ring. Residual piperidine was evaporated by heating at 60 ℃ in vacuo. The resulting pellets were brought up in 20 μL formamide-dye and sequentially loaded on a 10% denaturing PAGE (7 M urea, 10% acrylamide, 0.33% bisacrylamide in TBE) so that the T-tracts would be aligned.

3.3 Results and Discussion

While it is clear from this study of T_{11}-tracts (Chapter 2) and the previous one of various sized T-tracts in a section of promoter DNA (8) that the nucleosome can dramatically alter CPD formation in T-tracts, it is not clear to what extent that this is due to the histone proteins or to DNA bending. In a previous study, lambda repressor was used to constrain the formation of a protein-free DNA loop and show that DNA bending alone can modulate CPD formation (3). In that study, the site of maximum of CPD formation coincided with the site of maximum DNase I cleavage, which has been shown to occur 1-2 bases to the 3'-side of the dyad in a nucleosome phased by TG motifs (9). The exact shape, curvature, and rotational phasing of the DNA in the lambda repressor system is unknown, however, and therefore cannot be directly correlated with nucleosome core particles. We therefore, decided to investigate CPD formation in the T_{11}-tract of an 80 bp circular DNA section of the same rotationally phased sequence we used in the nucleosomal DNA studies to mimic one turn of the nucleosomal DNA. In the nucleosome crystal structure 1KX5.pdb, one complete turn of DNA around the nucleosome corresponds to about 79 bp (10). We included one more bp in our sequence so as not to interrupt the 10 bp repeat of the TG motifs used to rotationally phase the DNA (Figure ***3.1***).

The 80-mer single strand circular DNA complementary to the T_{11}-tract was prepared by ODN templated-directed ligation of a synthetic single strand 80-mer. The circular DNA was isolated and hybridized (Figure ***3.2***) to complementary strands 28, 41, 50, 60, 70, and 80 nucleotides in length with the T_{11}-tract near the center of each sequence (Figure ***3.1***). We expected that the single-stranded section of DNA would generate a bending force on the double strand DNA (dsDNA) section, when the length of the dsDNA segment exceeded the length of the remaining single strand, much like in a molecular vise (11). We therefore, expected that the DNA duplex in hybrids formed with the longer DNA would become increasingly bent with length, and that this would be reflected in the CPD distribution in the T_{11}-tract. To determine this, the hybrid DNA microcircles were then UVB irradiated at 0 and 40 °C, and then assayed for CPDs by T4-pdg (Figure ***3.3*** and Figure ***3.4***).

At 0 °C, the pattern of CPD formation for the 80-mer microcircle hybridized to the 28 bp DNA was similar to that for the 41 bp or 150 bp free DNA in that the maximum CPD yield was at the 3'-end, except that the distribution of peaks was broader. As the length of the duplex section increased to 41 and 50, the CPD pattern began to shift slightly towards the 5'-end with maxima at +2.0 and +1.4, respectively, relative to the 0 position corresponding to where the dyad axis would be in the nucleosome. When the segment reached 60, 70, and 80 bp, the CPD maxima shifted to the middle of the T tract, with maxima at positions -0.8, 0, and -0.5, respectively, which are close to the average of -0.9 observed for the nucleosome-bound DNAs (Figure ***3.5***). In addition, the standard deviation of the Gaussian fits became narrower, decreasing linearly from 2.5 for the 28-mer to 1.5 for the 80-mer, which was also close to the average of 1.4 seen for the nucleosome (Figure ***3.5***B). The close correlation between what was observed in the nucleosome and in the microcircle suggests that the microcircle is adopting an average structure with the same curvature

and rotational phase as in the nucleosome, and that these two parameters are sufficient to explain the modulation of CPD formation by the nucleosome.

At the higher temperature of 40 °C, the in phase 28-mer hybrid microcircle gave a fairly even pattern of CPDs, with a bias for the 5-side (Figure ***3.3*** and Figure ***3.4***), as was observed for the T_{11}-tracts of the nucleosome-free SHL 0 and -6 DNA duplexes at the same temperature (Figure ***2.14***B). The CPD pattern for the 41-mer hybrid microcircle could be fit to a Gaussian with a maximum at -3.3, whereas the maxima for the 60-, 70-, and 80-mer hybrid microcircles moved increasingly towards the center with maxima at -2.4, -1.5 and -1.4 (Figure ***3.5***A). The position of maximum CPD formation at 40 °C came within approximately one base to the 5'-side of that observed at 0 °C in the 80-mer hybrid. Again this may be attributed to the higher cleavage efficiency at 40 °C which resulted in a greater percentage of multiple cleavages that favors shorter end-labeled fragments. The 50-mer hybrid microcircle did not follow the general trend and for reasons not understood at this time had a maximum at -0.6 at 40 °C, which was much more towards the 3'-end than for any of the other microcircles. The standard deviation of the Gaussian fits is greater at 40 °C than at 0 °C, and in contrast to 0 °C, generally increased rather than decreased on going from the 41-mer to the 80-mer hybrid microcircles (Figure ***3.5***B), possibly owing to the more extensive cleavage.

The behavior of our fully duplex 80-mer microcircle is consistent with previous studies showing that covalently closed circular DNAs as small as 70 base pairs with the lowest superhelical density can adopt circular forms without kinking as judged from cryo-EM and enzymatic probe studies. By using sensitivity to BAL31 and S1 digestion, DNAs of 84-86 bp in length were found to form kink-free covalently closed circular DNAs (12). Because the fully complementary 80-mer DNA that we used contained a nick, it is possible that it could have kinked

at this site. Kinking at one end of a circular DNA, however, would increase the curvature of the opposite end and would be expected to lead to a second kink opposite the first kink (13). We see no evidence of such a kink that would have caused significant disruption to the CPD pattern in the T_{11}-tract which is almost directly opposite the nick in the 80-mer circular DNA duplex. Likewise, a cryo-EM study of 94 bp DNA circle containing nicks at opposite ends showed no significant evidence of such double kinking (14). T-tracts themselves have been found to be highly flexible by single molecule experiments that probe looping (15) and DNA cyclization (16).

To verify that the pattern of CPD formation was related to the rotational phasing, and not some other effect, we constructed am 80-mer nicked duplex in which the T_{11}-tract was out of phase by one half a turn (Figure ***3.6***). When this microcircle was irradiated at 0 °C, the CPD pattern completely changed. As expected, CPD formation was minimal at the center of the T-tract and maximal at the ends. When irradiated at 40 °C, the CPD was more evenly distributed, but still favored the ends.

3.4 Conclusion

We have shown that the pattern of CPD formation in nucleosomes can be reproduced with a nicked circular 80-mer DNA, corresponding to a full turn of DNA around the nucleosome that contains phased TG-motifs. The great similarity between the pattern of CPD formation in the nucleosome and in the microcircle suggests that the DNA in the microcircle is adopting the same rotational phase and curvature as in the nucleosome, and is not freely rotating about the helical axis or kinking. Such a rotationally phased unkinked 80-mer mini-circular duplex should therefore, be a good model for assessing the effect of DNA bending on hydrolytic deamination of cytosine containing CPDs, as well as other reactions of nucleosomes. The ability of the T_{11}-tract to smoothly bend

within the 80-mer microcircle is in accord with previous studies that found that T-tracts enhanced the bendability of DNA (16). The bend-dependent pattern of CPD formation within the T_{11}-tract might also be useful for reporting on the magnitude and phasing of bends in looped DNA structures in vitro and in vivo. Rotationally phased mini-circular DNA's might also find important applications for nano-scale construction and assembly of spatially organized materials.

3.5 Acknowledgements

We thank Vincent Cannistraro for advice and help with various experimental procedures. We also thank Stephen Lloyd for T4-pdg. Research reported in this chapter was supported by the National Cancer Institute of the National Institutes of Health under award number R01CA40463.

3.6 References

1. Gale, J.M. and Smerdon, M.J. (1988) Photofootprint of nucleosome core DNA in intact chromatin having different structural states. *Journal of Molecular Biology*, **204**, 949-958.

2. Pehrson, J.R. (1989) Thymine dimer formation as a probe of the path of DNA in and between nucleosomes in intact chromatin. *Proceedings of the National Academy of Sciences*, **86**, 9149-9153.

3. Pehrson, J.R. and Cohen, L.H. (1992) Effects of DNA looping on pyrimidine dimer formation. *Nucleic Acids Research*, **20**, 1321-1324.

4. Song, Q., Cannistraro, V.J. and Taylor, J.-S. (2014) Synergistic modulation of cyclobutane pyrimidine dimer photoproduct formation and deamination at a TmCG site over a full helical DNA turn in a nucleosome core particle. *Nucleic Acids Research*, **42**, 13122-13133.

5. Ikehata, H. and Ono, T. (2011) The mechanisms of UV mutagenesis. *Journal of Radiation Research*, **52**, 115-125.

6. Pfeifer, G.P., You, Y.H. and Besaratinia, A. (2005) Mutations induced by ultraviolet light. *Mutation Research/Fundamental and Molecular Mechanisms of Mutagenesis*, **571**, 19-31.

7. Ryabinina, O.P., Minko, I.G., Lasarev, M.R., McCullough, A.K. and Lloyd, R.S. (2011) Modulation of the processive abasic site lyase activity of a pyrimidine dimer glycosylase. *DNA Repair*, **10**, 1014-1022.

8. Schieferstein, U. and Thoma, F. (1996) Modulation of cyclobutane pyrimidine dimer formation in a positioned nucleosome containing poly(dA.dT) tracts. *Biochemistry*, **35**, 7705-7714.

9. Li, Q. and Wrange, O. (1993) Translational positioning of a nucleosomal glucocorticoid response element modulates glucocorticoid receptor affinity. *Genes and Development*, **7**, 2471-2482.

10. Davey, C.A., Sargent, D.F., Luger, K., Maeder, A.W. and Richmond, T.J. (2002) Solvent mediated interactions in the structure of the nucleosome core particle at 1.9 a resolution. *Journal of Molecular Biology*, **319**, 1097-1113.

11. Fields, A.P., Meyer, E.A. and Cohen, A.E. (2013) Euler buckling and nonlinear kinking of double-stranded DNA. *Nucleic Acids Research*, **41**, 9881-9890.

12. Du, Q., Kotlyar, A. and Vologodskii, A. (2008) Kinking the double helix by bending deformation. *Nucleic Acids Research*, **36**, 1120-1128.

13. Lionberger, T.A., Demurtas, D., Witz, G., Dorier, J., Lillian, T., Meyhofer, E. and Stasiak, A. (2011) Cooperative kinking at distant sites in mechanically stressed DNA. *Nucleic Acids Research*, **39**, 9820-9832.

14. Demurtas, D., Amzallag, A., Rawdon, E.J., Maddocks, J.H., Dubochet, J. and Stasiak, A. (2009) Bending modes of DNA directly addressed by cryo-electron microscopy of DNA minicircles. *Nucleic Acids Research*, **37**, 2882-2893.

15. Johnson, S., Chen, Y.J. and Phillips, R. (2013) Poly(dA:dT)-rich DNAs are highly flexible in the context of DNA looping. *PLoS One*, **8**, e75799.

16. Vafabakhsh, R. and Ha, T. (2012) Extreme bendability of DNA less than 100 base pairs long revealed by single-molecule cyclization. *Science*, **337**, 1097-1101.

3.7 Figures

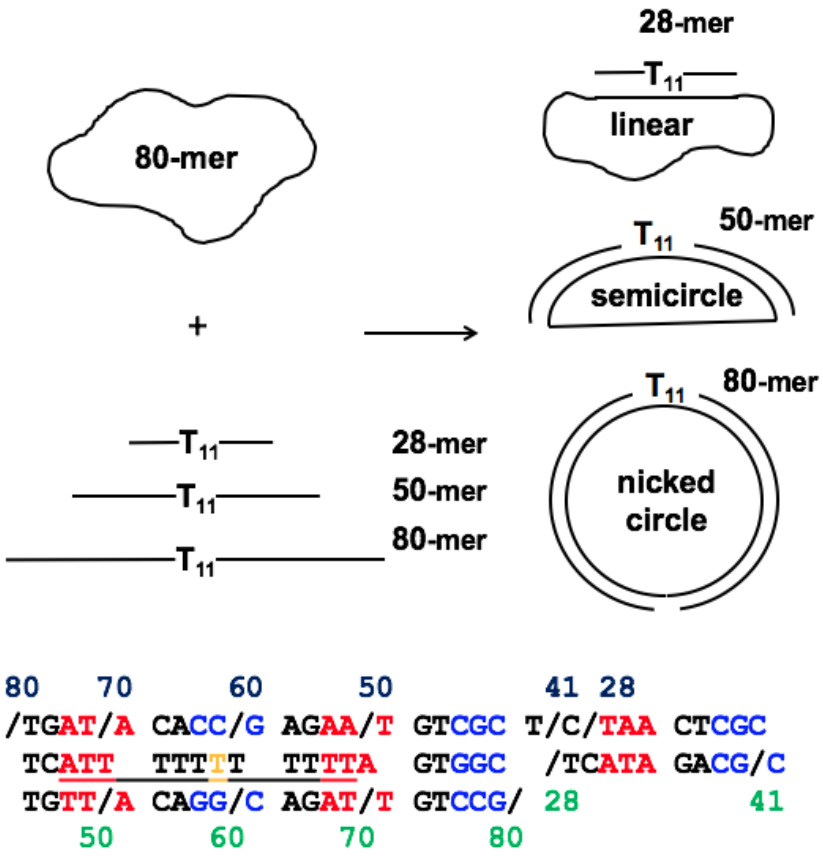

Figure 3.1: Scheme to determine the effect of bending on CPD yield in T_{11}-tracts. A single strand 80-mer corresponding to one full turn of the central section of the 150-mer nucleosomal DNA that is complementary to the T_{11}-tract was circularized by ligation using a ligation scaffold. The 80-mer was then annealed to increasing lengths of 5'-radiolabeled complementary strand containing a centrally located T_{11}-tract to form DNAs with different degrees of bending because of the length of the rigid duplex strand and flexible single strand. The sites of the 5'- and 3'-ends of the n-mers are indicated with a forward slash. Other features are as described in the Figure 2.3 caption.

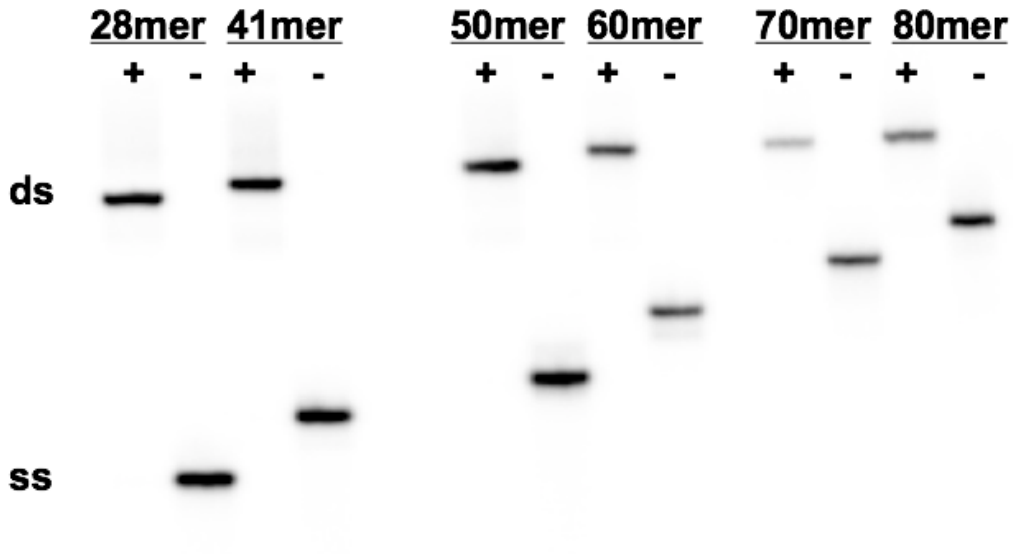

Figure 3.2: Quantitative hybridization of single strand oligomers to circular DNA. Annealing was done with radiolabeled single strand (ss) oligomers (-) to 80-mer linear circular DNA (+) at a ratio of 1:20 to give double stranded circular duplex (ds).

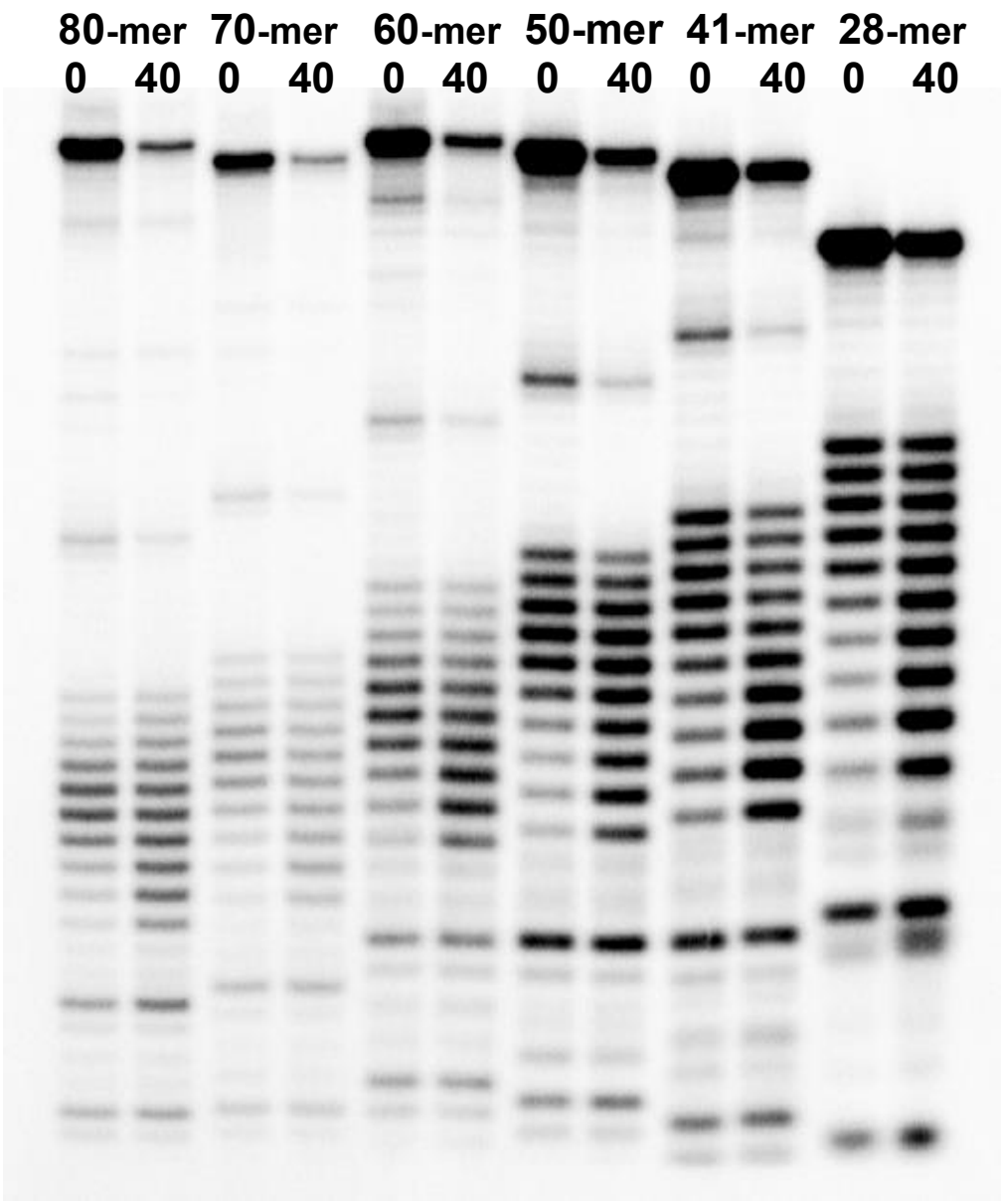

Figure 3.3: PAGE assay of CPD formation in the minicircular DNAs as a function of duplex length and temperature. The radiolabeled minicircular DNAs were irradiated with UVB light at 0 °C and 40 °C, treated with T4-pdg, and electrophoresed. The samples were loaded at different time intervals, so as to have the T_{11}-tract cleavage bands appear at roughly the same location in the gel.

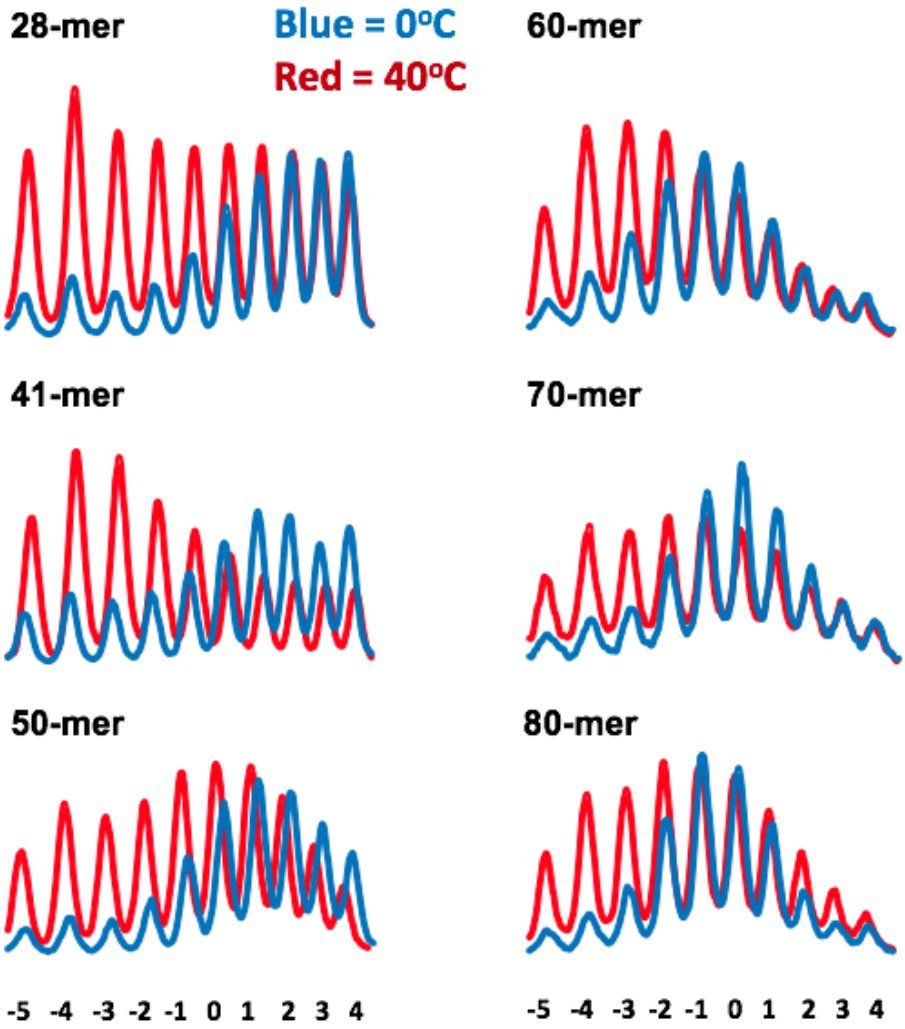

Figure 3.4: Frequency of CPD formation as a function of duplex strand length and temperature. The lanes in Figure 8 were scanned and the CPD formation patterns for the T_{11}-tracts for a given duplex length at 0 °C (blue) and 40 °C (red) are superimposed on each other.

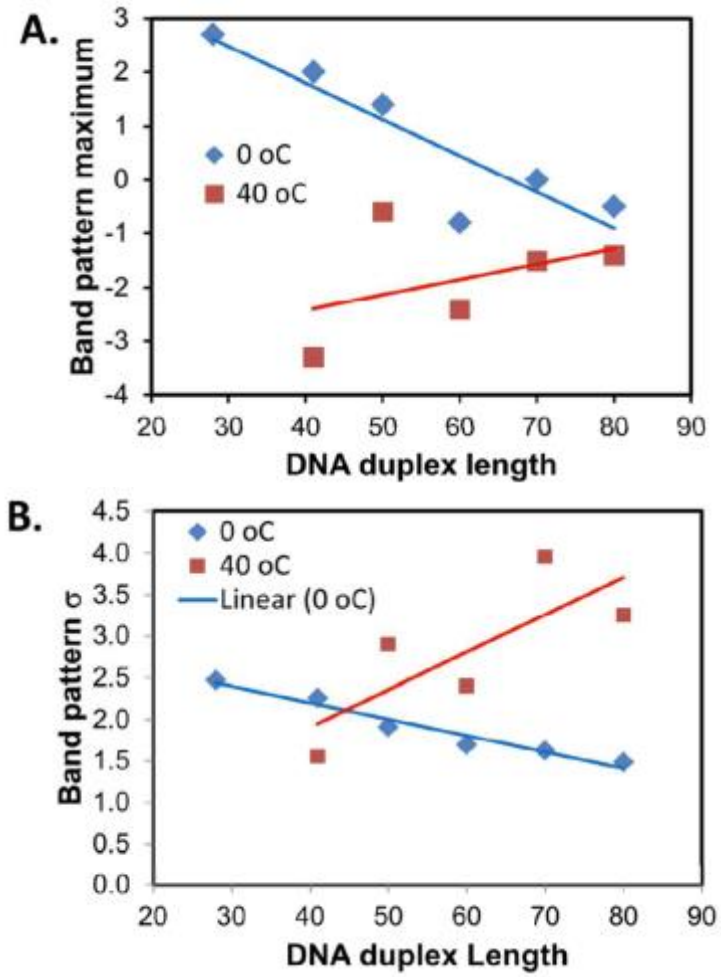

Figure 3.5: Plots of the maximum peak position and standard deviation of the Gaussian fits to the CPD cleavage pattern for the circular DNAs. A) A plot of the position of maximum CPD formation from fitting the cleavage patterns to a Gaussian function. B) The standard deviation of the Gaussian function. Data in blue are for 0 ^{o}C, data in red for 40 ^{o}C.

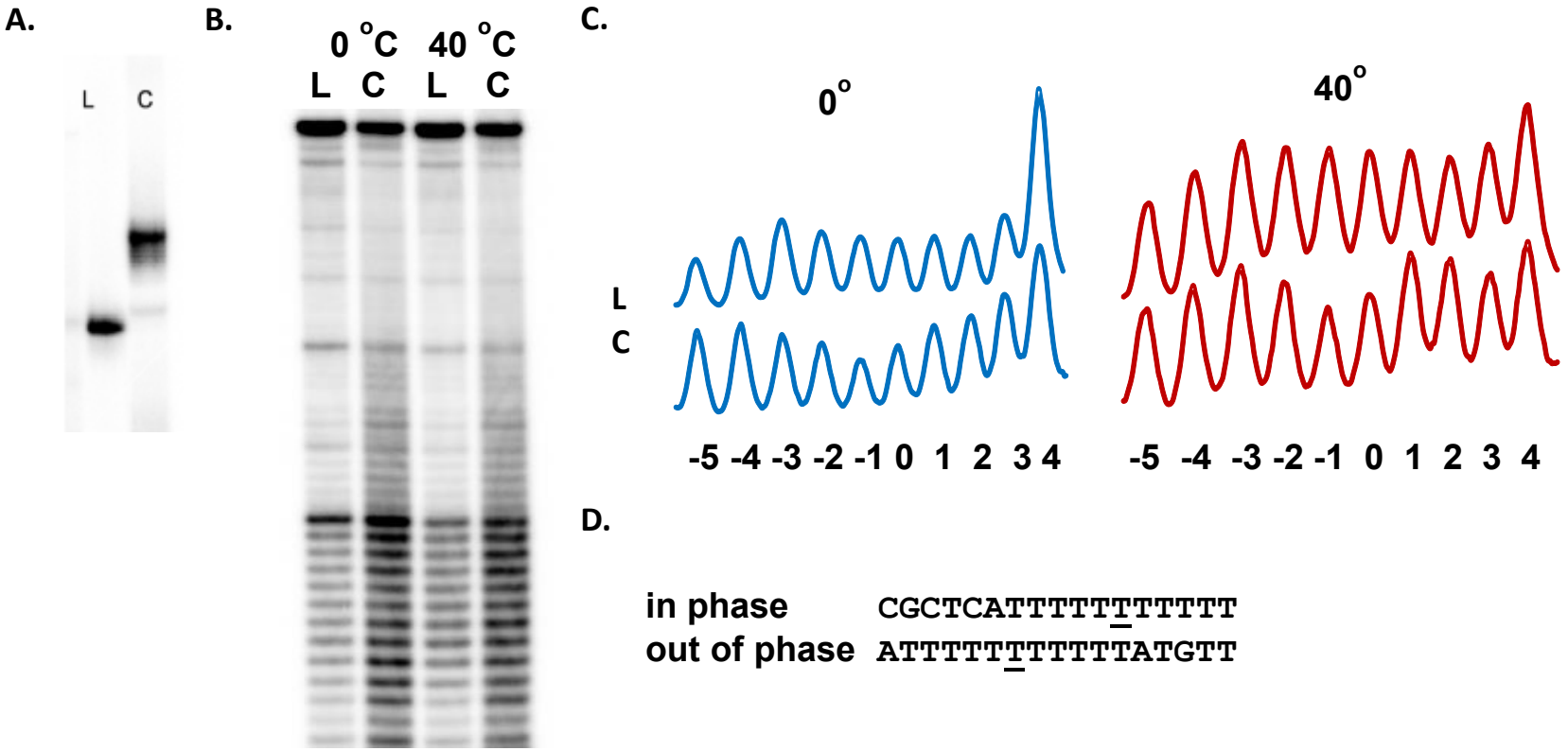

Figure 3.6: Shifting of the T_{11}-tract by half a turn of DNA shifts the CPD formation pattern towards the 5' and 3' ends. A) Gel electrophoresis of out-of-phase radiolabeled 80-mer linear duplex (Lane L) and 80-mer circular duplex (Lane C)B) Radio image of a PAGE gel of T4 pdg treated linear (L) and circular (C) forms of an 80-mer duplex containing an out of phase T_{11}-tract that were irradiated at 0° and 40 °C for 40 min and 20 min, respectively. C) Traces of the bands in the gel showing a shift of the bands in the out of phase circular form to the 5'- and 3'-ends compared to the major bands being in the center for the in phase form (Figure 3.4). D) The 80-mer sequence with an out of phase T_{11}-tract was constructed by changing the section of the in phase sequence shown to the out of phase sequence shown below it.

Chapter 4 Modulation of Cyclobutane Pyrimidine Photodimer Formation and Deamination in $d(TC)_6$ and $d(TC)_{35}$ Tracts in a Nucleosome Core Particle [1]

4.1 Introduction

The formation of cyclobutane pyrimidine dimers (CPD) by ultraviolet (UV) light speeds up C-to-T mutations in p53 tumor suppressor genes associated with skin cancers. The initial C or 5-methly-C (^{m}C) in CPD rapidly deaminates into U or T within hours to days (1), directing the insertion of A in the opposite strand by polymerase η (2), and thus leads to characteristic C-to-T or CC-to-TT UV signature mutations associated with skin cancers (3) (Figure ***4.1***). Chemically, C or ^{m}C deamination occurs in three steps under acidic conditions: protonation of C (or ^{m}C) at N3 position, attack at C4 by a water molecule, and loss of ammonia to form a U (or T). In free DNA duplex, the deamination process depends on sequence context, temperature and buffer conditions. For example, the deamination rate of T=^{m}C CPDs is approximately 25-fold faster when flanked directly by G's than by A's, T's or C's on the 3'-side, probably owing to catalysis by the O6 group of guanine (1). Furthermore, high salt concentrations slow down the deamination presumably by stabilizing the duplex structure and thereby inhibiting protonation of C and addition of water. Higher temperature or more acidic pH conditions create a favorable reaction environment and thus lead to faster deamination. In nucleosomes, another layer of complexity is added. Besides the factors mentioned above, deamination is also influenced by DNA structure and protein-DNA interactions that may determine DNA flexibility and reactivities. In regard to rotational setting, a

[1] All contents in this chapter are in manuscript preparation and have not been published.

12-fold difference in deamination rate was found between inward and outward facing T=^{m}CGs over a full helical turn in reconstituted nucleosomes (4), whereas a smaller fold change was determined from an *in vivo* study of deamination at TCG sites within the FOS promoter in HeLa cells (5).

Poly d(TC) tracts are highly dispersed and abundant sequences in eukaryotic genomes and are involved in various biological processes such as DNA synthesis and transcription (6,7). Nothing is known, however, about deamination at CT=CT or TC=TC sites in general, nor in nucleosomes. One early study, determined the deamination half-life of C-containing CPDs in an *E.coli* plasmid without attention to sequence context, and concluded that the deamination occurs rapidly with a half-life of about 5 h at 37 °C (8). In another study, Pfeifer and coworker examined the deamination of tripyrimidine sites within exon 8 of human p53 gene, and found 10-30% deamination after 24 h for most sites (9). However, in that study, the possible effect of chromatin structure was not considered. Recently, two studies in our group discovered that the deamination rate varied with rotational position of TCG or T^{m}CG sites in a nucleosome core particle and was greatest for outside facing positions (4,10).

To efficiently study the deamination rates of highly enriched TC repeats and their correlations with nucleosome positioning at the same time, we designed nucleosomal DNA containing two poly d(TC) sequences, one with a poly(TC)$_{6}$ and one with a poly(TC)$_{35}$ tract. With the help of TG bending motifs (11), these sequences were incorporated into nucleosome core particles (NCPs) *in vitro*, with specific rotational orientation, and sampling half of all superhelical locations. We will show that nucleosomes modulate CPD deamination, but less strongly than for TCG sites. Also in contrast with TCG sites, for which the sites of preferred CPD formation (also most flexible sites in conformation) coincided with the sites of fastest deamination, we found an

opposite correlation with TCT sites. One possible explanation is that the deamination rate for TCG sites depends on the orientation of the G, whereas with TCT sites, deamination depends on water reactivity of the C.

4.2 Material and methods

4.2.1 Materials

Oligodeoxynucleotides (ODNs) were purchased from Integrated DNA technologies (IDT). T4-pdg was prepared from a clone provided by Stephen Llyod as previously described (12). Photolyase was prepared from a clone provided by Aziz Sancar as previously described (13).

4.2.2 Preparation of nucleosomal DNA containing d(TC)$_6$-tract on dyad superhelix

The 168-bp parental nucleosomal DNA duplex was synthesized by hybridization of 96-mer and 95-mer ODNs (IDT) to form a 23-bp duplex at their 3'-ends by slowly cooling from 95 ℃ to room temperature in 50 mM NaCl, and extended by 3' to 5'-exo$^-$ Klenow Fragment (New England BioLabs) in 50 mM NaCl, 10 mM Tris-HCl (pH 7.5), 10 mM $MgCl_2$, 100 μM dNTPs and 1 mM dithiothreitol (DTT), for 30 min at 37 °C. The 168 bp duplex DNA was then digested by EcoRI (Promega) in 90 mM Tris-HCl (pH 7.5), 50 mM NaCl and 10 mM $MgCl_2$, for 30 min at 37 °C and cloned into pBlueScript II SK- vector DNA (Agilent) that had been restricted with EcoRI and then dephosphorylated with calf intestinal phosphatase (CIP) (New England BioLabs) in 100 mM NaCl 50 mM Tris-HCl (pH 7.5), 10 mM $MgCl_2$ and 1 mM DTT, for 30 min, at 37 °C, to prevent re-circularization. The cloning was performed using 1:3 and 1:5 molar ratios of vector:insert with T4 DNA ligase and 1 mM ATP at 10 °C overnight. The pBS vector with the d(TC)$_6$ insert was then transfected into TOP10 chemically competent *E.coli* cells (from Invitrogen) and plated on solid

LB media (15 g/L agar, 25g/L LB broth, 100 μg/mL ampicillin). A clone containing the desired insert was identified by restriction analysis and the sequence verified by DNA sequencing. The 150-bp nucleosomal DNAs were prepared from this plasmid by PCR amplification with LongAmp Taq DNA polymerase (New England Biolabs) for 35 cycles followed by phenol:chloroform:isopropanol (PCI) 25:24:1 extraction and ethanol precipitation. A typical 100 μL PCR reaction contained 0.5 μM of forward and reverse primers, 300 μM of dNTPs, 300 ng template DNA, and 4 μL of DNA polymerase ((2.5 U/ μL) in supplied buffer.

4.2.3 Preparation of nucleosomal DNA containing d(TC)$_{35}$-tract

The 150-mer single strand DNA containing d(TC)$_{35}$ at the 5'end was prepared by equimolar ligation of 3 short ODNs with T4 DNA ligase and 1mM ATP in the presence of 2 DNA scaffolds at 10 °C overnight and purified by denaturing polyacrylamide gel electrophoresis (PAGE) on a 10% acrylamide 0.33% bisacrylamide gel in 7 M urea in 100 mM Tris-borate 2 mM EDTA (TBE). Prior to ligation, 10% of the 6 μg of d(TC)$_{35}$-containing ODN was 5'-^{32}P labeled with [γ-^{32}P] ATP (Perkin Elmer) by T4 polynucleotide kinase (Thermo Scientific). The final 150-mer product was purified from the gel by crush elution followed by PCI extraction and ethanol precipitation and then re-suspended in 100 μL of water. Single-round PCR synthesis was performed to produce a 150-bp DNA duplex. A 500 μL reaction mix also contained 1X LongAmp Taq buffer (New England BioLabs), 300 μM of dNTP, 10 μg of the P1 primer complimentary to the 3' end of the ligated sequence and 6 μL of polymerase (2.5 U/ μL). A single cycle (95 °C - 7 min, 58 °C - 40 min and 68 °C - 15 min) was performed before terminating the reaction with 1% SDS. The sample was then PCI extracted, ethanol precipitated and re-suspended in 60 μL of 15% glycerol and 50 mM NaCl, followed by a native PAGE (6% acrylamide, 0.2% bisacrylamide in 1×TBE) purification, and was then taken up in 200 μL of 50 mM NaCl for further use.

4.2.4 Nucleosome reconstitution

Nucleosome core particles (NCPs) were isolated and purified from chicken erythrocytes following a simplified procedure provided by Dr. Michael Smerdon. DNA duplex 150-mers corresponding to $d(TC)_6$ and $d(TC)_{35}$ were incorporated into the nucleosomes by a salt mediated exchange process. Briefly, 150 bp duplex was incubated with nucleosomes at various ratios in 300 µL of 2 M NaCl, 10 mM Tris-HCl, 5 mM EDTA at pH 7.5 and room temperature for 2 h, and then dialyzed against 50 mM NaCl, 10 mM Tris-HCl, pH 7.5, at 4 °C overnight. The reconstituted NCPs were recovered from the dialysis tubing and equilibrated at 54 °C for 2 h to fix the nucleosomal phasing. The reconstituted particles were assayed by native PAGE (6% acrylamide, 0.2% bisacrylamide in 1×TBE), and the ratio of nucleosome-bound DNA to free DNA was quantified by Quantity One software.

4.2.5 Hydroxyl radical footprinting and Maxam-Gilbert G sequencing

Sodium ascorbate, $Fe(NH_4)_2(SO_4)_2 \cdot 6H_2O$ and H_2O_2 (15 mM, 1.5 mM, and 0.18% final concentrations respectively) were quickly added to 100 µL of the nucleosome-bound DNA sample in 50 mM NaCl, 10 mM Tris-HCl, pH 7.5 reaction buffer with gentle vortexing after the addition of each reagent. The reaction was incubated for 120 s at room temperature and quenched by addition of glycerol and EDTA solution to final concentrations of 5% and 12 mM, respectively. The samples were electrophoresed on a native PAGE (6% acrylamide, 0.2% bisacrylamide in 1×TBE), and gel sections containing the nucleosome bands were excised, crushed, and soaked in 1% SDS and 0.2 M NaCl. The proteins were then PCI extracted, and the DNA was ethanol precipitated. To align the bands, a Maxam-Gilbert G sequencing reaction was carried out on the nucleosome-free DNA sample in 50 mM cacodylate, 50 mM NaCl, 5 mM EDTA at pH 8.2. For a 100 µL reaction, 1µL of dimethyl sulfate was added to initiate the reaction. After 120 s of

incubation at room temperature, 60 µL of mercaptoethanol was added to quench the reaction. The DNA was ethanol-precipitated and the resulting pellet was solubilized in 100 µL of 1 M piperidine, followed by 5 min heating at 90 °C and evaporating to dryness at 60 °C.

4.2.6 T4-pdg assay for CPDs

DNA substrates were irradiated with 302-nm UVB light (Spectroline TR-302) at 0 °C for a dose of 36 kJ/m^2. Nucleosome-bound DNA was first PCI extracted twice, and ethanol-precipitated twice. The DNA samples were incubated with 8 µg of T4-pdg in 10 mM Tris-HCl, 50 mM NaCl, 5 mM EDTA, pH 7.5 for 30 min at 37 °C to and then heated at 90 °C in 1M piperidine for 5 min to insure complete elimination of the sugar ring. Residual piperidine was evaporated by heating at 60 °C *in vacuo*. The resulting pellets were brought up in 20 µL formamide-dye and loaded on a 10% denaturing PAGE (7 M urea, 10% acrylamide, 0.33% bisacrylamide in 1×TBE).

4.2.7 Deamination assay

Nucleosomes and DNA in deamination buffer (10 mM Tris-HCl, 50 mM NaCl, 0.5 mM EDTA, pH 7.2) were irradiated as described above. After irradiation, the sample was placed in a 37 °C water bath for the deamination time course. Aliquots of 50 µL were taken at time intervals and then quickly frozen before storage at -80 °C. After the last time point was collected, nucleosome samples were PCI extracted twice, and ethanol-precipitated twice. Then all samples were brought up in 100 µL of the photolyase reaction mix (10 mM Tris-HCl, 50 mM NaCl, 5 mM EDTA, 5 mM DTT, pH 7.5). The completion point for deamination was determined with a separate aliquot after irradiation where the free DNA was isolated from the nucleosome sample as described above and brought up in 3 mM of 2-(N-morpholino) ethanesulfonic acid (Mes), 50 mM NaCl and 0.5 mM

EDTA, pH 6, at 55 °C for 48 h. After deamination, the sample was ethanol precipitated and re-suspended in 100 μL of the photolyase reaction mix.

4.2.8 Photoreversion and uracil-DNA glycosylase cleavage

Photolyase (2 μg) was added to each 100 μL sample followed by pre-incubation in the dark for 7 min at room temperature. The samples were then laid out underneath a 352-nm light for 1 h to catalyze the photoreversion. The reaction was terminated with addition of 1% SDS before PCI extraction twice and ethanol precipitation twice. Each pellet was re-suspended in 100 μL of Uracil-DNA glycosylase (UDG) buffer (supplied) and 2 μL of UDG (New England BioLabs), and then incubated at 37 °C for 1 h. the reaction was then stopped with 1% SDS before PCI extraction and ethanol precipitation. Each sample was re-suspended in 1M piperidine and heated at 90 °C for 5 min to insure complete elimination of the sugar ring. Residual piperidine was evaporated by heating at 60 °C *in vacuo*. The resulting pellets were brought up in 20 μL formamide-dye and loaded on a 10% denaturing PAGE (7 M urea, 10% acrylamide, 0.33% bisacrylamide in 1×TBE).

4.2.9 Rate constant calculation

The gel bands corresponding to deamination sites were integrated following phosphorimaging by the BioRad Quantity One program. The deamination rate constants were then obtained from the slope of a linear least squares fit of the log of the fraction of remaining C versus deamination time, $\mathrm{Ln}\,(1-U_t/U_\infty) = -kt$, where t is deamination time, k is deamination rate constant, U_t is amount of deaminated C at time t, U_∞ is total amount of C obtained from complete deamination. Deamination half-life equals to Ln (2/k), error bars were calculated by linear least squares curve fitting function.

4.3 Results and Discussion

4.3.1 Design and synthesis of DNA substrates

The main purpose of this study was to determine the deamination rates for C-containing CPDs in $(TC)_n$ tracts in a nucleosome to gain more insight about the effect of chromatin structure on the frequency of mutations rising from a deamination-bypass mechanism. Nucleosome core particles were designed to contain TC repeats at various superhelix locations (SHLs). In our first design, a $d(TC)_6$-tract was centered on the dyad to cover all rotational positions at SHL 0. To translationally and rotationally position the CPD sites, TG bending motifs, $(T/A)_3NN(G/C)_3NN$, were incorporated every 10 bp in the flanking DNA (11,14). With this motif, bending is toward the major groove at the central GC base pair of the $(G/C)_3$ sequence and toward the minor groove at the central TA base pair of the $(T/A)_3$ sequence (Figure ***4.2***A). In this way, the $d(TC)_6$ tract spans nucleotide positions from +6 to -5 rotational (Figure ***4.2***C), with the nucleotides to the 5'-side assigned negative numbers, and to the 3'-side, positive numbers. EcoRI digestion sites were engineered into the ends of the sequence for cloning, with six extra bp's added to the end to ensure efficient digestion. The designed 168-mer DNA was prepared by primer extension of two overlapping 95-mer and 96-mer synthetic ODNs (Table ***4.1***). The EcoRI digested 168-mer was cloned into the EcoRI site of a pBlueScript SK- vector. Individual clones were verified by sequencing (Figure ***4.3***).

In our second design, a 70-bp long $poly(TC)_{35}$ tract was incorporated into a 150-bp nucleosomal DNA by scaffold-directed ligation (Figure ***4.2***B, Table ***4.1*** and Figure ***4.4***). The TG bending motif was used again to rotationally position the $d(TC)_{35}$ tract from nucleotides -7 to -76, covering SHLs from -1 to -7 along a nucleosome core particle (Figure ***4.2***C).

4.3.2 Nucleosome reconstitution and assay by hydroxyl radical footprinting

To determine the optimal conditions for NCP reconstitution, the 150-bp DNA duplexes were 5'-end labeled and titrated with NCPs isolated from chicken erythrocytes under the high salt conditions that promote nucleosomal DNA exchange, followed by lowering of the salt concentration and thermal annealing (15). Electrophoresis on a native gel showed that about 95% of both 150-mer DNAs could be incorporated into a single NCP band at an NCP:DNA ratio of 600:1 (Figure ***4.5***). To determine the rotational and translational setting of the DNA on the nucleosome, the reconstituted NCPs were subjected to HO• footprinting. The HO• cleavage pattern exhibited a pronounced 10–11 bp periodicity, indicating that the 150-mer DNAs were rotationally phased. The cleavage pattern was mapped onto the DNA sequence by alignment with the Maxam-Gilbert G reaction bands (Figure ***4.6***B and Figure ***4.14***A). The HO• footprinting pattern was used to verify the rotational setting of the TC-tract based on the expectation that the periodic modulation of the HO• cleavage pattern would only be apparent where the DNA is in direct contact with the histone core. Hydroxyl radicals preferentially cleave DNA at sites where the sugar phosphate backbone is most exposed and faces away from the histone surface, and is inhibited where it faces the histone surface. For the poly$(TC)_6$-tract on dyad position, one can clearly see the expected seven repeats of HO• cleavage bands above (to the 3'-side of) the band at the TC-tract region, with the last band appearing at the edge of the large uncleaved band corresponding to full length DNA. For the d$(TC)_{35}$-tract, we were worried that, with flanking TG motifs on only one side of the TC repeats, that the long 70-bp TC-tract would not be fully bent around the nucleosome. Nevertheless, the HO• cleavage pattern shows 14 clear repeats, indicating a complete rotational phasing of the full-length DNA. These results, coupled with the observation of a single nucleosomal band in the electrophoresis gel following nucleosomal DNA exchange (Figure ***4.5***) indicates that the 150-mer

DNA's were all largely adopting a single, centered translational position that maximizes histone–DNA contacts. Had the DNA shifted by 10 bp to either side, contact between one turn of the helix and the nucleosome would have been lost, which would be thermodynamically unfavorable. The maximum of HO• cleavage band is shifted by about two nucleotides to the 3'-side of that for CPD formation, which is consistent with what was observed for CPD formation in a T_{11}-tract in a similarly positioned nucleosome core particle (16).

4.3.3 CPD formation in free and nucleosomal DNA containing d(TC)$_6$-tract

The site of CPD formation was assayed by T4-pdg cleavage, a glycosylase that cleaves the the DNA at the 5'-pyrimidine of the CPD. This enzyme first hydrolyzes the N-glycosidic linkage of the 5'-pyramidine of the CPD, and then causes strand cleavage (Figure ***4.6***A) by an associated lyase activity. The lyase first yields a 5'-phosphate-terminated end by a β-elimination reaction, which is followed by formation of a 3'-phosphate terminated end by a slower δ-elimination reaction (17). In a previous study of CPDs formed in T_{11}-tract (16), we found that the CPDs in free DNA duplexes showed essentially the opposite intensity pattern compared to that in nucleosome-bound DNA. In free DNA, CPDs form with highest frequency at the 3' end, decreasing to a minimum in the center, and increasing slightly at the 5' end, as observed by others in T-tracts of various lengths (18,19). In nucleosome-bound DNA, the band pattern changed dramatically, with the highest CPD frequency in the middle of the T-tract and tapering off towards the 5' and 3' ends. Unlike the T_{11}-tract, the d(TC)$_6$-tract showed an even distribution of CPDs in the free DNA, which is probably because TC tracts do not adopt the unique structure of T-tracts in solution at low temperature, but in nucleosomes, they both showed the same CPD pattern suggesting that they have similar conformation and reactivity (Figure ***4.9***A).

We also compared the CPD yields in d(TC)$_6$-tract with previous studies at TCG sites (Figure ***4.10***) (4). Both results showed the same CPD pattern with highest CPD yield at position +2 that corresponds to an outward-facing DNA backbone, and decreasing yields towards the ends. Despite the difference between the 3'-flanking bases, the CPD yields showed great similarity between TCT and TCG sites, suggesting that the CPD formation is irrelevant with sequence context.

Next, we compared individual C-containing CPD yields in free and nucleosome-bound d(TC)$_6$-containing DNA, by normalizing all yields to the T=C CPD formed between -10 and -11, which had the same yield in DNA and in an NCP as determined in a previous study (16). It can be clearly seen from Figure ***4.6***B and Figure ***4.8*** that a T=C CPD forms more frequently than a C=T CPD in free DNA with about a 1.5-fold difference at all positions. A similar difference between the yields for CPD formation at TC and CT sites in AT=^{m}CA and A^{m}C=TA in duplex DNA have also been observed (1). In nucleosomes, the relative CPD yield for the TC and CT sites in the d(TC)$_6$-tract varies from 0.6- to 2.4-fold depending on the rotational positions (Table ***4.2***). These differences can be understood to result from the fact that the position of the CPDs containing the same C differ in position by one nucleotide, leading to a shift in the CPD formation pattern.

4.3.4 Deamination of cytosine in CPDs in a d(TC)$_6$-tract

To determine the effect of the nucleosome on the deamination rate of the C-containing CPDs, we used a combined enzymatic electrophoresis assay that detects deamination through cleavage at uracils by uracil DNA glycosylase (UDG), following photoreversion of the CPDs by DNA photolyase. Although T4-pdg assays can distinguish between CPD formation at T=CT and TC=T sites, because they give different length products, UDG cannot distinguish between a uracil having arisen from a T=CT and TC=T CPD. Therefore, we decided to use the combined yields of CPDs

at the T=CT and TC=T sites in our analysis of deamination rates as both CPDs contribute to the deamination of the same C. In the following analyses, if not otherwise specified, CPD yields at TCT sites will correspond to the combined yields as described. As can be seen in Figure ***4.9***A, the highest CPD yield in nucleosome-bound DNA appears near the middle of the TC-tract with a 4.3-fold increase as compared to that of free DNA. The average yield per site in nucleosome-bound DNA is two times greater that in free DNA, which is consistent with the previous finding in nucleosome-bound T_{11}-tract at SHL 0 (16).

The deamination rates of the cytosines in the C-containing CPDs were determined by tracking the conversion of C to U by an enzyme-coupled gel electrophoresis assay (Figure ***4.6***A). In the first step, free or nucleosome-bound 150-mer DNA duplexes were irradiated with 302 nm light at 0 °C to minimize deamination of the *cis-syn* CPDs produced. The samples were then incubated at 37°C and pH 7.2 to allow deamination to occur, and aliquots were removed at various time intervals. An additional aliquot was made to undergo complete deamination for the calculations of rates constants and half-lives, by lowering the pH to 6 and heating the sample at 55 °C for a minimum of 48 h. The aliquots were then phenol extracted to remove the histone proteins, ethanol precipitated and incubated with photolyase under black light to photorevert the *cis-syn* CPDs back to two individual pyrimidines. The samples were then treated with UDG to form an abasic site (AP site) at the site of the U. The AP site was then converted to a strand cleavage site by hot piperidine treatment. Non-photorevertible dipyrimidine photoproducts, such as (6–4) and Dewar DNA photoproducts, cannot be cleaved by UDG; though they can lead to strand cleavage upon hot piperidine treatment. If they were present, however, they would not result in deamination time dependent cleavage, and thus would not affect the deamination rate measurements. The

digested DNA was electrophoresed on a denaturing gel (Figure ***4.6***C) to separate the cleavage products, which are then quantified by phosphorimaging.

The rate constants for C deamination were determined from the slopes of lines fit to the natural log of the fraction of undeaminated cytosines in CPDs (Figure ***4.6***D and Figure ***4.7***) as described in the Experimental Procedures section. The initial amount of U present was non-zero and varied between samples, likely due to varying amounts of deamination that occurred during purification steps prior to photoreversion with photolyase, or due to piperidine cleavage of (6-4) or Dewar photoproducts. Table ***4.3*** summarizes the deamination half-lives, as well as relative CPD yields at nucleosomal SHL 0 and in free DNA. Although as large as a 4.3-fold increase was seen with CPD frequency in nucleosomes compared to free DNA at +2 position (Figure ***4.9***A), there was much less of a difference in the deamination rates between free and nucleosomal DNA (Figure ***4.9***B). The same was true for +4, 0, and -2 positions, where CPD yields in nucleosomes are 2.1-, 2.9-, and 1.6-fold greater than that in free DNA, while the corresponding differences in deamination rates were only 0.7, 1.0, and 0.9, respectively. Comparing the general pattern of relative CPD formation and deamination half-lives, one can clearly see greater modulation of CPD formation by rotational position than for deamination. These differences are also reflected in the relative standard deviations (RSD) for CPD formation and deamination (Table ***4.4***). There was a 38% RSD for CPD formation as a function of position in the nucleosome, compared to 8.3% in free DNA, which is an almost 5-fold difference. A RSD of 23% in deamination half-lives in the nucleosome, however is only 2-fold greater than in free DNA (RSD 10%). These results further confirm that nucleosome structure is capable of modulating CPD formation and deamination, but that the modulating effect is greater on CPD formation than deamination.

The rates of CPD formation and deamination appear to correlate in an opposite manner. In nucleosomes, CPD formation is maximal in the middle of the $d(TC)_6$ tract (+2 and 0 positions), tapering off towards 5' and 3' ends (Figure ***4.9***A and Figure ***4.12***). An opposite pattern can be seen for the deamination rate constants as a function of rotational position, where the slowest deamination coincides with that for maximum CPD formation (+2 and 0 positions) (Figure ***4.12***). In free DNA, the deamination rates, like CPD formation, are essentially independent of position (Figure ***4.9***). What is very curious is that the rates of T=C/C=T deamination do not follow the pattern of deamination observed for T=^{m}CG sites studied previously (Figure ***4.11***) (4). For T=^{m}CG sites, the deamination rate directly correlated with CPD formation frequency and was maximal for outside facing T^{m}C sugar phosphate backbones. The enhanced rate at these positions was correlated with increased flexibility of the DNA. In contrast, deamination at T=C/C=T sites was slowest at these sites. We suspect that other structural or dynamic properties other than sugar phosphate backbone flexibility dominate the deamination process for $d(TC)_6$.

4.3.5 Mutagenic potential of TCT sites as a function of rotational position

Given that UV-induced C-to-T mutations arise principally from the deamination bypass mechanism, the mutagenic potential of TCT sites as a function of rotational position is expected to depend on the rate of photoproduct formation, deamination, repair and replication. We have shown that the rates of photoproduct formation and deamination are affected by rotational positions, and that the nucleosome modulating effect on formation is much larger than on deamination at TCT sites. The mutagenic potential corresponding to the combined rates of the photoproduct formation and deamination would therefore largely conform to the trend of the photoproduct formation, and greatly increases for TCT sites positioned away from the surface (also the most flexible conformation). The largest mutagenic potential based on the products of the

photoproduct formation and deamination rates is at position +2, which shows almost a 4-fold higher mutagenic potential compared to free DNA (Figure ***4.13***). However, as large as a 7-fold increase was observed at the same position for a TCG site, owing to the significantly increased deamination rate caused by the catalysis of 3'-flanking G (4).

4.3.6 CPD formation and deamination of cytosine in CPDs in a $d(TC)_{35}$-tract

To determine whether the rotational dependence of the deamination rates observed in the $d(TC)_6$-tract at the dyad also extends to other superhelical sites, we constructed a 70-mer $d(TC)_{35}$ tract to span the all the remaining superhelical locations (-1 to -7) to the 5'-side of the $d(TC)_6$ sequence at SHL 0. Knowing that long d(TC)-tracts are known to arrest DNA synthesis near the middle of the sequence due to formation of triplexes (6), we prepared the $d(TC)_{35}$ duplex by scaffold-directed ligation, followed by a single-round of PCR, to reduce the synthesis errors caused by repetitive thermal cycling. The HO• cleavage pattern confirmed that the poly(TC) sequence was being held with the expected rotational phasing. In the nucleosome-bound DNA, the CPD formation pattern exhibits a pronounced 10-bp periodicity from SHL -3 to -6, with CPD formation peaks at exactly -30, -40, -50 and -60 (Figure ***4.14***A and Figure ***4.15***), in perfect alignment with the phasing predicted to be induced by the TG bending motifs placed every 10-bp in the 3'-side of the sequence. An unusually large amount of CPDs form at nucleotide position -40, showing a 4-fold increase compared with average CPD yields in nucleosomes, possibly due to the out-extending H2A tail at this region.

Deamination half-lives were determined by 3-point fitting of 46, 70 and 92 h deamination data (Figure ***4.16***). The sites of fastest deamination appeared at -17, -27 and -37, which are all 3 nucleotides to the 3' of the base pair whose major groove faces the nucleosome, as it does at the dyad. These sites therefore correspond to -7 and +3 relative the dyad, and are consistent with the

results of $d(TC)_6$ experiment, where -7 and +4 positions showed shortest half-lives of 60 and 66 h, compared with 57 h at -17 in $d(TC)_{35}$.

4.4 Conclusion

By the use of $d(TC)_6$ and $d(TC)_{35}$ tracts incorporated into nucleosomes, we have shown that rotational position in a nucleosome affects the rates of CPD formation and deamination at the TCT sites within every superhelical turn from SHL 0 to SHL -7. We also determined that the nucleosome modulated CPD formation at TCT sites to a greater extent than deamination. Furthermore, deamination was slowest at sites where CPD formation was the greatest, and fastest at sites where CPD formation was least, which is opposite to what was found for CPDs formed at ATCG sites. Although phosphate backbone flexibility and conformation seem to be the major controlling factors for CPD formation at both TCG and TCT sites, deamination appears to be controlled by different factors. For ATCG sites, the strong effect of rotation on the rate of deamination of the C may have to do with the presence of the G, and in its absence, some other factors dominates that shows an opposite dependence on rotational position. The origin of UV signature C to T mutations are widely accepted to arise from two main pathways: (1) the error-prone DNA replication at CPD sites; and (2) the error-free translesion synthesis at deamination sites. This combined study on CPD formation and deamination at $d(TC)_n$ tracts suggest that C-to-T mutations in such sequences in nucleosomes would largely depend on the CPD formation rate, rather than the deamination rate, because the nucleosome modulating effect on formation is much larger than on deamination at TCT sites.

4.5 Acknowledgements

We thank Vincent Cannistraro for constructing and carrying out the deamination studies on the d(TC)$_{35}$ sequence and for advice and help with various experimental procedures. We also thank Stephen Lloyd for T4-pdg and Aziz Sancar for photolyase. Research reported in this chapter was supported by the National Cancer Institute of the National Institutes of Health under award number R01CA40463.

4.6 References

1. Cannistraro, V.J. and Taylor, J.-S. (2009) Acceleration of 5-Methylcytosine Deamination in Cyclobutane Dimers by G and Its Implications for Uv-Induced C to T Mutation Hotspots. *Journal of Molecular Biology*, **392**, 1145-1157.

2. Song, Q., Sherrer, S.M., Suo, Z. and Taylor, J.-S. (2012) Preparation of Site-Specific T=(M)Cg Cis-Syn Cyclobutane Dimer-Containing Template and Its Error-Free Bypass by Yeast and Human Polymerase H. *The Journal of Biological Chemistry*, **287**, 8021-8028.

3. Ziegler, A., Leffell, D.J., Kunala, S., Sharma, H.W., Gailani, M., Simon, J.A., Halperin, A.J., Baden, H.P., Shapiro, P.E. and Bale, A.E. (1993) Mutation Hotspots Due to Sunlight in the P53 Gene of Nonmelanoma Skin Cancers. *Proceedings of the National Academy of Sciences of the United States of America*, **90**, 4216-4220.

4. Song, Q., Cannistraro, V.J. and Taylor, J.-S. (2014) Synergistic Modulation of Cyclobutane Pyrimidine Dimer Photoproduct Formation and Deamination at a T(M)Cg Site over a Full Helical DNA Turn in a Nucleosome Core Particle. *Nucleic Acids Research*, **42**, 13122-13133.

5. Cannistraro, V.J., Pondugula, S., Song, Q. and Taylor, J.-S. (2015) Rapid Deamination of Cyclobutane Pyrimidine Dimer Photoproducts at Tcg Sites in a Translationally and Rotationally Positioned Nucleosome in Vivo. *Journal of Biological Chemistry*, **290**, 26597-26609.

6. Baran, N., Lapidot, A. and Manor, H. (1991) Formation of DNA Triplexes Accounts for Arrests of DNA Synthesis at D (Tc) N and D (Ga) N Tracts. *Proceedings of the National Academy of Sciences*, **88**, 507-511.

7. Manor, H., Rao, B.S. and Martin, R.G. (1988) Abundance and Degree of Dispersion of Genomic D (Ga) N· D (Tc) N Sequences. *Journal of Molecular Evolution*, **27**, 96-101.

8. Barak, Y., Cohen-Fix, O. and Livneh, Z. (1995) Deamination of Cytosine-Containing Pyrimidine Photodimers in Uv-Irradiated DNA Significance for Uv Light Mutagenesis. *Journal of Biological Chemistry*, **270**, 24174-24179.

9. Tu, Y., Dammann, R. and Pfeifer, G.P. (1998) Sequence and Time-Dependent Deamination of Cytosine Bases in Uvb-Induced Cyclobutane Pyrimidine Dimers in Vivo. *Journal of Molecular Biology*, **284**, 297-311.

10. Song, Q., Cannistraro, V.J. and Taylor, J.-S. (2011) Rotational Position of a 5-Methylcytosine-Containing Cyclobutane Pyrimidine Dimer in a Nucleosome Greatly Affects Its Deamination Rate. *The Journal of Biological Chemistry*, **286**, 6329-6335.

11. Shrader, T.E. and Crothers, D.M. (1989) Artificial Nucleosome Positioning Sequences. *Proceedings of the National Academy of Sciences*, **86**, 7418-7422.

12. Ryabinina, O.P., Minko, I.G., Lasarev, M.R., McCullough, A.K. and Lloyd, R.S. (2011) Modulation of the Processive Abasic Site Lyase Activity of a Pyrimidine Dimer Glycosylase. *DNA Repair*, **10**, 1014-1022.

13. Worthington, E.N., Kavakli, İ.H., Berrocal-Tito, G., Bondo, B.E. and Sancar, A. (2003) Purification and Characterization of Three Members of the Photolyase/Cryptochrome Family Blue-Light Photoreceptors from Vibrio Cholerae. *Journal of Biological Chemistry*, **278**, 39143-39154.

14. Svedružić, Ž.M., Wang, C., Kosmoski, J.V. and Smerdon, M.J. (2005) Accommodation and Repair of a Uv Photoproduct in DNA at Different Rotational Settings on the Nucleosome Surface. *Journal of Biological Chemistry*, **280**, 40051-40057.

15. Kosmoski, J.V. and Smerdon, M.J. (1999) Synthesis and Nucleosome Structure of DNA Containing a Uv Photoproduct at a Specific Site. *Biochemistry*, **38**, 9485-9494.

16. Wang, K. and Taylor, J.-S.A. (2017) Modulation of Cyclobutane Thymine Photodimer Formation in T11-Tracts in Rotationally Phased Nucleosome Core Particles and DNA Minicircles. *Nucleic Acids Research*, **45**, 7031-7041.

17. Latham, K.A. and Lloyd, R.S. (1995). Delta.-Elimination by T4 Endonuclease V at a Thymine Dimer Site Requires a Secondary Binding Event and Amino Acid Glu-23. *Biochemistry*, **34**, 8796-8803.

18. Lyamichev, V. (1991) Unusual Conformation of (Da) N·(Dt) N-Tracts as Revealed by Cyclobutane Thymine–Thymine Dimer Formation. *Nucleic Acids Research*, **19**, 4491-4496.

19. Suter, B., Schnappauf, G. and Thoma, F. (2000) Poly (Da· Dt) Sequences Exist as Rigid DNA Structures in Nucleosome-Free Yeast Promoters in Vivo. *Nucleic Acids Research*, **28**, 4083-4089.

20. Lemaire, D.G. and Ruzsicska, B.P. (1993) Kinetic Analysis of the Deamination Reactions of Cyclobutane Dimers of Thymidylyl-3', 5'-2'-Deoxycytidine and 2'-Deoxycytidylyl-3', 5'-Thymidine. *Biochemistry,* **32**, 2525-2533.

4.7 Tables and Figures

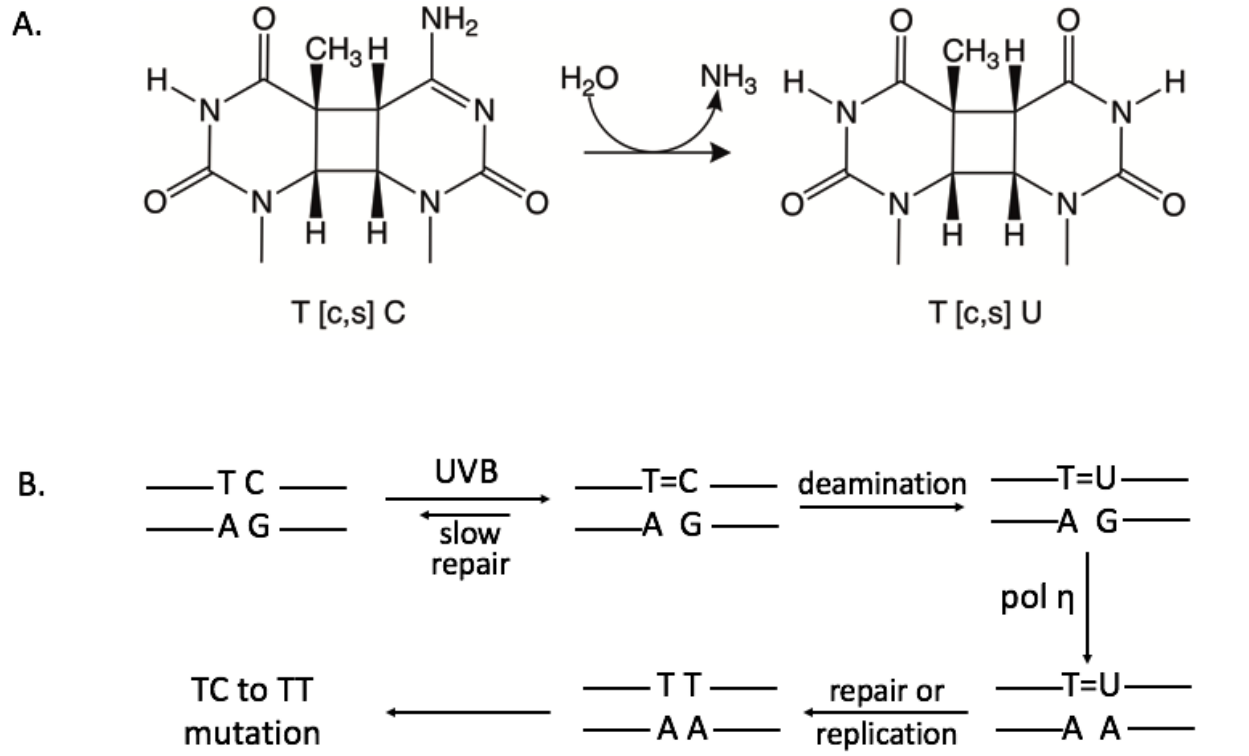

Figure 4.1: Deamination-bypass mechanism for UV-induced C to T mutations. (A) *cis-syn* CPD deamination at a TC site. (B) formation of UV-induced C to T mutation at a TC site in which polymerase η inserts an A opposite the U resulting from deamination of the C in the CPD formed by UV light.

A.

AC AGATG|AATTC GGCTC ATTCA GCGTC TATGT CGGTC TTAGA
GGCTG ATACA CCGAG AATGT CGCTC TTACT CGCTC ATCTC TCTCT
CTCGT GGCTC ATAGA CGCTG TTACA GGCAG ATTGT CCGTG TAACA
CGGTG ATACT GCGAC AATGA CGCTG|AATTC ACAGAT

B.

5′TC-(TC)$_{33}$-TC- ATACC GGGCG
5′pAAAGT GGCTC ATAGA CGCTG
TTACA GGCAG
5′pATTGT CCGTG TAACA CGGTG
ATACT GCGAC AATGA CGCTG

C.

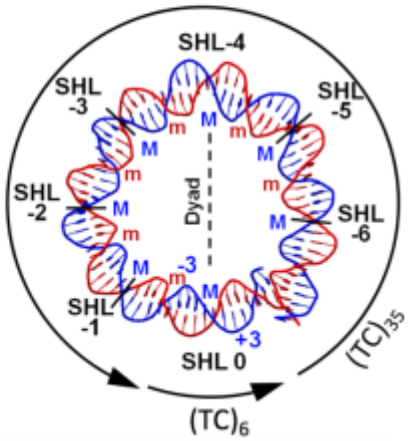

Figure 4.2: Nucleosomal DNA sequence design. (A) A 168-mer DNA was designed to have a centrally located d(TC)$_6$-tract (underlined), terminal EcoRI restriction sites (green italic), phased minor groove bending (T/A)$_3$ sequences in red and major groove bending (G/C)$_3$ sequences in blue. The C in orange in the d(TC)$_6$-tract corresponds to the position at which the major groove is expected to bend towards the histone surface at the dyad axis. (B) A 150-mer DNA was made from 3 oligomers by scaffold-directed ligation: an 80-mer with d(TC)$_{35}$-tract, a 30-mer with 5'-phosphate and a 40-mer with 5'-phosphate. Other features are as described in (A). (C) In our design, d(TC)$_6$ covers dyad SHL from +6 to -5, d(TC)35 covers SHLs from -1 to -7. The SHLs are identified by the number of helical turns from the dyad axis on the blue strand containing the d(TC)$_6$ tract. They are negative to correspond with the negative numbers assigned to the nucleotides on the d(TC)$_6$-tract strand that are 5'- to the C at the dyad axis which is assigned as 0. The -3(inside) and +3(outside) nucleotide positions are shown in blue. The positions at which the major and minor grooves face the histone surface are indicated by M and m, respectively, and are color coded blue and red to match the major and minor groove bending motifs in (A) and (B).

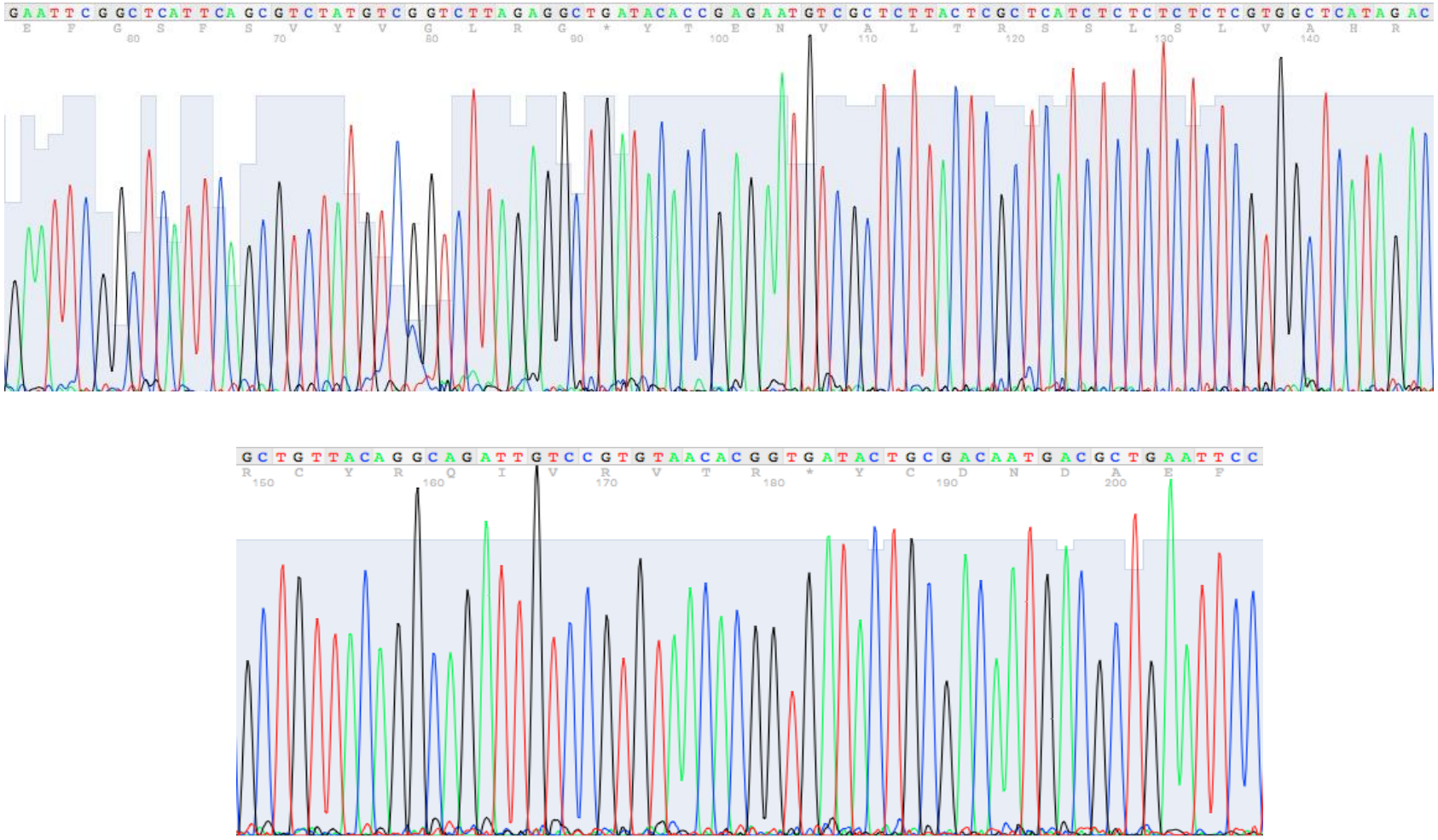

Figure 4.3: Sequencing results for clone 16 used in this study.

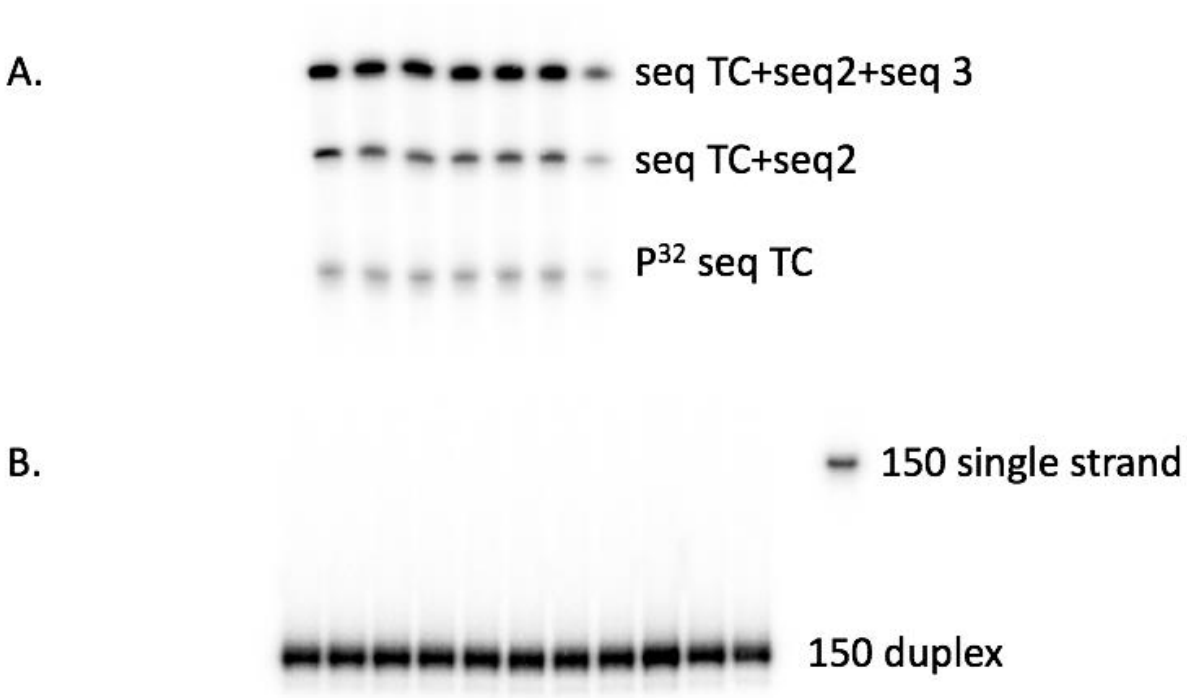

Figure 4.4: PAGE analysis of 150-mer DNA duplex containing d(TC)$_{35}$-tract. (A). Scaffold-mediated ligation products loaded on a 10% denaturing PAGE. (B). Single-round of PCR products loaded on a10% native PAGE.

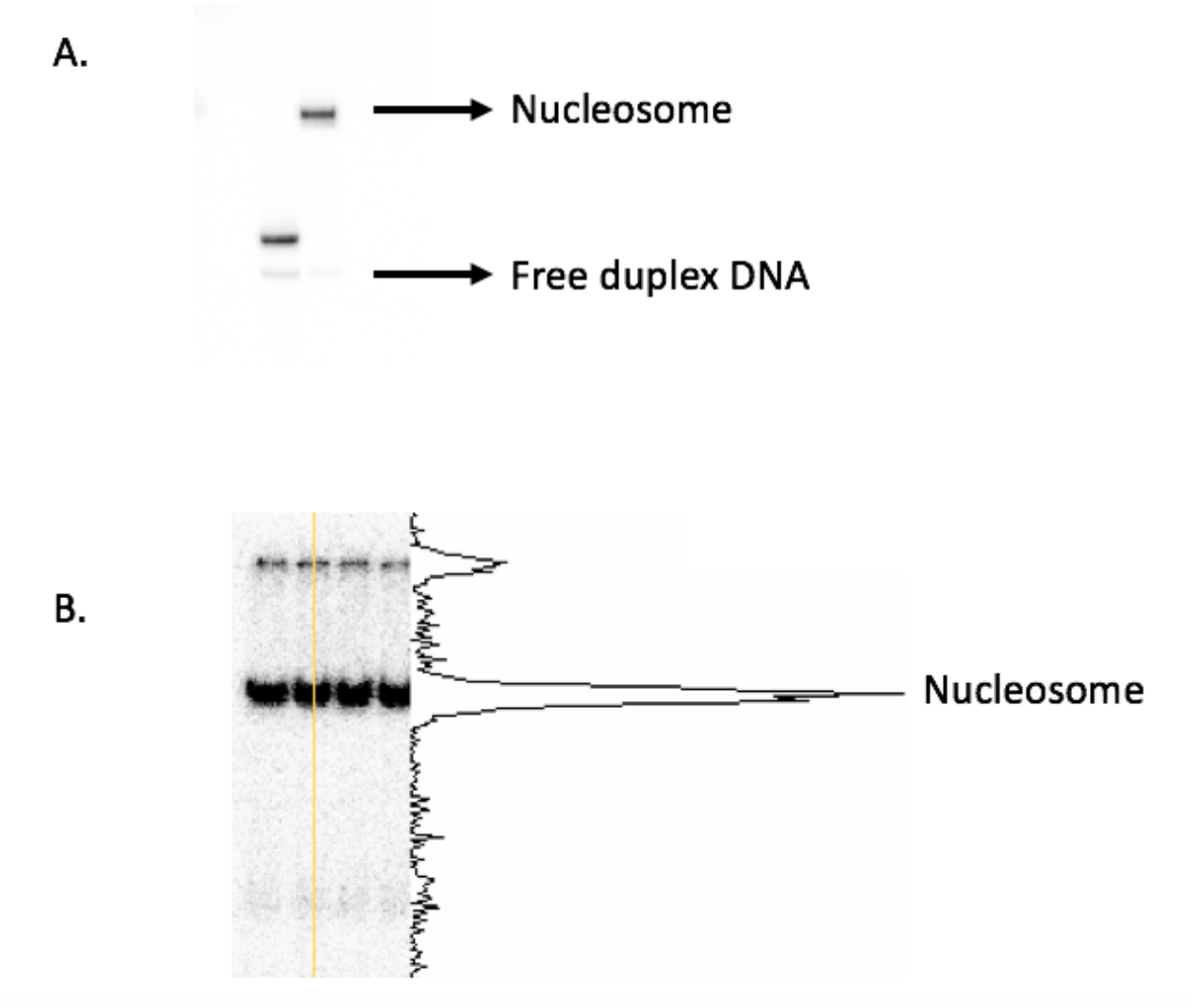

Figure 4.5: PAGE analysis of reconstituted nucleosomes. Greater than 95% incorporation was achieved after nucleosome reconstitution for d(TC)$_6$-DNA (A) and d(TC)$_{35}$-DNA (B).

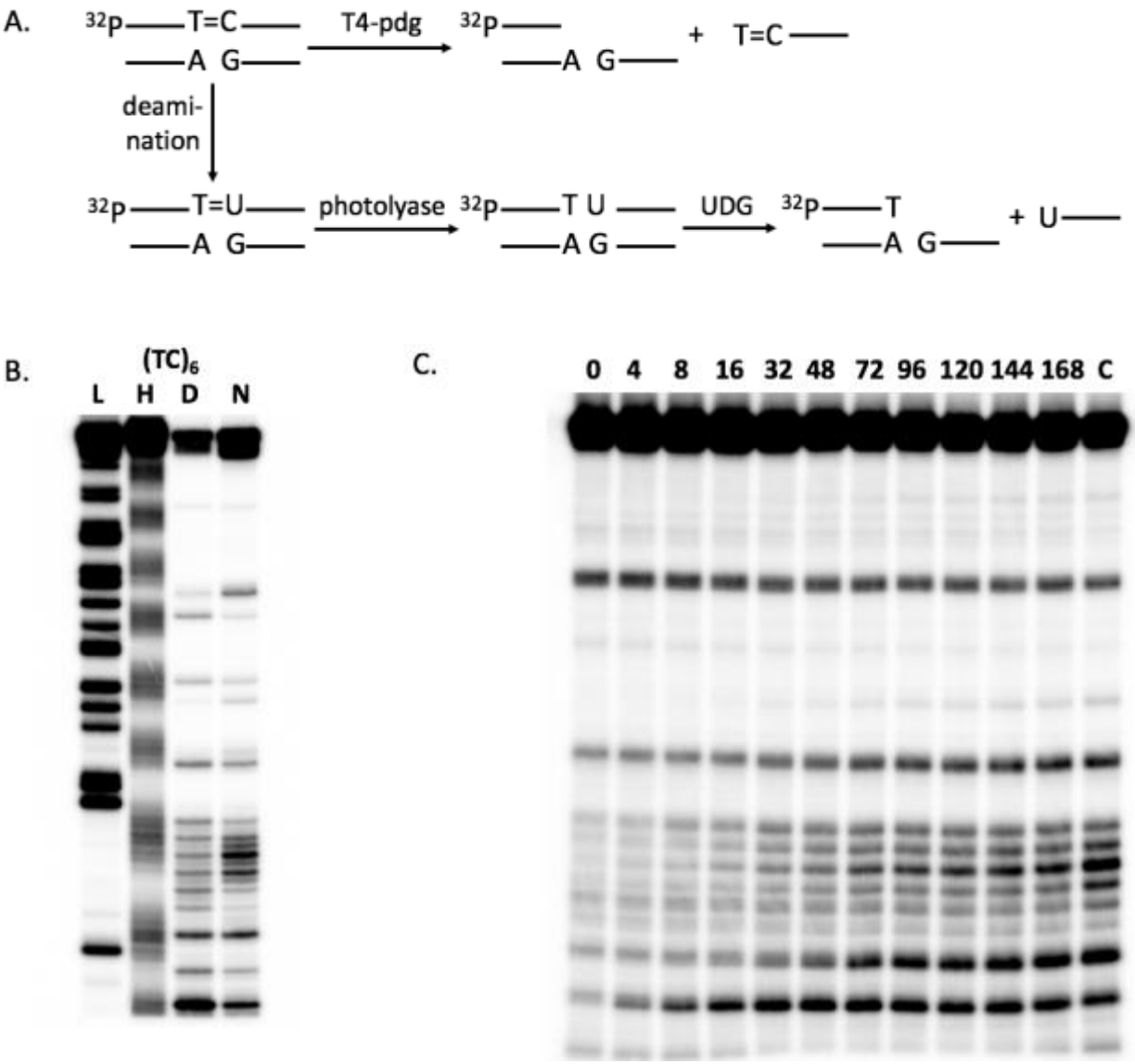

Continued on next page.

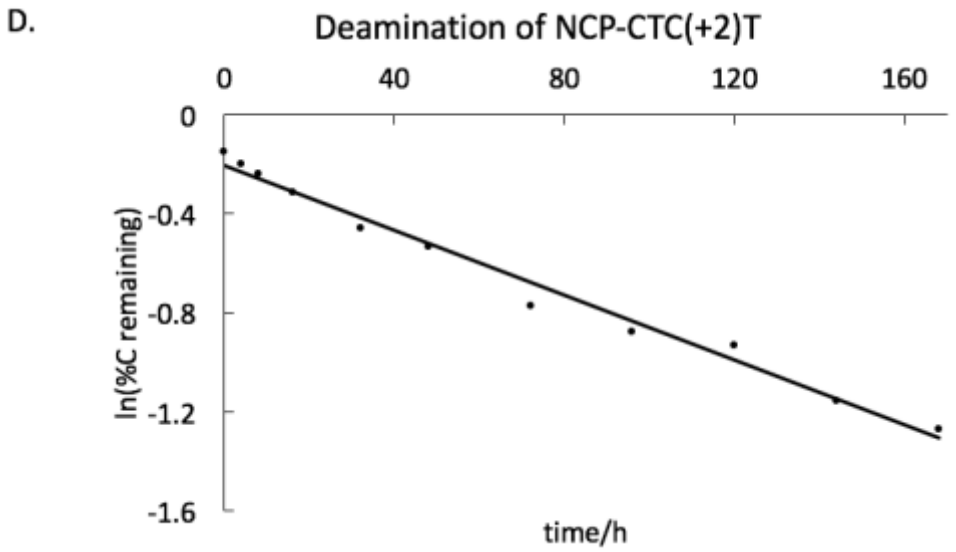

Figure 4.6: Determination of deamination rates. (A) General scheme for the T4-pdg assay to quantify CPD formation (top) and the photolyase/UDG cleavage assay to determine deamination rates (bottom). Free 150-mer duplex DNA containing $d(TC)_6$-tract or chicken nucleosomes that had been exchanged with 150-mer duplex DNA were irradiated to form T=CT or TC=T CPDs that were allowed to deaminate over time, converting C to U within the CPD. At specific time intervals aliquots of the reaction were removed and photoreverted with photolyase and cleaved by UDG. (B) PAGE analysis of hydroxyl radical footprinting of nucleosome core particles (lane H) and assay of CPD formation in free (lane D) and nucleosome-bound DNA (lane N). Lane L is the Maxam Gilbert G ladder. (C) PAGE analysis of deamination time course (hours) with reconstituted nucleosomes. The last lane C represents complete deamination. Panel (D) shows the plot of the extent of deamination with time that has been fit to a first order process at CTC(+2)T.

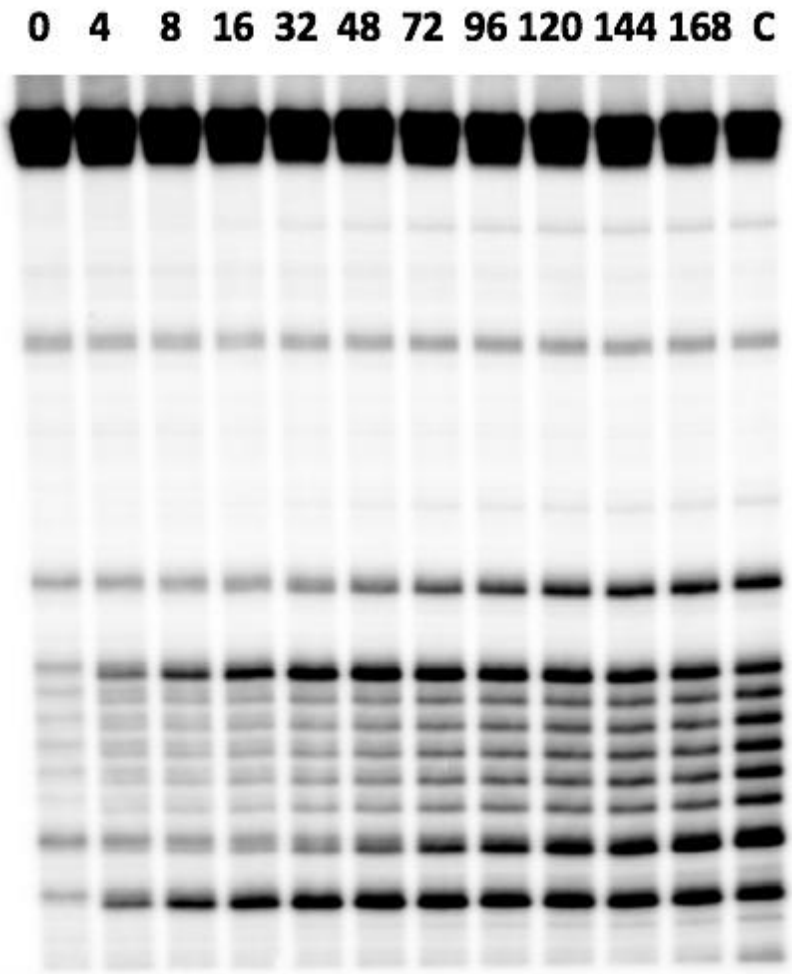

Figure 4.7: PAGE analysis of CPD deamination in free DNA containing d(TC)$_6$-tract. Numbers on top indicate deamination time in hours, lane C is the deamination completion point.

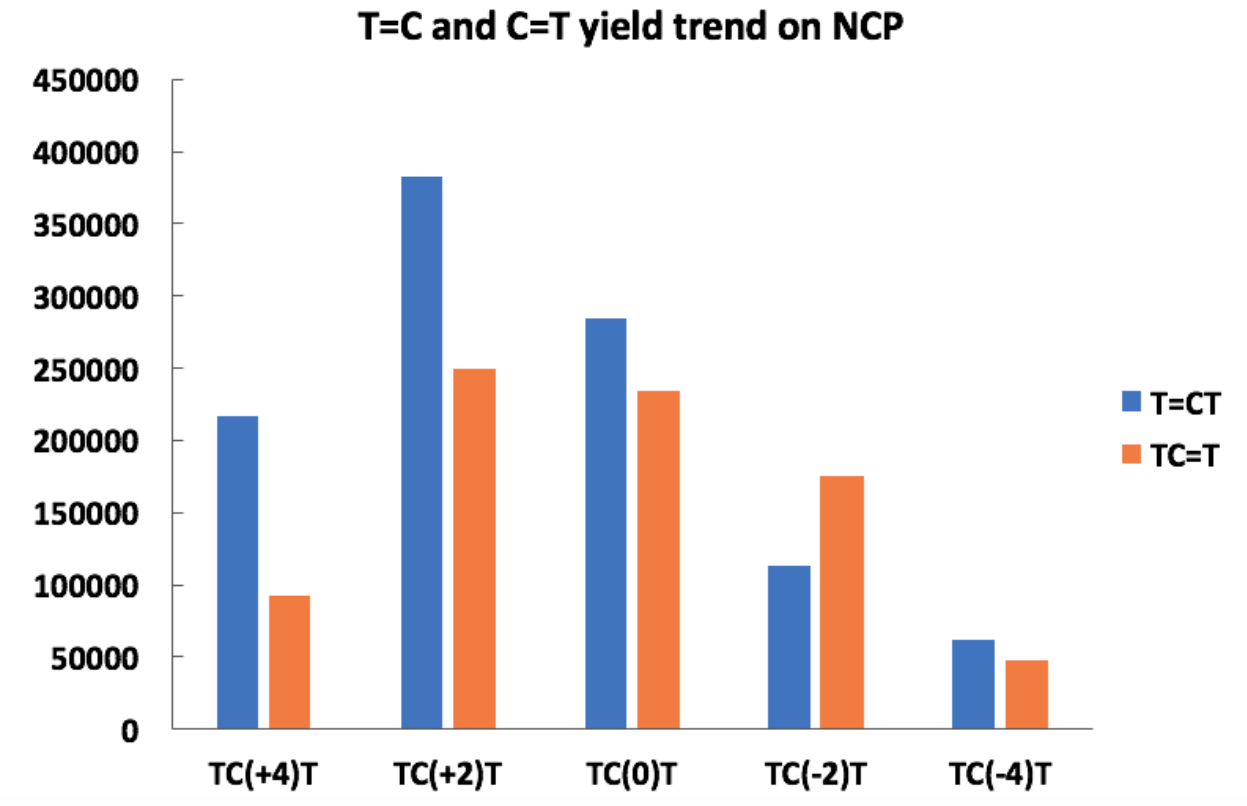

Figure 4.8: CPD yields for T=CT and TC=T sites as a function of rotational position in d(TC)$_6$-NCP. The difference inmaxima reflects the fact that the TC and CT CPDs differ in position by one nucleotide

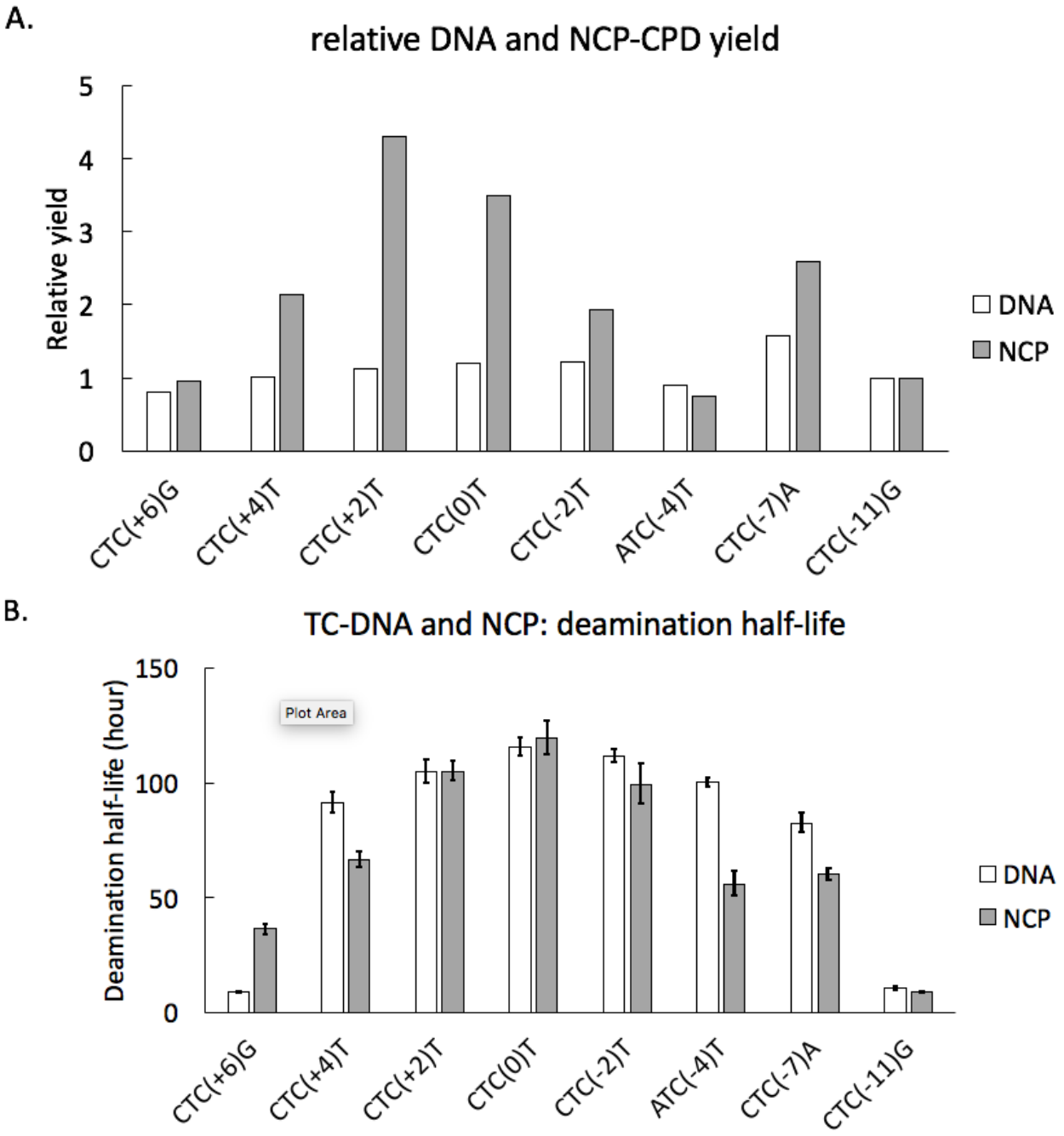

Figure 4.9: Photoproduct yield and deamination half-lives as a function of nucleotide position. (A) Bar graph of T=C and/or C=T CPD relative yield at each rotational position compared to that at T=C(-11)G. A previous study showed that CPDs between -12 and -11 nucleotide positions formed with equal frequency between free and nucleosome-bound DNA. (B) Bar graph of the deamination half-life at 8 rotational positions.

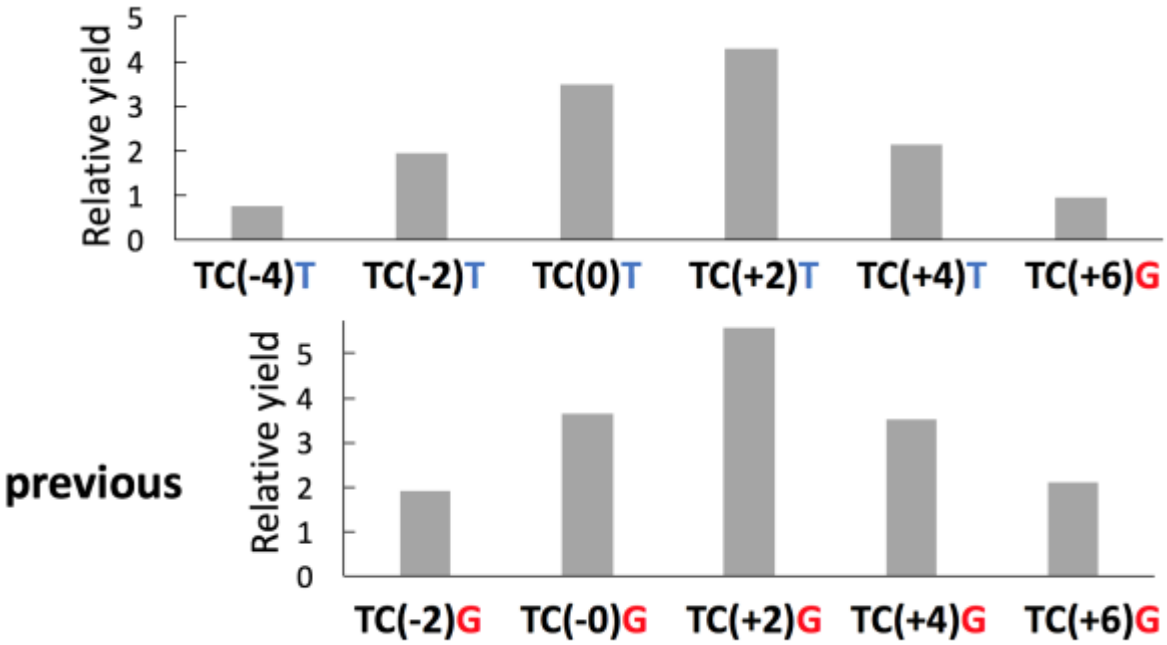

Figure 4.10: Comparison of relative yields between TCT and TCG sites. Top bar graph shows relative CPD yields at TCT and TCG sites within d(TC)$_6$-tract. Bottom bar graph shows relative CPD yields at TCG sites in a previous study by our group.

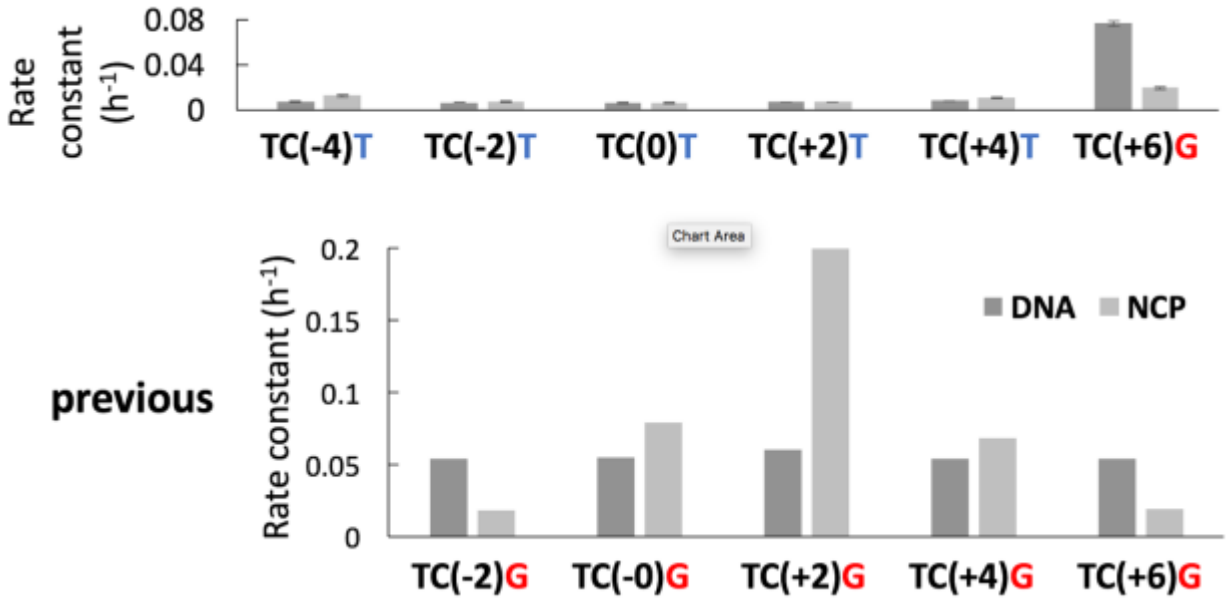

Figure 4.11: Comparison of deamination rate constants between TCT and TCG sites. Top bar graph shows relative CPD yields at TCT and TCG sites within d(TC)$_6$-tract. Bottom bar graph shows relative CPD yields at TCG sites in a previous study by our group.

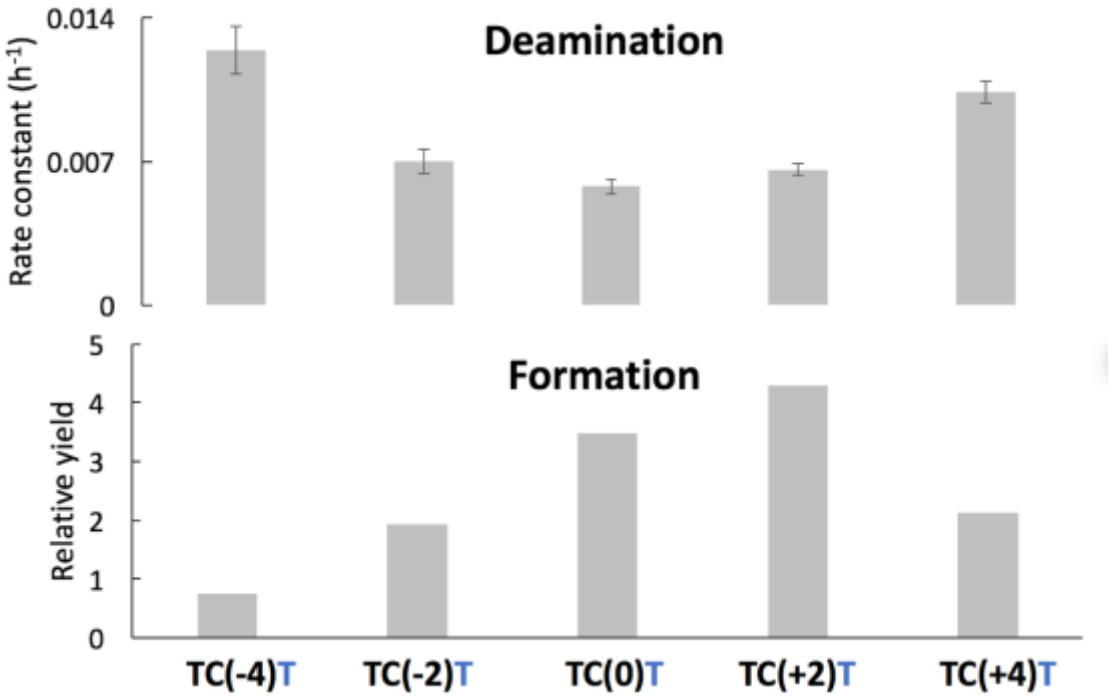

Figure 4.12: Correlation between deamination rate constant and CPD formation yields as function of rotational positions at TCT sites within d(TC)$_6$-tract.

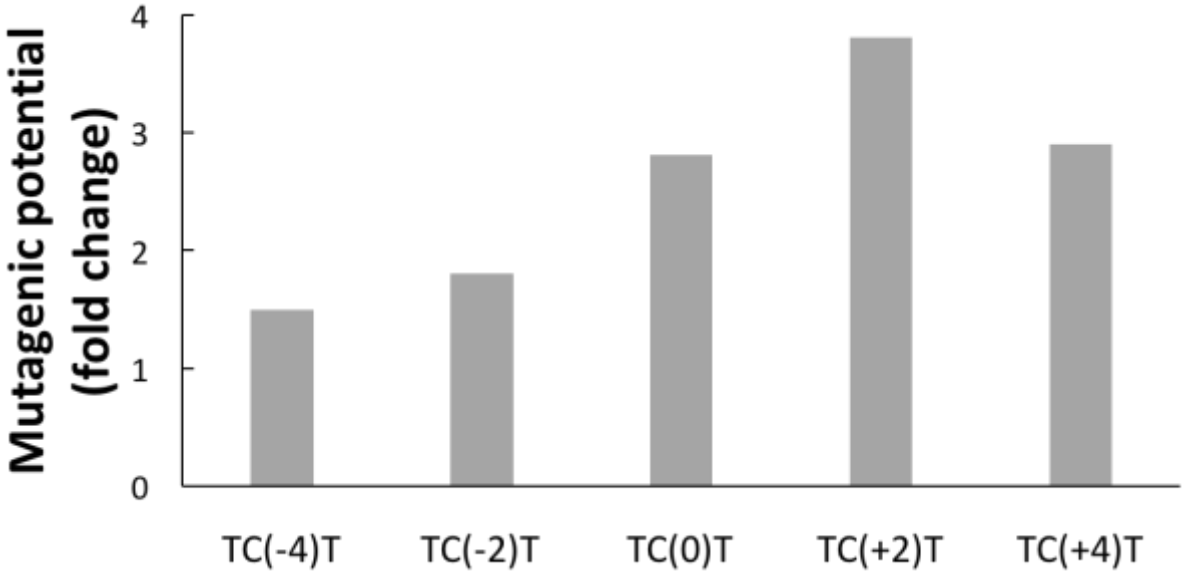

Figure 4.13: Mutagenic potential of TCT sites as a function of rotational position. The product of the relative rate of CPD formation and CPD deamination is plotted versus rotational position.

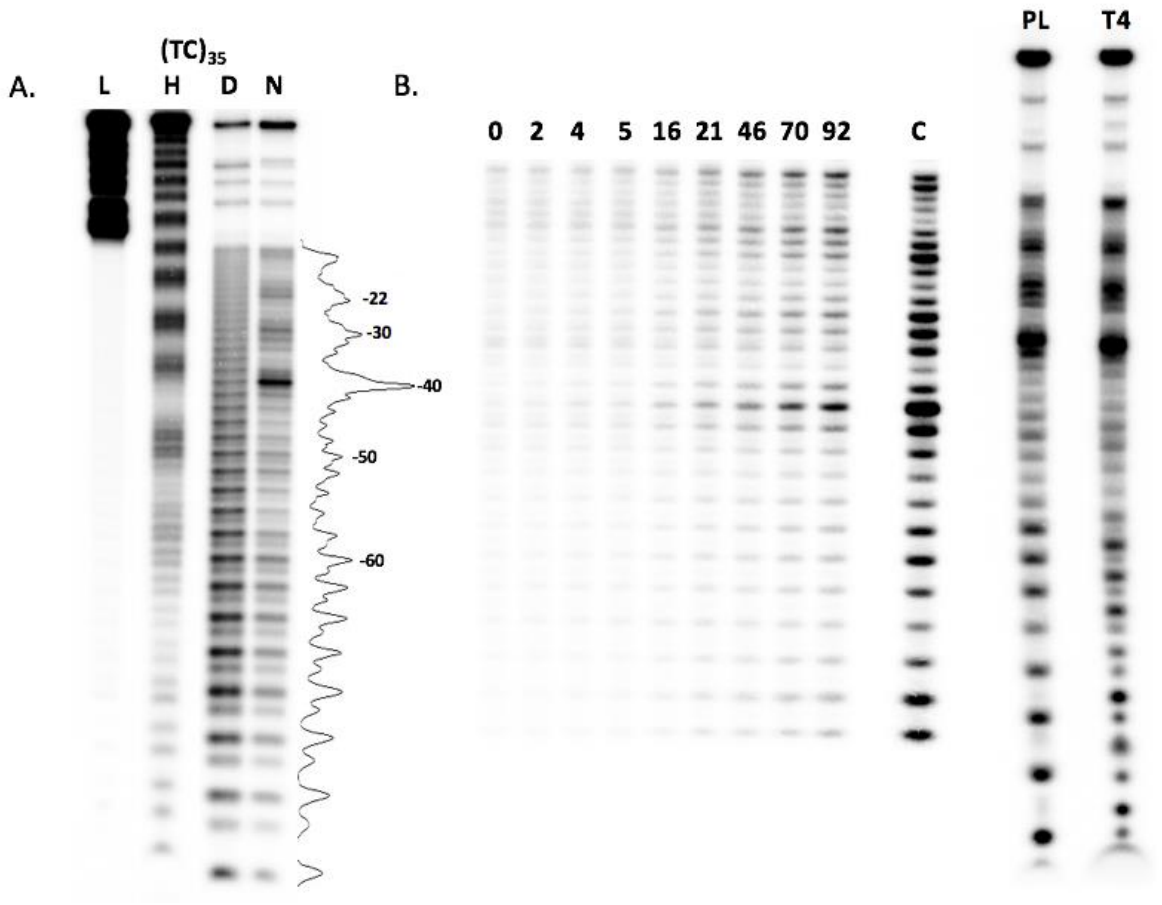

Figure 4.14: PAGE analysis of CPD deamination in free or nucleosome-bound DNA containing d(TC)$_{35}$-tract. (A) Lane H: hydroxyl radical footprinting of nucleosome core particles; Lane D and N: assay of CPD formation in free and nucleosome-bound DNA; Lane L: Maxam Gilbert G ladder. (B) deamination time course (hours) with reconstituted nucleosomes. The last lane C represents complete deamination. Lane PL: whole picture of deamination pattern on nucleosome-bond DNA; Lane T4: whole picture of CPD pattern on nucleosome-bond DNA.

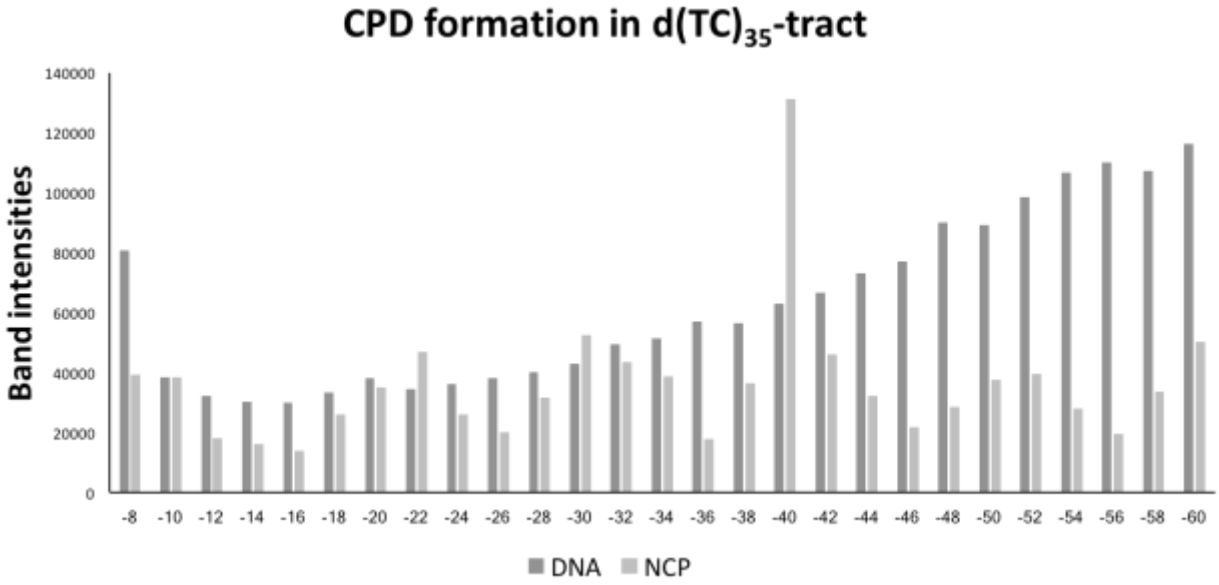

Figure 4.15: CPD formation as a function of nucleotide position in d(TC)$_{35}$-tract.

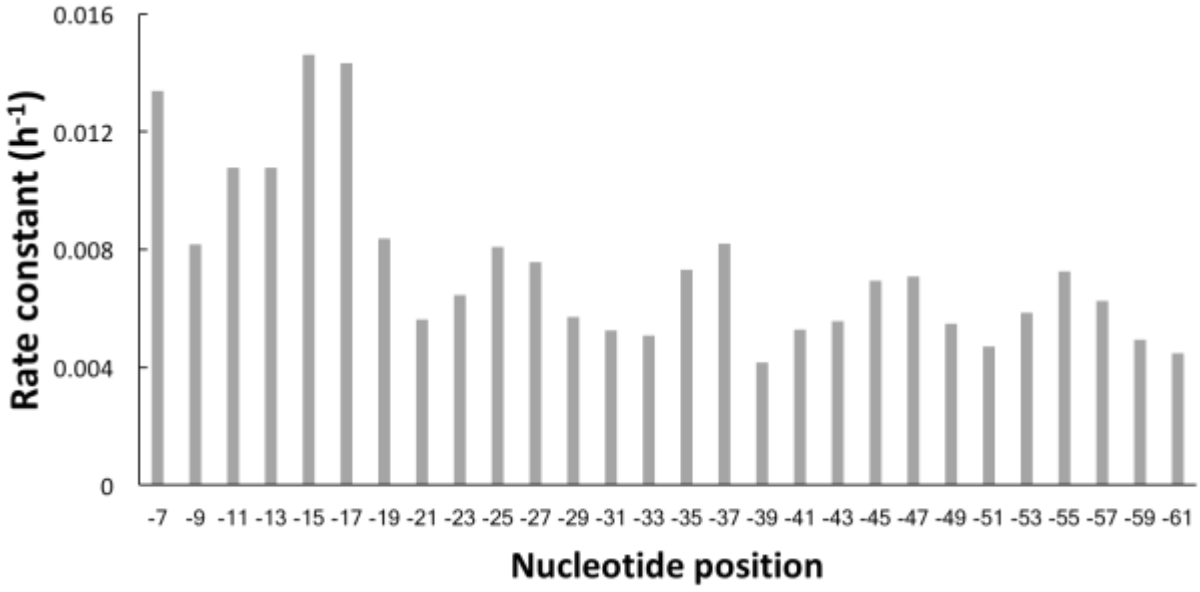

Figure 4.16: Deamination rate constants as a function of nucleotide position in d(TC)$_{35}$-NCP.

PCR primer set to make $d(TC)_6$-DNA:

Forward: 5'-AATTC GGCTC ATTCA GCGTC TATG

Reverse:5'-CA GCGTC ATTGT CGCAG TATCA C

ODNs used in scaffold-mediated ligation and single-round PCR to make $d(TC)_{35}$-DNA :

scaffold 1: 3'-TATGGCCCGCTTTCACCGAGTATCTG-5'

scaffold 2: 3'-CCACTATGACGCTGTTACTGCGACP-5'

reverse primer: 3'-GACAATGTCCGTCTAACAGGCACATAGTG-5'

Table 4.1: Primer set and scaffold DNA used in synthesis of $d(TC)_6$- and $d(TC)_{35}$-contatining nucleosomal DNA.

	fold change in CPD yield (T=C/C=T)		HO• cleavage pattern
	DNA	NCP	
TC(+4)T	1.68	2.37	peak
TC(+2)T	1.57	1.54	
TC(0)T	1.53	1.21	
TC(-2)T	1.45	0.64	valley
TC(-4)T	1.31	1.29	

Table 4.2: Fold change in CPD yields between T=CT and TC=T at TCT sites.

	Relative T=C yield		Fold change	Deamination half-life (h)		Fold change
	DNA	NCP		DNA	NCP	
CTC(+6)G	0.81	0.95	1.2	9.0 ± 0.3	36 ± 2	4.0
CTC(+4)T	1.01	2.13	2.1	91 ± 4	67 ± 3	0.7
CTC(+2)T	1.13	4.30	3.8	105 ± 5	105 ± 4	1.0
CTC(0)T	1.20	3.49	2.9	115 ± 4	119 ± 7	1.0
CTC(-2)T	1.21	1.93	1.6	112 ± 3	99 ± 8	0.9
ATC(-4)T	0.91	0.75	0.8	100 ± 2	56 ± 5	0.6
CTC(-7)A	1.58	2.59	1.6	82 ± 4	60 ± 3	0.7
CTC(-11)G	1.00	1.00	1.0	10.5 ± 0.8	9.0 ± 0.1	0.8

Table 4.3: Nucleosome rotational positioning effect on photoproduct yield and deamination half-life.

	CTC(+4)T	CTC(+2)T	CTC(0)T	CTC(-2)T	average	Std. dev.	RSD
DNA relative CPD yield	100.60%	113.00%	120.00%	121.00%	1.14	0.09	8.3%
NCP relative CPD yield	213.30%	430.10%	348.80%	193.30%	2.96	1.13	38.1%
DNA deamination half-life	91.184	105	115.5	111.774	105.86	10.71	10.1%
NCP deamination half-life	66.6	105	119.5	99	97.53	22.34	22.9%

Table 4.4: Relative CPD yields and deamination times and standard deviations for all 4 CTCT sites within d(TC)$_6$-tract.

Chapter 5 Summary and Future Research

5.1 Summary

Cyclobutane pyrimidine dimers (CPDs) are the most abundant UV-induced DNA lesions, and CPDs formed at C-containing sites are also the ones that are most closely associated with skin cancer induction. The mutagenicity of a particular CPD will depend on its induction frequency, deamination rate, repair rate and DNA damage polymerase bypass rate. To study the effects of nucleosome translational and rotational positions on T=T CPD formation and deamination systematically and efficiently, we designed a circular permutation synthetic strategy for the rapid preparation of the substrates with any translational or rotational position. We found that nucleosome positioning greatly altered the T=T CPD distribution pattern in a T_{11}-tract at all seven helical turns located across one half of a symmetric nucleosome core particle compared to free DNA. Compared with its characteristic pattern in free DNA, T=T CPD distributions within each helical turn are dramatically changed, favoring the middle of the T_{11}-tract, correlating with outside positions. While raising the temperature changed the CPD pattern in free DNA, the pattern was temperature invariant in the nucleosome. Irradiation of a circular DNA corresponding to one full turn of DNA in the nucleosome resulted in the same pattern as in the nucleosome proving the dominant role of DNA curvature in determining CPD distribution.

The CPDs of TC or CC sites have been correlated with C-to-T mutations. Unlike T=T CPDs that are stable, the C in C-containing CPDs readily deaminates to U within hours to days, which then directs the insertion of A during bypass by DNA polymerase eta, resulting in the characteristic C-to-T signature mutation of UV light. In Chapter 4, we studied the deamination of TC CPDs at all rotational positions in the nucleosome using DNA sequences containing poly $(TC)_n$

tracts, and found that, compared with free DNA, nucleosomes can only moderately modulate deamination rates and that the modulation is opposite that for CPD formation. Because the modulation on formation is much stronger than on deamination in nucleosomes, the net mutagenicity of $d(TC)_n$-tracts mainly depends on the photoproduct formation rates with high mutagenic potential at outward-facing nucleotide positions.

5.2 Future Research

5.2.1 Quantitative analysis of parameters that can alter deamination kinetics of C-containing CPDs in nucleosomes

In free DNA, the deamination rates of C-containing CPDs highly depend on their flanking sequences, salt concentration, temperature, and other factors (1). The same systematic investigation of the effects of these factors on deamination, however, is lacking within nucleosomes and worth studying, because these factors are associated with nucleosome structure stability. It would also be interesting to know the extent to which other types of DNA photoproducts, such as (6-4) PPs and Dewar photoproducts, are influenced by nucleosome structure, sequence context, salt and temperature. Deamination of C-containing CPDs is subject to a complex interplay of various factors, and dissecting the contributions of these factors quantitatively will enhance our understanding of deamination process, and furthermore, how to control them.

5.2.2 Use of minicircular DNA to study bending effects on deamination and other reactions of DNA

Before the establishment of our DNA minicircular model, a protein-free DNA loop held by lambda repressor was used to assess the effects of DNA curvature on pyrimidine dimer formation (2). The exact shape, curvature, and rotational phasing of the DNA in the lambda repressor system is

unknown, however, and therefore cannot be directly correlated with nucleosome core particles. Our minicircular DNA model incorporates exactly a complete turn of nucleosomal binding DNA, and faithfully reproduces the pattern of CPD formation in nucleosomes. Such a minicircle should therefore, be of general value for assessing the effects of nucleosome curvature on DNA modifications, such as hydrolytic deamination, by examining the bend-dependent pattern of CPD formation.

5.2.3 Crystal structure analysis of site-specifically photodamaged nucleosomes

There are numerous crystal structures of nucleosome core particles in the Protein Data Bank (PDB), varying in resolution, DNA sequence and nucleosome source. These structures can contribute to the understanding of nucleosome assembly (3), DNA sequence-dependent binding affinity (4) and positioning (5). Structures of nucleosome-containing defects, especially UV lesions, are rare in PDB (6,7). The difficulty resides in synthesis of nucleosome-binding DNA containing site-specific UV damages or other lesions. So far there are two major ways to prepare such DNA substrates: i) Use dinucleotide phosphoramidite building blocks, such as developed for the *cis-syn* thymine dimer (8) and 6–4PP (9) for solid-phase DNA synthesis technology; ii) Irradiate with UV the oligonucleotides containing photodamage-forming sites and then elongate to desired length by ligation (10). Both ways are subject to yield and length limitations, preventing their application in preparing nucleosome crystal structures. It was only recently that Osakabe and coworkers determined the nucleosome structure containing 6–4PPs to elucidate the lesion recognition by UV-damaged DNA-binding (UV-DDB) in chromatin (6). Compared with damage recognition and repair, we are most interested in the structure distortion induced by DNA photodimers and are currently working on crystalizing nucleosomes containing the T_{11}-tract, in order to explain the

unusual shifts and abnormalities found in CPD formation patterns at different superhelical locations and to better understand how TG-motifs phase DNA on a nucleosome (11).

5.3 References

1. Cannistraro, V.J. and Taylor, J.-S. (2009) Acceleration of 5-methylcytosine deamination in cyclobutane dimers by G and its implications for UV-induced C-to-T mutation hotspots. *Journal of Molecular Biology*, **392**, 1145-1157.

2. Pehrson, J.R. and Cohen, L.H. (1992) Effects of DNA looping on pyrimidine dimer formation. *Nucleic Acids Research*, **20**, 1321-1324.

3. Luger, K., Mader, A.W., Richmond, R.K., Sargent, D.F. and Richmond, T.J. (1997) Crystal structure of the nucleosome core particle at 2.8 angstrom resolution. *Nature*, **389**, 251.

4. Chua, E.Y., Vasudevan, D., Davey, G.E., Wu, B. and Davey, C.A. (2012) The mechanics behind DNA sequence-dependent properties of the nucleosome. *Nucleic Acids Research*, **40**, 6338-6352.

5. Tsunaka, Y., Kajimura, N., Tate, S. and Morikawa, K. (2005) Alteration of the nucleosomal DNA path in the crystal structure of a human nucleosome core particle. *Nucleic Acids Research*, **33**, 3424-3434.

6. Osakabe, A., Tachiwana, H., Kagawa, W., Horikoshi, N., Matsumoto, S., Hasegawa, M., Matsumoto, N., Toga, T., Yamamoto, J. and Hanaoka, F. (2015) Structural basis of pyrimidine-pyrimidone (6–4) photoproduct recognition by UV-DDB in the nucleosome. *Scientific Reports*, **5**.

7. Horikoshi, N., Tachiwana, H., Kagawa, W., Osakabe, A., Matsumoto, S., Iwai, S., Sugasawa, K. and Kurumizaka, H. (2016) Crystal structure of the nucleosome containing ultraviolet light-induced cyclobutane pyrimidine dimer. *Biochemical and Biophysical Research Communications*, **471**, 117-122.

8. Taylor, J.S., Brockie, I.R. and O'Day, C.L. (1987) A building block for the sequence-specific introduction of cis-syn thymine dimers into oligonucleotides. Solid-phase synthesis of TpT [c, s] pTpT. *Journal of the American Chemical Society*, **109**, 6735-6742.

9. Iwai, S., Shimizu, M., Kamiya, H. and Ohtsuka, E. (1996) Synthesis of a phosphoramidite coupling unit of the pyrimidine (6− 4) pyrimidone photoproduct and its incorporation into oligodeoxynucleotides. *Journal of the American Chemical Society*, **118**, 7642-7643.

10. Smith, C.A. and Taylor, J.-S. (1993) Preparation and characterization of a set of deoxyoligonucleotide 49-mers containing site-specific cis-syn, trans-syn-I, (6-4), and Dewar photoproducts of thymidylyl (3'--> 5')-thymidine. *Journal of Biological Chemistry*, **268**, 11143-11151.

11. Wang, K. and Taylor, J.-S.A. (2017) Modulation of cyclobutane thymine photodimer formation in T11-tracts in rotationally phased nucleosome core particles and DNA minicircles. *Nucleic Acids Research*, **45**, 7031-7041.